The Pennsylvania State University

The Graduate School

College of Engineering

A PHOTOCHEMICAL PROCESS TO FABRICATE THIN FILMS AND PATTERNS OF UNSUBSTITUTED POLYTHIOPHENE

A Thesis in

Chemical Engineering

by

Sudarshan Natarajan

© 2005 Sudarshan Natarajan

Submitted in Partial Fulfillment
of the Requirements
for the Degree of

Doctor of Philosophy

December 2005

The thesis of Sudarshan Natarajan was reviewed and approved* by the following:

Seong H. Kim
Assistant Professor of Chemical Engineering
Thesis Adviser
Chair of Committee

Henry C. Foley
Professor of Chemical Engineering

Themis Matsoukas
Associate Professor of Chemical Engineering

Ayusman Sen
Professor of Chemistry

Andrew L. Zydney
Walter Robb Chair and Professor of Chemical Engineering
Head of the Department of Chemical Engineering

*Signatures are in file in the Graduate School

Abstract

Polythiophenes have great potential in the field of electronics, sensors, solar-cells, displays so on. Despite its superior thermal and environmental stability and ease of synthesis, unsubstituted polythiophene is not widely utilized in the aforementioned applications. One of the main reasons is its intractability. The unsubstituted polythiophene is insoluble and not fusible, hence cannot be processed into useful devices using conventional micro-fabrication methods. To address this issue an *in-situ* photochemical polymerization process is developed and detailed in this thesis. The process involves vapor deposition of monomer 2,5-diiodothiophene on a substrate in ambient condition, followed by UV irradiation of the deposited precursor film in an argon environment. The photochemical process synthesizes polythiophene directly from the monomer adsorbed on a substrate thus avoids the intractability issues of unsubstituted polythiophene in fabrication of thin films and patterns.

The most significant contribution is the discovery of photo-activated Ullmann coupling reaction. Photo-activation of a thin film of 2,5-diiodothiophene on a copper substrate produces unsubstituted polythiophene with an average conjugation length of ~ 7, while the same process on Au, Pt, Pd, and SiO_2 produces polymer of conjugation length ~ 4. This enhanced conjugation length on copper is explained by the mediation of Ullmann coupling pathway in the photochemical reaction. The photo-activation of monomer molecules removes the need for reflux at a high temperature as in conventional Ullmann coupling reaction and enables *in-situ* Ullmann coupling synthesis of thin films

and micro-patterns of unsubstituted polythiophene from the monomer film in ambient conditions.

Experimental evidences showing a decrease in the extent of mediation of Ullmann coupling with an increase in the thickness of monomer are presented. A diffusion-reaction model is developed to qualitatively explain the experimental evidences. Also, a stochastic model is developed to explain the mass spectrum of polythiophene synthesized on non-reactive substrate such as glass. Extent of reaction is calculated by fitting this model to the experimental results.

A mask-less technique for fabrication of periodic patterns of polythiophene is also demonstrated by regio-selective condensation of 2,5-diiodothiophene followed by photochemical conversion of the condensed monomer into polythiophene.

Table of Contents

List of Tables ……..... vii
List of Figures ……... viii
Acknowledgements ……... xii

Chapter 1. Introduction ….……..... 1
1.1 Background……..... 1
1.2 Factors affecting the material properties …… 1
1.3 Current methods of processing …..…….. 4
1.4 Organization of the thesis …… 8
1.5 References ……..…. 9

Chapter 2. Photochemical conversion of 2,5-diiodothiophene condensed on a substrate to polythiophene thin films and micro-patterns. ……..……... 16
2.1 Introduction ……. 16
2.2 Experimental …… 16
2.3 Results and discussion ……..……..……. 18
2.4 Conclusion ……... 28
2.5 References ……... 28

Chapter 3. Synthesis of polythiophene films and patterns on copper substrates using photo-activated Ullmann coupling reaction. …… 39
3.1 Introduction ……..... 39
3.2 Experimental …… 40
3.3 Results and discussion ……..……... 42
3.4 Conclusion ……... 46
3.5 References ……... 47

Chapter 4. Insights on the mechanism of the photochemical and the photo-activated Ullmann coupling processes ……..…….. 58
4.1 Introduction…...……..... 58
4.2 Mass spectrum of photochemcially synthesized polymer ……..……. 59
4.3 Mechanism and kinetics of polymerization …….……..…….. 59
4.4 Stochastic model for the mass spectrum ……..……... 63
4.5 Diffusion-reaction model to predict the extent of copper mediation …….. 66
4.6 References ……... 72

Chapter 5. Mask-less fabrication of polythiophene patterns by photochemical conversion of the regio-selectively condensed 2 5-diiodothiophene …… 86
5.1 Introduction ……..... 86
5.2 Experimental …… 87

5.3 Results and discussion ……..……..……. 89
5.4 Conclusion ……... 93
5.5 References ……..……. 94

Appendix A: Additional notes on chapter 2 …….. 100
Appendix B: Additional notes on chapter 3 …….. 115
Appendix C: Additional notes on chapter 4 …….. 119
Appendix D: Additional notes on chapter 5 …….. 124

List of Tables

3.1	C_α=C_β symmetric and anti-symmetric stretching vibration peak positions and the intensity ratio of α-α' oligothiophenes.	49
4.1	Parameters used for various monomer thickness (L).	74
5.1	Surface chemistry dependence of the contact angle of 2,5-diiodothiophene liquid on various substrates at ~50 ˚C.	96

List of Figures

1.1 Examples of conjugated polymer 12

1.2 Polaron in a polythiophene chain Top: Geometrical change in the molecular structure Bottom: Localized levels in the forbidden gap. 12

1.3 Charge transport in the localized state material is by tunneling of charge from one site to the next. 13

1.4 Conjugated polymer with defects in structure and architecture. 13

1.5 Dependence of mobility on the morphology. 14

1.6 Chemical synthesis procedures of unsubstituted polythiophene. 14

1.7 Self-assembled structures formed in regioregular polythiophenes. 15

1.8 Mechanism of electrochemical polymerization. 15

2.1 Schematic of the photochemical synthesis of polythiophene patterns on a substrate by deposition of 2,5-diiodothiophene followed by UV irradiation through a photomask. The structure of 2,5-diiodothiophene with the α- and β- position indication is also shown. 31

2.2 **(a)** XPS survey spectrum and high resolution spectra of **(b)** C1s, **(c)** S2p, and **(d)** $I3d_{5/2}$ regions of the polythiophene thin film photochemically synthesized on a glass substrate. 32

2.3 **(a)** Photoluminescence excitation and emission spectra of the photochemically synthesized polythiophene films on a glass substrate and **(b)** color photograph of the photoluminescence emission from the THF extract of the photochemically synthesized polymer films. (Excitation wavelength is 435nm). 34

2.4 S_L edge and C_K edge of grazing incidence NEXAFS spectra: **(a)** Photochemically synthesized polythiophene film, **(b)** Electrochemically deposited polythiophene film, **(c)** Electrochemically deposited poly-3,dodecyl-thiophene film. 35

2.5 IR spectra of **(a)** 2,5-diiodothiophene, **(b)** polythiophene thin film produced by 2 min UV irradiation, **(c)** polythiophene thin film produced by 5 min UV irradiation, and **(d)** chemically synthesized polythiophene (purchased from Aldrich). The polythiophene thin film shown in **(b)** and **(c)** are produced directly on gold substrates by the photochemical method described in the text. The thin film spectra shown in **(b)** and **(c)** are 36

obtained by the reflection-absorption technique and the powder spectrum shown in **(d)** is obtained by the diffuse-reflection technique. The monomer spectrum shown in **(b)** is from the Aldrich reference library.

2.6 **(a)** Fluorescence microscope and **(b)** tapping-mode AFM images of polythiophene patterns generated on a thiophene thiol terminated gold substrate. **(c)** Fluorescence microscope image of polythiophene patterns on a melt-cast polyethylene film. A 600-mesh TEM grid is used as a photo-mask for making patterns. 38

3.1 An example of traditional thermally activated Ullmann coupling. 49

3.2 Photoluminescence emission of the polymer film synthesized on copper is compared to that synthesized on other substrates such gold, palladium, and silicon with native oxide. 50

3.3 Raman spectrum of chemically synthesized polythiophene powder, surface-enhanced Raman spectrum (SERS) of photochemically synthesized polythiophene film on copper and on gold are compared. 51

3.4 Mechanism of photo-activated Ullmann coupling on a copper substrate. 52

3.5 **(a)** I $3d_{5/2}$ region of the polymer film synthesized on copper is compared to that synthesized on other substrates such gold, palladium, platinum, silicon with native oxide. **(b)** Cu 2p3/2 region of the polymer film synthesized on copper. **(c)** Cu $L_3M_{4,5}M_{4,5}$ region of the polymer film synthesized on copper is compared with the standard CuI and Cu metal spectrum. 53

3.6 **(a)** S 2p region **(b)** C 1s region **(c)** Survey spectrum of the polymer film synthesized on copper. 55

3.7 Snapshots of 200x optical microscope video showing liquid formation during irradiation of solid 2,5-diiodothiophene film. 56

3.8 Pseudo colored fluorescence microscope image of photo-patterned polythiophene on a copper substrate. 57

4.1 MALDI-MS of photochemically synthesized polythiophene film. 75

4.2 Spreadsheet to calculate the molecular mass of the oligothiophenes with varying number of iodine substitutions. Highlighted molecular masses represent the locations of the prominent peaks in the experimental result shown in Fig. 4.1. 77

4.3 Reactions of photo-generated thienyl radical. 78

4.4 Reactions of photo-generated iodine radical. 79

4.5 Flory's derivation for number average distribution in a linear condensation (or step) polymer. 80

4.6 Plot showing the experimental mass spectrum of the polythiophene sample and the prediction based on equation 4.4. Extent of reaction is 0.665 and the probability of finding a Th and ThI are 0.63 and 0.37 respectively. 81

4.7 Photoluminescence (PL) emission redshifts with the decrease in the thickness of the polythiophene film synthesized on copper. Top – Pseudo colored PL image showing the redshift. Bottom – Spectroscopic data confirming the redshift. 82

4.8 High resolution XPS of I $3d_{5/2}$ region showing the increase in the iodide content with the decrease in the polythiophene film thickness. Iodide content is a representative of the extent of mediation of Ullmann coupling reaction. 83

4.9 Schematics of the photo-activated Ullmann coupling. Concentration of organo-copper intermediates depends on the intensity of photons reaching the surface of copper. 84

4.10 Dimensionless average diffusion constant (D_{avg}/D_o) and concentration of organo-copper intermediates at the surface of copper (C*) versus monomer film thickness (L). 84

4.11 Results of numerical solution of diffusion-reaction model capturing the effect of thickness on the extent of mediation of Ullmann coupling reaction. As the thickness decreases, the concentration of reacted organo-copper intermediates or the extent of mediation of Ullmann coupling increases. 85

5.1 Schematics of wettability patterning of the substrate, regio-selective deposition of 2,5-diiodothiophene, and photochemical conversion of the adsorbed monomer patterns to polythiophene patterns **(a)** PDMS stamping approach is used to generate wettability contrast patterns on gold substrates. **(b)** On Au/SiO_2 substrates, selective formation of thiol SAM on gold followed by hexamethyldisilazane treatment of SiO_2 surface is used. 97

5.2 Fluorescence microscope images of the polymer patterns produced on the gold substrates periodically patterned with the thiophene-terminated SAM square regions surrounded by **(a)** OH-terminated and **(b)** CH_3-terminated SAM lines. Image (b) is pseudo colored to show the readers an idea of photoluminescence emission. **(c)** Schematics to show the maximum amount of monomer that can be pinned inside the more wettable region. Insets in (a) and (b) are digitally magnified by ×4 to show individual patterns. 98

5.3 Bridging defect often formed in thiophene/OH combination due to poor wettability contrast. 99

5.4 Fluorescence microscope image of the polymer patterns produced on the thiophene-terminated SAM covered Au square patches surrounded by HMDS-treated SiO_2 regions. 99

Acknowledgements

First and foremost, I thank Prof. Janna Maranas and Prof. Larry Duda for giving me a recommendation letter that allowed me to continue my Ph.D. at Penn State. I thank Prof. Hank Foley for patiently mediating the process of my transfer to Prof. Seong Kim's group. I am greatly indebted to Prof. Kim for accommodating me in his group. I really appreciate the motivation and encouragement he gave me for new research ideas. I learned a great deal about the critical analysis of data and presentation skills from him. I really enjoyed his way of teaching and advising me by constantly challenging my analysis and interpretation. I thank Prof. Foley, Prof. Themis Matsoukas and Prof. Ayusman Sen for serving in my committee and challenging me during exams to help me make a better scientist out of myself. I thank the National Science Foundation for funding my project through various grants.

Many people have been supportive for the completion of my project and this thesis would be incomplete without thanking them. I thank Mr. Bob Hengstebeck of Material Research Institute for helping me with XPS data collection and analysis. I thank Mr. Tom Larrabee of Prof. Thomas Mallouk's group for AFM data collection & analysis and stamping experiments. I thank Prof. Michael Pishko and his graduate students for allowing me to use the photoluminescence spectroscopy. I thank Ms. Elaine Kunze and Ms. Susan Magargee of the Huck Institute of Life Sciences for helping me with fluorescence microscopy. I thank Ms. Jackie Bortiatynski of Department of Chemistry for allowing me to use the UV-Vis, DRIFTS and GC-MS of the Organic Chemistry lab. I thank Dr. Dan Jones and Dr. Lian-Chao Li for helping me with MALDI data collection. I

thank Dr. Ram Rajagopalan of Prof. Foley's group and Dr. Keith Rider of Longwood University, for explaining me some of the concepts in polymer science and physical chemistry respectively. I thank Mr. Matt Dixon and Ms. Christine McGuiness of Prof. David Allara's group for helping me with Raman and Contact angle experiments respectively. I thank Ms. Susan Fullerton of Prof. Kim's group for helping me with the photolithography process. I thank Prof. Duda again for helping me with diffusion-reaction modeling. A special thanks to Mr. Sujith Nair and Mr. Krishna Dronavajjala of Chemical Engineering for helping me in numerous ways to complete my research. I thank Prof. Chris Keating's group and Mr. Nitesh Kumar of physics department for helping me with thermal evaporation of metals. I thank all my previous and current group members for their suggestions on my research, comments on my presentations and assistance with my experiments. I thank all my previous and current roommates for providing me with good Indian food. Last but not least, I thank this great country for providing me with the opportunity for an enriching experience.

Chapter 1

Introduction

1.1 Background

Conjugated polymers are polymeric molecules with alternating single and double bonds, as shown in the example of polyacetylene and polythiophene in Fig. 1.1. After the discovery of metal-like conductivity in polyacetylene on doping with iodine in 1977, both fundamental and applied research on these conjugated polymers gained a huge momentum. Discovery of electroluminescence in the early 90's further fuelled the research interests as it opened the possibility of flexible displays and solar cells. In addition to these well known applications, conjugated polymers have potential in many other applications such as optical modulators and switches, sensors, corrosion prevention and antistatic coating owing to their electronic and optical properties. Apart from the practical applications, these materials are instrumental in furthering our knowledge on chemical structure-property relationships. Prof. Alan Heeger, Prof. Alan MacDiarmid, and Prof. Hideki Shirakawa are the researchers who discovered and pioneered the development of conjugated polymer and their contributions have been honored with the Nobel Prize in Chemistry for the year 2000 [1].

1.2 Factors affecting the material properties

Conjugated polymers are considered as one-dimensional form of carbon materials as graphite and diamond being considered as 2d and 3d form of carbon respectively. Electronic and optical properties in conjugated polymers arise due to the

delocalization of π bond electrons along the backbone polymer molecule [2,3]. One dimensional nature of these polymers leads to anisotropy in the physical properties such as conductivity, optical absorption so on. Delocalization of π bond electrons gives rise to low band gaps in these polymers. Degree of conjugation is the measure of average number of monomer units over which electrons are delocalized. The band gap decreases as the degree of conjugation increases. The band gap typically ranges from 3 – 2 eV and this value corresponds to the energy of the photons in the visible region. Hence conjugated polymers strongly absorb the portions of visible light and are intensely colored. For the same reasons, conjugated polymers find applications in photovoltaics and displays.

Delocalization of π bond electrons also leads to the possibility of doping the polymer through charge transfer from electron donor or acceptor species. The terminology "doping" is borrowed from the inorganic semiconductor science, and it actually means oxidation (removal of electron/injection of hole) or reduction (injection of electron) of molecules in the context of conjugated polymer materials. Doping of the conjugated polymer leads to increase in the conductivity of the material. For example, addition of iodine to polythiophene leads to formation of holes in the polythiophene and the conductivity of the polymer increases nearly seven or eight folds (from 10^{-10} S/cm to ~ 10^{-3} S/cm). Doping of conjugated polymers such as polythiophene, polypyrrole or polypheneylene leads to formation of polarons. Polarons are the deformation in the geometric structure of the polymer due to presence of the charge. As shown in Fig. 1.2, polarons are also visualized as localized states in the forbidden gap (i.e. the gap between the conduction and valence band) and the presence of polarons results in a change of the

optical absorption. Hence the doped polymer has a different color then the original polymer. Application of voltage across the doped polymer leads to transport of these charge carriers or the polarons. Mobility of the polarons in conjugated polymer materials is typically explained by the hopping transport model as schematically shown in Fig. 1.3. In this model, the polaron is assumed to tunnel from one localized energy state to another site. Typically, highest possible mobility values (> 0.1 $cm^2V^{-1}s^{-1}$) are desired for many of the applications of conjugated polymers. Hence, research efforts have been focused on understanding the factors affecting the mobility and developing process strategies to improve it. In general, mobility values have been found to deteriorate with several factors, some of them being defects in the chain architecture, non-conjugated defects, lack of molecular level packing and morphological defects.

Fig. 1.4 illustrates the defects in chain architecture such as mislinking, crosslinking and non-conjugated defects. These defects deteriorate the mobility for two reasons. Firstly, these defects prevent the delocalization of electrons (or decreases degree of conjugation) creating deep localized energy states. These deeply localized states entrap the polarons and prevent their mobility. Secondly, presence of these defects leads to poor packing of chains and thereby reducing inter-chain transport of polarons. Linear chains with α–α' linking not only maximizes the π electron cloud delocalization, but also allows better molecular packing by Van der Waal's interaction. As shown in Fig. 1.5, the overall mobility not just depends on the molecular level morphology but also depends on inter & intra fiber charge transport. So, it is highly desirable to have densely packed morphology without any discontinuities.

1.3 Current methods of processing

Among all conjugated polymers, polythiophenes are the most extensively studied because of their superior thermal and environmental stability [4]. Extensive studies for the past two decades have led to the development of many synthesis and processing techniques for fabrication of thin films and patterns of polythiophene. Current processing techniques can be divided in two categories − post-synthesis fabrication and *in-situ* polymerization. In the post-synthesis fabrication method, oligomers and substituted polythiophenes are synthesized chemically and fabricated into thin films using conventional processes such as physical vapor deposition or spin-casting. In the *in-situ* polymerization process, polythiophene thin films are directly synthesized on target substrate. That is, synthesis and fabrication are combined into one step. Popular examples of *in-situ* polymerization process are electrochemical and plasma polymerization technique [5-8]. Advantages and disadvantages of various methods are summarized in the followings sections.

Post-synthesis fabrication: As shown in Fig. 1.6, α–α' coupled linear unsubstituted polythiophene can be synthesized by well defined coupling of Grignard reagent using di-halo monomer or oxidative coupling of unsubstituted monomers. Chemical synthesis procedure in general can produce polymers without structural defects, but in certain cases catalyst or salt residues are present in the polymer. Although unsubstituted polythiophene can be synthesized easily, they suffer from serious processing hurdles. Unsubstituted polythiophene is insoluble and infusible. Even oligomers longer than hexamer are completely insoluble in almost all common organic solvent. Usually above-mentioned

chemical methods are used for synthesis of well defined oligomers and the purified oligomers are fabricated into single crystals or thin films [9]. Single crystals of soluble oligomers such as tetramer can be made using solvent recrystallization technique. But, single crystals of longer oligomers like octamer can be made only by extremely slow (~ 1 day) process of vacuum sublimation. Also, single crystals of oligomers are extremely fragile and cannot be cut or polished. Thin films of oligomers are usually made by physical vapor deposition (PVD) process. In the PVD technique the oligomers are filled into Knudsen or Langmuir type evaporation cell and heated up to their sublimation temperature. Sublimation temperature of pentamer is around room temperature and that of hexamer is 373K. PVD can also be used for polythiophene with a polymerization degree of 20-25 monomeric units. One of the disadvantages of PVD is that it is a slow process and typical rates of deposition are 0.1 nm/s or lesser. A higher rate typically leads to poor morphology and random orientation of oligomer resulting in poor mobility.

Researchers have resolved the issue of insolubility of unsubstituted polythiophene by synthesizing polymer with side groups that aid solubility. But, they have found that the presence of irregular side groups will sterically twist the thiophene rings resulting in loss of conjugation. A breakthrough in the field came about, when McCullough et al first synthesized regioregular poly (3-alkylthiophenes) (PATs) with almost 100% HT-HT coupling [4]. These polymers are not only soluble in common solvents like chloroform, they also self-assemble in solid state as shown in Fig.1.7. Self-assembled structure leads to a large increase in conductivity (or mobility) and average conductivities reported are as high as 1000 S/cm^{-1}. Spin coating is the most common technique used to fabricate thin films of PATs [9,10,11].

Spin coating is a simple and economical process, but the morphology of the final polymer films is difficult to control. Morphological defects such as pin holes and disorder in self-assembly are often observed and these defects affect the device performance and reproducibility [10,11]. Even if thin films of soluble polythiophenes can be easily prepared on desired substrates, patterning of these thin films into desired device structures has remained as a challenging task. Laser direct-write lithography or conventional lithography require high intensity laser beams or presence of photo-sensitive side groups, which results in photo-oxidation, deterioration of material properties and/or reduced environmental stability [12]. Inexpensive printing techniques such as screen printing [13,14] inkjet printing [15,16] has not been able to achieve truly micron scale features. High resolution approaches reported in the literature including e-beam lithography [17], scanning electrochemical microscopic lithography [18,19], and dip-pen lithography [20] suffer from low throughput. Microcontact printing can be used for patterning single molecular layer of polymer, but the reliability is poor because of the deformation of the elastomeric stamp [21, 22]. Recently attempts are made to combine the printing techniques with regio-selective wetting approach to generate features much smaller than that accessible by just printing alone [23, 24].

Electrochemical Methods: This *in-situ* polymerization technique is one of the generic methods for quick synthesis of various conjugated polymers [5]. In this method, the monomer molecules undergo oxidative coupling at the anode as shown in Fig. 1.8 and gets deposited on the anode. Reductive coupling can also be employed for polymerization and this method produces neutral insulating polymer which leads to rapid passivation of

electrode. Passivation of electrode limits the attainable film thickness to around 100nm. Electrochemical methods can be employed only with a solvent and substrate that have higher oxidation potential than thiophene. Presence of easily oxidizable impurities such as water in the system leads to formation of non-conjugated defects. Grade of the polymers is often affected by over oxidation of oligomers and mislinking defects. Mislinking defects become prevalent once oligomers are formed because of the increase in the concentration of C_β-H relative to C_α-H. Electrochemical methods are routinely employed for applications such as corrosion prevention where the target substrate is conductive and the grade of the polymer synthesized is not very critical.

Plasma Polymerization: This process is not well defined on the issues relating to initiation and propagation mechanism and the presence of high energy species leads to fragmentation of monomer [6,7,8]. Random coupling of monomer and monomer fragments usually produces highly cross-linked polymer with lots of structural defects. Plasma processes are suitable for applications such as antistatic coatings where the substrate is non-conductive and the grade of the polymer can be compromised. Processes such as laser induced chemical vapor deposition [25,26,27], x-ray [28,29], ion [30] and electron induced polymerization [31-35] usually involve high energy species and suffer from the same disadvantages as plasma polymerization.

1.4 Organization of the thesis

An *in-situ* photochemical polymerization process is developed and detailed in this thesis. In contrast to the popular *in-situ* electrochemical polymerization approach, the photochemical method described here doesn't require a conducting substrate. Also this photochemical process can be easily integrated with the traditional photolithography for large scale fabrication of micro-patterns of polythiophene. The process involves vapor deposition of monomer 2,5-diiodothiophene on a substrate in ambient condition, followed by UV irradiation of the deposited film in an argon environment. In chapter 2, experimental details and the characterization of material and structural properties of photochemically polymerized polythiophene are presented. Proof of concept for photolithographic patterning of polythiophene is also presented. One of the interesting discoveries during the course of this research is the the effect of copper on the photochemical reaction. Photo-activation of a thin film of 2,5-diiodothiophene on a copper substrate produces unsubstituted polythiophene with an average conjugation length of 6 ~ 7, while the same process on Au, Pt, Pd, and SiO_2 produces polymer of conjugation length 4 ~ 5. This enhanced conjugation length on copper is explained by the involvement of Ullmann coupling pathway in the photochemical reaction. This photoactivated Ullmann coupling is detailed in chapter 3. In chapter 4, models are developed to explain the mass spectrum of the photochemically synthesized polymer and to explain the effect of monomer thickness on the extent of mediation of Ullmann coupling in the photochemical reaction. In chapter 5, a mask-less technique to fabricate periodic patterns of a polythiophene is detailed. In this technique, monomer patterns are

generated by regio-selective condensation of 2,5-diiodothiophene and these monomer patterned are converted to polymer patterns by blanket UV irradiation without a mask.

1.5 References

[1] *Advanced Information* – The Nobel Prize in Chemistry 2000, Nobel e-Museum.

[2] Chandrasekhar, P. *Conducting Polymers Fundamentals and Applications;* Kluwer Academic Publishers, USA **1999**.

[3] Horowitz, G; Delannoy, P In *Handbook of Oligothiophenes and Polythiophenes*; Fichou, D., Ed.; Wiley-VCH: Weinheim, **1999**

[4] McCullough, R. D. In *Handbook of Oligothiophenes and Polythiophenes*; Fichou, D., Ed.; Wiley-VCH: Weinheim, **1999**

[5] Roncali, J. *Chem. Rev.* **1992**, *92*, 711.

[6] Tanaka, K.; Yoshizawa, K.; Takeuchi, T.; Yamabe, T.; Yamauchi, J. *Synthetic Metals* **1990**, *38*, 107.

[7] Ryan, M.E.; Hynes, A.M.; Wheale, S.H.; Badyal, J.P.S.; Hardacre, C.; Ormerod, R.M. *Chem. Mater*. **1996**, *8*, 916.

[8] Groenewoud, L.M.H.; Engbers, G.H.M.; Terlingen, J.G.A.; Wormeester, H.; Feijen, J. *Langmuir* **2000**, *16*, 6278.

[9] Fichou, D.; Ziegler, C. In *Handbook of Oligothiophenes and Polythiophenes*; Fichou, D., Ed.; Wiley-VCH: Weinheim, **1999**

[10] Relini, A.; Bolognesi, A.; Botta, C.; Marinelli, M.; Mendichi, R.; Schieroni, A.G.; Rolandi, R. *Materials science & engineering C-Biomimetic and Supramolecular systems* **2002,** *22*, 313.

[11] Kwong, C.Y.; Djurisic, A.B.; Chui, P.C.; Cheng, K.W.; Chan, W.K. *Chem. Phys. Lett.* **2004,** *384*, 372.

[12] Holdcroft, S. *Adv. Materials* **2001**, *13*, 1753.

[13] Garnier, F.; Hajlaoui, R.; Yassar, A.; Srivastava, P. *Science* **1994**, *265*, 1684.

[14] Bao, Z.; Feng, Y.; Dodabalapur, A.; Raju, V.R.; Lovinger, A. *Chem. Mater*. **1997**, *9*, 1299.

[15] Paul,K.E.; Wong, W.S.; Ready, S.E.; Street, R.A. *Appl. Phys. Lett.* **2003**, *83*, 2070.

[16] Sirringhaus, H.; Kawase, T.; Friend, R.H.; Shimode, T.; Inbasekaran, M.; Wu, W.; Woo, E.P. *Science* **2000**, *290*, 2123.

[17] Persson, S.H.M.; Dyreklev, P.; Inganäs, O. *Adv. Mater.* **1996,** *8*, 405.

[18] Borgwarth, K.; Rohde, N.; Ricken, C.; Hallensleben, M.L.; Mandler, D.; Heinze, J. *Adv. Mater.* **1999,** *11*, 1221.

[19] Maynor, B.W.; Filocamo, S.F.; Grinstaff, M.W.; Liu, J. *J. Amer. Chem. Soc.* **2002,** 124, 522.

[20] Lim, J.H.; Mirkin, C.A. *Adv. Mater.* **2002,** 14, 1474.

[21] Granlund, T.; Nyberg, T.; Roman,L.S.; Svensson, M.; Inganäs, O. *Adv. Mater.* **2000,** *12*, 269.

[22] Schmid, H.; Michel, B. *Macromolecules* 2000, *33*, 3042.

[23] Chabinyc, M.L.; Wong, W.S.; Salleo, A; Paul, K.E.; Street, R.A. *Appl. Phys. Lett* **2002**, *81*, 4260.

[24] Wang, J.Z.; Zheng, Z.H.; Li, H.W.; Huck, W.T.S, Sirringhaus, H. *Nature Materials* **2004**, *3*, 171.

[25] Nishio, S.; Okumura, M.; Okada, S.; Minamimoto, Y.; Taketani, Y.; Matsuzaki, A.; Sato, H. *J. Photopolymer Sci. Tech.* **1998,** *2,* 347.

[26] Nishio, S.; Okada, S.; Minamimoto, Y.; Okumura, M.; Matsuzaki, A.; Sato, H. *J. of Photochemistry and Photobiology A: Chemistry* **1998**, *116*, 245.

[27] Wochnowski, C.; Metev, S. *Appl. Surf. Sci.* **2002**, *186*, 34.

[28] Salaneck, W.R.; Wu, C.R.; Nilsson, J.O.; Bredas, J.L. *Synthetic Metals* **1987**, *21*, 57.

[29] Land, T.A.; Hemminger, J.C. *Surface Science* **1992**, *268*, 179.

[30] Tepavcevic, S.; Choi, Y.; Hanley, L. *J. Amer. Chem. Soc.* **2003,** *125*, 2396.

[31] Baumgärtner, K.M.; Volmer-Uebing, M.; Taborski, J.; Bäuerle, P.; Umbach, E. *Ber. Bunsenges. Phys. Chem.* **1991**, *95*, 1488.

[32] Raza, H.; Wincott, P.L.; Thornton, G.; Casanova, R.; Rodriguez, A. *Surf. Sci.* **1997**, *390*, 256.

[33] Nambu, A.; Kondoh, H.; Nakai, I.; Amemiya, K.; Ohta, T. *Surf. Sci*. **2003**, *530*, 101.

[34] Hernandez, J.E.; Ahn, H.; Whitten, J.E. *J. Phys. Chem. B* **2001**, *105*, 8339.

[35] Ahn, H.; Whitten, J.E. *J. Macromolecular Sci. – Pure and Applied Chem.* **2004**, *A40*, 1357.

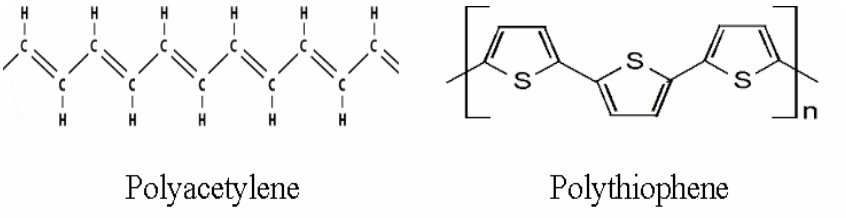

Fig. 1.1 Examples of conjugated polymers.

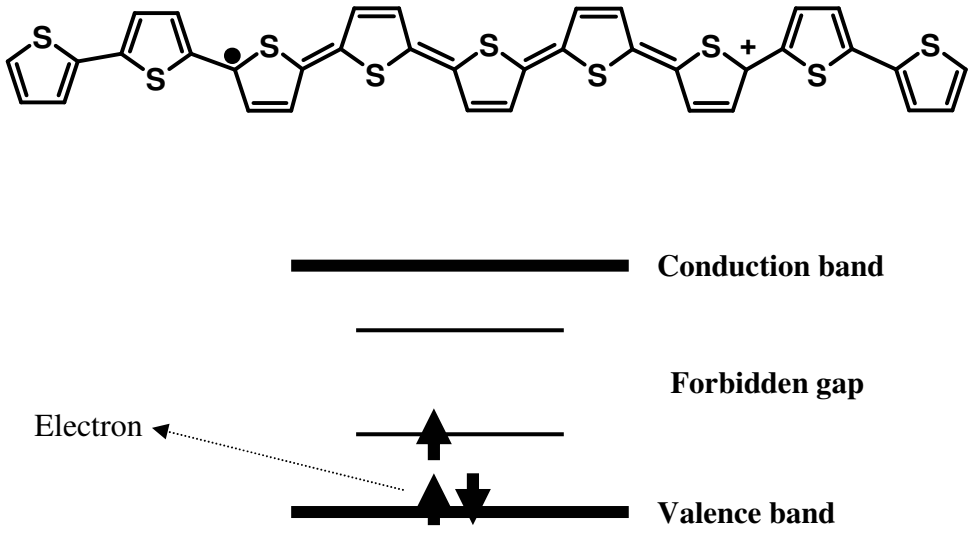

Fig 1.2 Polaron in a polythiophene chain Top: Geometrical change in the molecular structure Bottom: Localized levels in the forbidden gap [3].

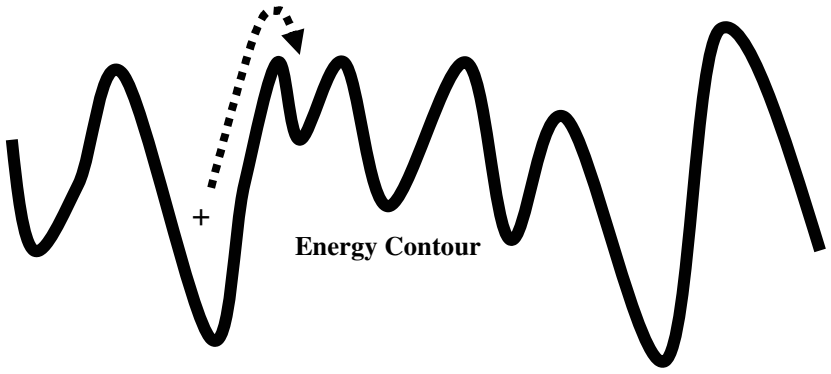

Fig 1.3 Charge transport in the localized state material is by tunneling of charge from one site to the next [3].

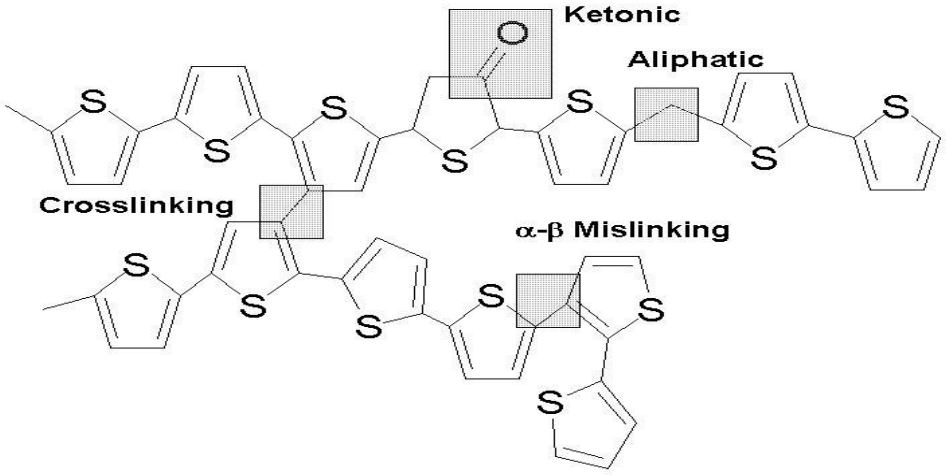

Fig 1.4 Conjugated polymer with defects in structure and architecture.

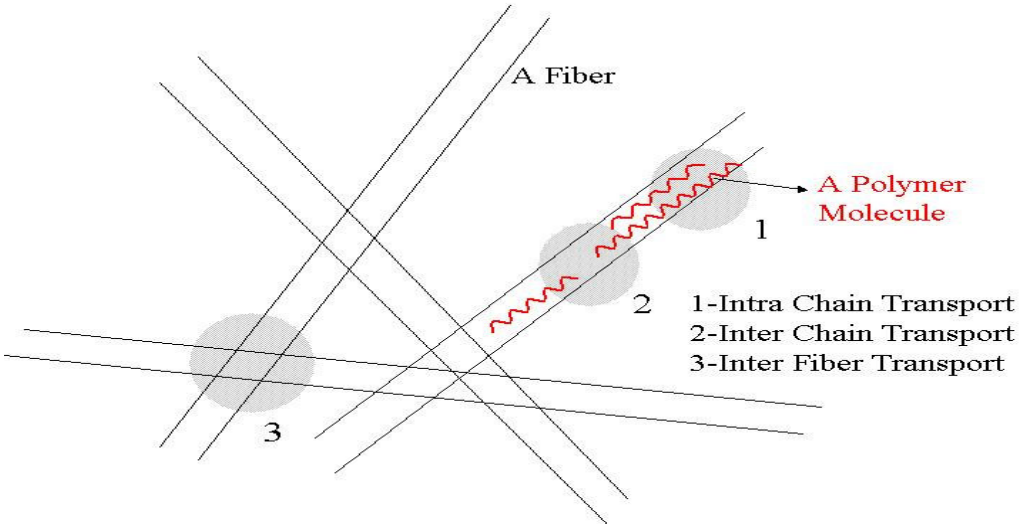

Fig 1.5 Dependence of mobility on the morphology [2].

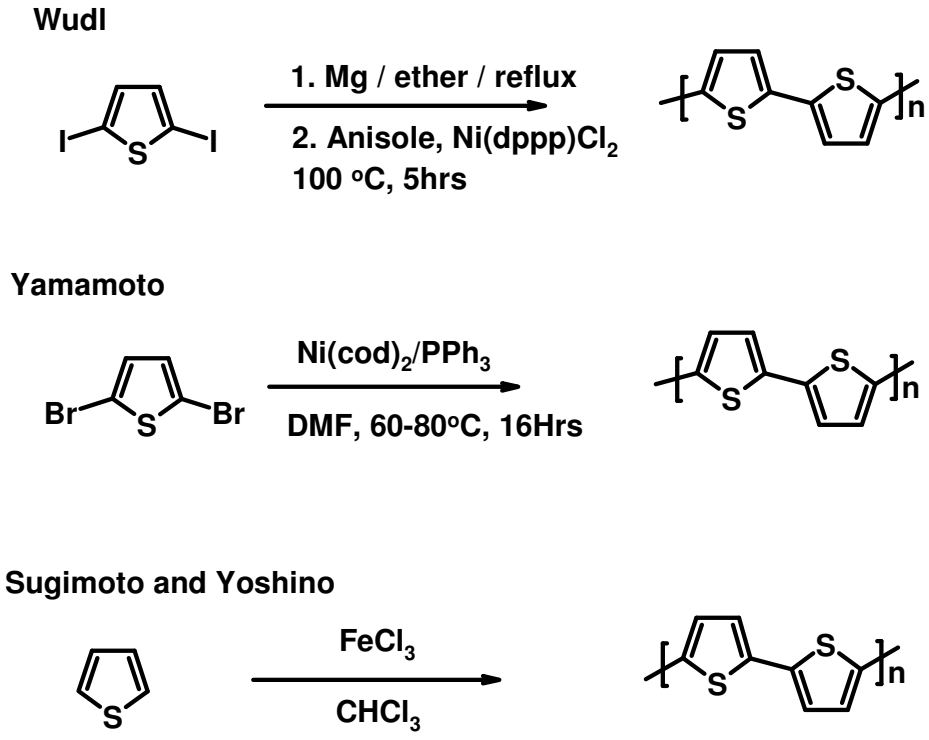

Fig. 1.6 Chemical synthesis procedures of unsubstituted polythiophene [4].

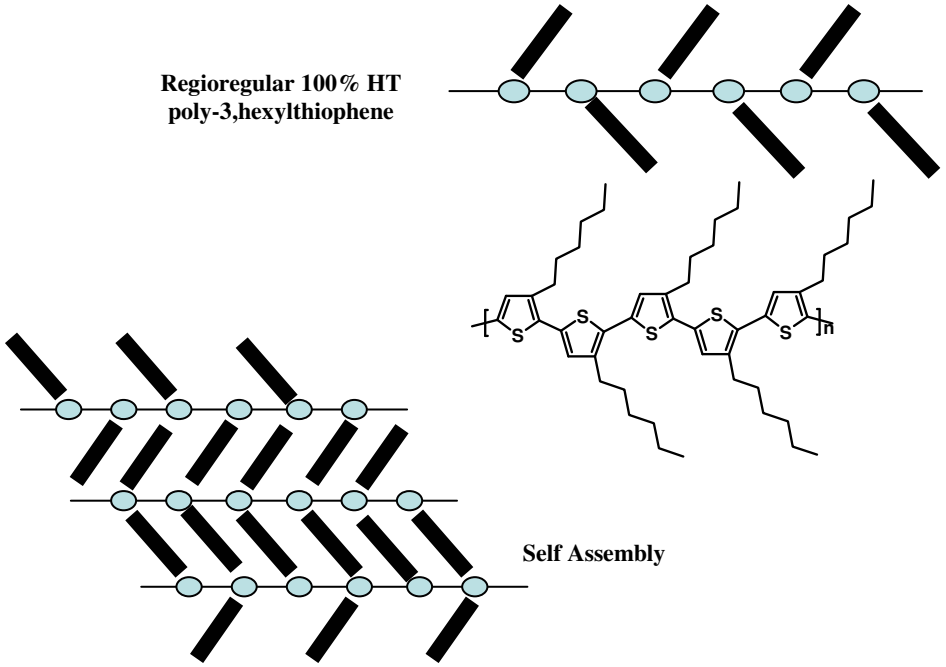

Fig 1.7 Self-assembled structures formed in regioregular polythiophenes [4].

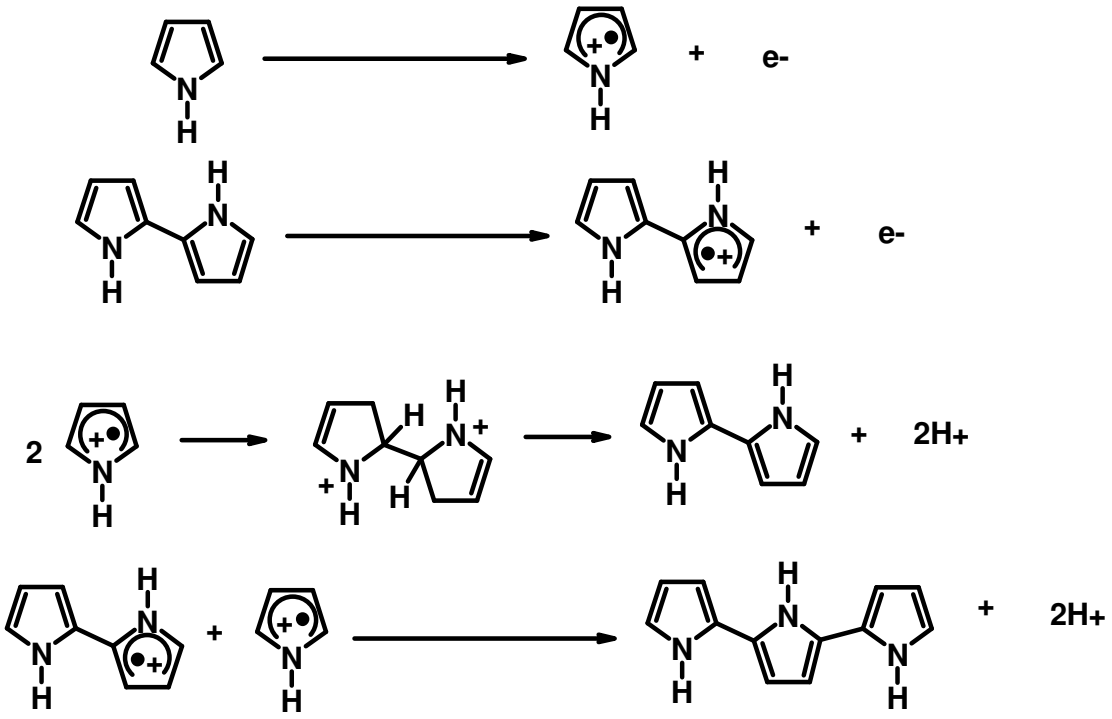

Fig 1.8 Mechanism of electrochemical polymerization [5].

Chapter 2

Photochemical conversion of 2,5-diiodothiophene condensed on a substrate to polythiophene thin films and micro-patterns

2.1 Introduction

In this chapter, a simple photochemical process for the in-situ fabrication of unsubstituted polythiophene thin films and patterns is described. The schematic of the entire process is shown in Fig. 2.1. The process involves vapor deposition of monomer (2,5-diiodothiophene) on a substrate in ambient condition, followed by UV irradiation in argon environment. The selective photodissociation of the C-I bond in the monomer molecule produces monomer radicals with intact π-ring structure, which can be polymerized in the condensed film. Since the photochemical process synthesizes polythiophene directly from the monomer adsorbed on a substrate, the intractability issues of unsubstituted polythiophene in the fabrication of thin films and micro-patterns are bypassed. Micron scale patterns of polythiophene can be made easily by regio-selective irradiation of the monomer film through a photomask.

2.2 Experimental

2,5-diiodothiophene (Aldrich, 98%) monomer was deposited on a substrate by physical vapor deposition from a heated evaporation source in ambient conditions. Glass, silicon wafer, gold film, and polyethylene were used as substrates in this study. Glass,

silicon wafer and gold substrates were cleaned with 5:1:1 mixture of H_2O:NH_4OH:H_2O_2 at 70 °C for 10 minutes prior to use. Polyethylene substrates were prepared by melt casting just prior to use. The substrate was directly placed on the evaporation source and the monomer film thickness was controlled by varying deposition time. Typical monomer thickness was 200-500nm. The deposited monomer film was subsequently irradiated for 120 ~ 600 s with a collimated UV beam from a 200 W Hg lamp (Oriel 6283) in argon environment. In order to prevent substrate heating during UV irradiation, the infrared radiation emitted from the lamp was removed with a water filter.

The chemical structure of the synthesized polymer films were characterized with photoluminescence spectroscopy (PL), near-edge X-ray absorption fine structure (NEXAFS), reflection-absorption infrared spectroscopy (RAIRS) and x-ray photoelectron spectroscopy (XPS). PL emission and excitation spectra were acquired using a Photon Technologies International QM-4-2000-SE instrument. Reflection absorption inferred spectra were obtained using a Thermo Nicolet Nexus 670 system with a mercury cadmium telluride detector. X-ray photoelectron spectra were obtained using a Kratos Axis Ultra instrument equipped with a monochromatic Al Kα source. Charging during data collection was compensated with a charge neutralizer. The reported binding energies are referenced to carbon 1s at 285eV. The XPS spectra of 2,5-diiodothiophene could not be obtained due to evaporation of the sample in vacuum. Tetrahydrofuran (THF) extracts of the polymer films were prepared by sonicating the films synthesized on glass substrates in THF for 300 s. The color photograph of the extract was obtained using a digital camera with a suitable filter to remove the scattered excitation light. The direct current conductivity was measured by the four probe technique using HP 3468A

multimeter. Samples for the four probe conductivity measurements were prepared by contacting a thin film of the doped polymer sample with four parallel lines of gold electrodes, prepatterned on a glass slide. The thickness of the electrodes was 100nm. The thin film doping was carried out by exposing the sample to iodine vapors.

A commercially available transmission electron microscope (TEM) grid was used as a model photomask for photolithographic patterning. The irradiated film was then washed with hexane to remove unreacted monomers from the substrate. Atomic force microscopy (AFM; Digital Instruments Multimode Nanoscope IIIa) measurements revealed that the film thickness can be controlled in the range of 100 ~ 500 nm. An Olympus BX60 Fluorescence microscope with appropriate cube (excitation 415 - 485 nm; emission 510 - 800 nm) and tapping mode AFM were used to analyze the produced patterns.

2.3 Results and discussion

Electronic properties in conducting polymers are determined by the degree of conjugation of π electrons along the polymer backbone. The critical requirement for attaining "high-quality" conjugated polymers is to avoid defects such as monomer fragmentation, mislinking of monomer units (α-β and β-β coupling) and cross-linking of polymer chains. Material property and chemical structural analyses of the polythiophene produced by the photochemical reaction of the condensed monomer film indicate that the fragmentation and crosslinking defects are negligible. These results are described below

in detail and compared with other direct deposition process like plasma polymerization, laser-induced CVD, electron-induced polymerization so on.

XPS spectra of the photochemically synthesized polythiophene film on a glass substrate are shown in Fig. 2.2 The XPS spectra of the film synthesized on other substrates – silicon wafer and gold surfaces, are essentially the same as this one. The survey spectrum shown in Fig. 2.2a clearly indicates the absence of covalently bonded oxygen defects. The fact that there are no substrate peaks in the survey spectrum indicates the macroscopic homogeneity of the films synthesized. The C region shown in Fig. 2.2b displays two components - the C1s peak at 285 eV (FWHM = 1.25 eV) and the broad shakeup extending from 287.5 to 292.5 eV (Fig. 2.2b) [1].The binding energy difference of the α and β carbons in thiophene is only 0.34eV [1], which is smaller than the resolution of our XPS instrument (0.6eV). Absence of other carbonaceous species suggests the homogeneity of the carbon in the polymer. The shakeup peak originates from π-π^* transitions between HUMO and LUMO of the conjugated polymer backbone. Its intensity is about 50 times smaller than the C1s peak.

In the high-resolution S 2p XPS region, there is a well-resolved spin-orbit doublet peak at 164.1 and 165.3 eV with a FWHM of 0.97 eV, as shown in Fig. 2.2c. These peaks are attributed to $2p_{3/2}$ and $2p_{1/2}$. Their positions are consistent with the reported values for polythiophene indicating the intactness of the thiophene monomeric unit in the synthesized polymer film [1]. The ratio of the doublet peak areas is found to be 2:1, which is consistent with theoretical value. The average S/C atomic ratio is found to be around 0.24. This is in agreement with the theoretical value of 0.25 within experimental error ranges, indicating the absence of sulfur loss during UV irradiation. This result

clearly indicates that the C-S bond in the thienyl ring is preserved during the photochemical process.

The high-resolution I $3d_{5/2}$ is shown in Fig. 2.2d. There is only one dominating peak observed at 621 eV, which is attributed to the C-I bond remaining in the film. Although this is very close to the peak position of I_2, it is concluded that this peak is mainly due to the iodine covalently bonded to the carbon, because I_2 readily desorbs from the film in UHV. The average I/C ratio after 5min UV irradiation is found to be 0.13, which is 26% of the theoretical value for the 2,5-diiodothiophene monomer. For some samples, a very weak shoulder peak at 619.1eV can be found. This shoulder may be due to I_3^- doping of the polymers by iodine generated during photochemical reaction [2]. However, this peak is not observed always due to its low intensity. This indicates that the intrinsic iodine doping during the synthesis occurs only to a very small or negligible extent.

The efficacy of the described photochemical process is clearly revealed by the comparing the XPS spectra shown in Fig. 2.2 with those of plasma, X-ray, and electron beam polymerized samples reported in the literature. For the samples prepared by other in-situ deposition methods, multiple or unresolved sulfur 2p doublet peaks are often observed, indicating the presence of multiple sulfur species in the sample [3-5]. Dissociation of the C-S bond leads to extensive crosslinking and deterioration of conjugation. Studies on high-intensity UV laser induced CVD of polythiophene directly from the halogen-substituted thiophene by Sato et al. show that at least 30 % of the C-S bonds are broken and considerable carbonyl defects are formed [6,7]. Multiple photon absorption during high intensity laser irradiation may have resulted in the fragmentation

of the thienyl structure. Multiple photon absorption does not occur in our experimental conditions, where much lower photon flux from a mercury vapor lamp is used. Also, as their reaction is carried out at a low temperature (~220K) in a rough vacuum, the physisorbed water molecules on the substrate may have reacted with radicals generating oxygenated defects. In our experiments, the production of unwanted oxygenated defects due to the physisorbed water is negligible because the UV irradiation of the deposited monomer film is carried out at room temperature in argon environment.

Photoluminescence excitation and emission spectra of the polythiophene films synthesized on a glass substrate are shown in Fig. 2.3a. The presence of strong photoluminescence emission with the maximum at 545nm clearly indicates the presence of polymers with an average conjugation length (α-α' connection of thienyl monomer units) of 4-5 mer. The excitation maximum is observed at around 425nm, which is in good agreement with those of the chemically synthesized unsubstituted α-oligothiophenes [8]. Fig. 2.3b shows the color photograph of the photoluminescence emission from the THF extract of polymer films. The extracted polymer in THF emits a very intense green to greenish yellow light upon UV excitation, which is consistent with the observed photoluminescence spectra of the thin film. The fact that the photochemically synthesized polymer films are soluble in THF strongly supports the absence of polymer chain crosslinking. Ahn and Whitten reported the production of oligo-hexylthiophene by low energy (185eV) electron induced polymerization of hexylthiophene in UHV conditions [5]. They reported that the electron beam polymerized films are insoluble in organic solvents and attributed this to the cross-linking of oligomers.

Further evidence for intactness of ring structure and absence of fragmentation comes from the NEXAFS analyses of thin films of polythiophene synthesized by the same process in ultra-high vacuum (UHV) instead of argon environment. Experimental details of sample preparation and spectroscopic analyses are in reference 9. Essentially, thins films of polythiophene are produced by simultaneous dosing and UV irradiation of monomer in UHV. A thin film of gold evaporated onto silicon wafer is used as the substrate. Polythiophene thin films prepared in ultra-high vacuum have different morphology due to hindered mobility of radicals and monomers at a low temperature (~120K), but the polymerization chemistry producing thin films (~ 100nm) is expected to same as that of the process in argon environment, as the gold substrate is chemically inert. Even if the gold substrate takes part in the polymerization chemistry, the substrate effect will vanish once few monolayers (~ 5nm) of polythiophene are formed. Also, it is found that the photoluminescence emission maximum of the polythiophene film synthesized in UHV is also ~ 540nm supporting the assumption that the polymerization chemistry is same in both in UHV and argon environment. The NEXAFS spectra give the detailed electronic structure of the photochemically synthesized thin films. Fig. 2.4 compares grazing incidence NEXAFS spectra of the sulfur L=edge and carbon K-edge regions of the photochemically synthesized polymer film with reference spectra reported earlier [10]. The sulfur L-edge is not well resolved due to overlap of electronic transitions from two states S $2p_{1/2}$ and S $2p_{3/2}$. The first three at 163.3 eV, 164.7 eV and 166.5eV are ascribed to the $2p_{3/2}$ -> $2\pi^*$, the superimposition of $2p_{3/2}$ -> $2\sigma^*$ (C-S) and $2p_{1/2}$ -> $2\sigma^*$, and the $2p_{1/2}$ -> $2\sigma^*$ (C-S) transitions, respectively [10,11]. The shoulder peak at 170.7

eV corresponds to the σ* (C=C) resonance, the broad peak at 173.5eV is attributed to transitions to the S atomic 3d levels.

In the carbon K-edge region, there are two sharp transition peaks at 286.0 and 287.7 eV, one shoulder peak at 289.0 eV, and one broad transition at 295.0 eV. These peak positions are in good agreement wit the theoretical calculation [10]. Comparing with the NEXAFS spectra of polythiophene and poly-3-dodecyl-thiophene compounds [11,12], the peaks at 286.0 eV and 287.7 eV are ascribed to the C1s -> π^*_1 ($3b_1$) and C1s -> π^*_1 (C-S $5b_2$) transitions, respectively. The shoulder peak at 289.0 eV is attributed to C 1s -> π^*_2 transition. The broad feature appearing at 295.0 eV is associated to the C 1s -> σ* (C-C) thiophene ring resonance. The NEXAFS spectra of the ~ 200nm thick polythiophene film are found to be polarization independent.

It should be noted that there is no discernible peak around 292.5 eV in the carbon K-edge of the photochemically synthesized polymer film, which is associated with σ* (C-C) resonance of alkyl chain [11,12]. Moreover, if there is alkyl chain, the 289.0 eV peak would be much stronger due to the σ* (C-H) resonance of alkyl chain overlapping with C 1s -> π^*_2 ($2a_2$) transition at this position (C in Fig. 2.4). These results support that the photochemically synthesized polymer has intact ring structure and decomposition or fragmentation defects are negligible.

The detailed molecular structure of the photochemically synthesized polythiophene can be obtained from IR spectra of the synthesized film and comparison of the same with those of the chemically synthesized polythiophene (purchased from Aldrich) and the 2,5-diiodothiophene monomer. The length of π conjugation and the

absence of monomer fragmentation and crosslinking defects in the photochemically synthesized films are inferred from the IR spectra shown in Fig. 2.5. 2,5-diiodothiophene shows two peaks at 1388 cm^{-1} and 1497 cm^{-1} corresponding to the C=C symmetric and anti-symmetric stretching vibration of the thienyl ring, respectively [13]. The chemically synthesized α-α' coupled polymer shows the C=C symmetric and anti-symmetric stretching vibrations at 1440 and 1490 cm^{-1}, respectively [14,15]. The change of these IR peaks upon conversion from monomer to polymer is well studied in the literature [14,15]. There are three discernable changes. First, as the polymerization progresses the C=C antisymmetric peak intensity increases and become comparable the symmetric counterpart. Second, the C=C symmetric stretching shifts towards a higher wavenumber as the degree of π conjugation increases. This value reaches upto 1440cm^{-1} for chemically synthesized polymers. Third, the C=C antisymmetric stretching shifts slightly to a lower wavenumber. The photochemically synthesized polymer exhibits all the three characteristic changes: the significant growth of the C=C antisymmetric peak at 1492 cm^{-1} and gradual shift of the C=C symmetric peak to higher wavenumbers as well as a peak growth at 1430cm^{-1}. The photochemically synthesized polythiophene has a distribution of conjugation length, but based on the prominent C=C antisymmetric stretching peak at 1492 cm^{-1} and symmetric stretching peak at 1430cm^{-1}, the average conjugation length can be estimated to be ~ 4 mer, which is consistent with the photoluminescence results. The C-H in-plane and out-of-plane bending vibration peak are observed at 1080 cm^{-1} and 795 cm^{-1} respectively, which is consistent with the reported values for oligothiophenes Also we observe a C-I stretching vibration peak at 943 cm^{-1} in the polymer due to the presence of unreacted C-I bonds. The intensity of the C-I bond (relative to the intensity of C-H out-of-plane vibration) is significantly reduced in the polymer, as compared to the monomer.

The two peaks at 1345cm^{-1} and 1200cm^{-1} can be attributed to a trace amount of iodine molecules inside the film [16]. The photodissociation occurs inside the film as well as at the film-air interface. It is likely that the iodine molecules produced near the film/air interface escape into the atmosphere. Some of the iodine molecules produced inside the film will be trapped and dope the produced polymers; however, the amount of trapped iodine appears to be very small. The C=C stretching and C-H deformation peaks are still very intense in the IR spectra. It is known that even with a low level of doping, the dopant-induced peaks become dominant and the C=C stretching and C-H deformation peaks disappear. This is consistent with the XPS analysis, in which we find that the I_3^- dopant species are just barely detectable. There are no significant peaks detected in the 1675 ~ 1750 cm^{-1} region, reinforcing the XPS results indicating the absence of oxygenated species.

The intactness of the monomer structure is strongly supported from the C-H stretching vibration peak observed in the range 3060 ~ 3125 cm^{-1}, corresponding to the hydrogen at the β positions in the thienyl group. A very weak shoulder at 3020 cm^{-1} is somewhat close to the C-H stretching at the α position in the thienyl group that appears at 3050 cm^{-1} [14]. This might imply a trace of mislinking in the polymer. More important aspect of the IR spectra is that there are no aliphatic C-H stretch peaks (-CH_2- and CH_3) at around 2830-2970cm^{-1} and no ≡C-H stretch peak at around 3288cm^{-1} that are commonly observed in plasma polymerization due to fragmentations of the monomeric repeat unit [17,18].

The photochemically synthesized polythiophene film exhibits an electrical conductivity comparable to the chemically synthesized polythiophene. The thick

polythiophene films (500 ~ 600 nm thick) were prepared and doped with iodine vapor for 24 hours. The color of the thin film turns deep dark brown and the photoluminescence is completely quenched due to formation of polarons and bipolarons [19]. The DC conductivity of these doped samples, measured with a four probe method, ranges from 1 to 3 S/cm. These values are close to the conductivity values of doped chemically-synthesized unsubstituted polythiophene samples reported in the literature. [20,21].

The key for successful production of high-quality polythiophene in in-situ fabrication lies in the careful control of the intermediate species generation. The well-established photodissociation mechanism of iodo-organic compounds supports the selective dissociation of the C-I bond of the iodothiophene molecule upon absorption of UV photons (λ = 250 ~ 300 nm) generating a thienyl radical and an iodine atom [22,23]. The excess kinetic energy imparted to the photo-generated radicals will be rapidly quenched via collisions in the condensed phase [24]. During this collision process, photogenerated radicals may react with unreacted monomers or recombine with another radical, forming dimers. The dimers produced in these reactions contains two iodine atoms at both ends; so they can be further activated by photons and get involved in further reactions forming oligomers and polymers. Our photochemical process is apparently similar to the process recently reported by Wudl et al. [25] in solid state 2,5-dibromo-3,4-ethylenedioxythiophene. Their process is initiated by heat in solid state without any catalyst and is attributed to the oxidative property of the bromine by-product. In contrast, our process is driven completely by spatially controlled radical generation by photon induced dissociation of C-I bond. They demonstrated that the iodine molecule cannot induce the oxidative polymerization.

The direct photochemical synthesis can be easily incorporated into the conventional photolithography process to make integrated devices containing organic functional materials. In this work, the patterning capability is demonstrated with a 600-mesh TEM grid as a model photomask. This process does not require the use of sacrificial photoresist layers and generate the patterns by regio-selective direct conversion of the monomer molecules adsorbed on the substrate to the polymer. Fig. 2.6a and 2.6b show the fluorescence microscope and tapping-mode AFM images of square patterns of polythiophene directly synthesized on a gold substrate. The gold surface was pre-treated with a monolayer of 2-thiophenethiol to aide the formation of homogenous monomer film before the UV irradiation. The tapping mode AFM reveals that the surface of the polymer films are extremely smooth (RMS value = 2Å over 5μm×5μm area). The average height of the final polythiophene patterns is around 250nm for an initial monomer thickness of around 400nm. This decrease can be attributed to slow but continuous evaporation of unreacted monomers before and during UV irradiation as well as desorption of photo-generated radicals during UV irradiation. To further prove the versatility of the direct photochemical synthesis, polythiophene patterns are made on a clean polyethylene substrate (Fig. 2.6c). This approach can also be used for fabrication of polythiophene micro-patterns on other substrates such as glass and silicon wafer surfaces with high reproducibility. The photoluminescence of the polymer patterns stored in ambient conditions are found to be stable over six months (longest storage time tested in our lab). Successful demonstration of high-quality conducting polymer pattern production will open a new route to fabrication of organic devices with complete control of both material properties and morphology.

2.4 Conclusion

A photochemical process for making thin films and patterns of polythiophene on a wide range of substrates is developed. The photoluminescence spectra and reasonably high conductivity (1-3 S/cm) results confirm the successful synthesis of polythiophene with an average conjugation length of 4 ~ 5 monomer units. XPS and IR analyses reveal that the ring structure of the monomer unit is intact and the polymer chains are not cross-linked. Fabrication of polythiophene micro-patterns is demonstrated by regio-selective conversion of the monomer film by UV irradiation through a photomask.

2.5 References

[1] Tourillon, G.; Jugnet, Y. *J.Chem. Phys.* **1988**,*89*,1905.

[2] Salaneck,W.R.; Thomas, H.R.; Bigelow,R.W.; Duke,C.B.; Plummer, E.W.; Heeger, A.J.; MacDiarmid, A.G. *J.Chem. Phys* **1980**, *72*, 3674.

[3] Tanaka, K.; Yoshizawa, K.; Takeuchi, T.; Yamabe, T.; Yamauchi, J. *Synthetic Metals* **1990**, *38*, 107.

[4] Ryan, M.E.; Hynes, A.M.; Wheale, S.H.; Badyal, J.P.S.; Hardacre, C.; Ormerod, R.M. *Chem. Mater.* **1996**, *8*, 916.

[5] Hernandez, J.E.; Ahn, H.; Whitten, J.E. *J. Phys. Chem. B* **2001**, *105*, 8339.

[6] Nishio, S.; Okumura, M.; Okada, S.; Minamimoto, Y.; Taketani, Y.; Matsuzaki, A.; Sato, H. *J. Photopolymer Sci. Tech.* **1998**, *2*, 347.

[7] Nishio, S.; Okada, S.; Minamimoto, Y.; Okumura, M.; Matsuzaki, A.; Sato, H. *J. of Photochemistry and Photobiology A: Chemistry* **1998**, *116*, 245.

[8] Fichou, D.; Ziegler, C. In *Handbook of Oligothiophenes and Polythiophenes*; Fichou, D., Ed.; Wiley-VCH: Weinheim, **1999**.

[9] Liu, G.; Natarajan, S.; Kim, S.H. *Surf. Sci. Lett.* **2005** (in press).

[10] Hitchcock, A.P.; Horsley, J.A.; Stöhr, J. *J. Chem. Phys.* **1986**, *85*, 4835.

[11] Tourillon, G.; Mahatsekake, C.; Andrieu, C.; Williams, G.P.; Garrett R.F.; Braun, W. *Surf. Sci* **1988**, *201*, 171.

[12] Hitchcock, A.P.; Tourillon, G.; Garrett R.F.; Williams, G.P.; Mahatsekake, C.; Andrieu, C. *J. Phys. Chem. B* **1990**, *94*, 2327.

[13] Yamamoto, T.; Kamijoh, T.; Wataru, I. *J. Polym. Sci. Part A: Polym. Chem* **200l**, *38*, 1642.

[14] Louarn, G.; Buisson, J.P.; Lefrant, S.; Fichou, D. *J. Phys. Chem.* **1995**, *99*, 11399.

[15] Furukawa, Y.; Akimoto, M.; Harada, I. *Synthetic Metals* **1987**, *18*, 151.

[16] Hotta, S.; Shimotsuma, W.; Taketani, M. *Synthetic Metal* **1984/85**, *10*, 85.

[17] Groenewoud, L.M.H.; Engbers, G.H.M.; Terlingen, J.G.A.; Wormeester, H.; Feijen, J. *Langmuir* **2000**, *16*, 6278.

[18] Groenewoud, L.M.H.; Engbers, G.H.M.;Feijen, J. *Langmuir* **2002**,*19*, 1368.

[19] Hotta, S.; Ito, K. In *Handbook of Oligothiophenes and Polythiophenes*; Fichou, D., Ed.; Wiley-VCH: Weinheim, **1999**.

[20] McCullogh, R. In *Handbook of Oligothiophenes and Polythiophenes*; Fichou, D., Ed.; Wiley-VCH: Weinheim, **1999**.

[21] Kossmehl, G.; Engelmann, G. In *Handbook of Oligothiophenes and Polythiophenes*; Fichou, D., Ed.; Wiley-VCH: Weinheim, **1999**.

[22] Dzvonik,M.; Yang,S.; Bersohn, R. *J. Chem. Phys.* **1971**, *61*, 4408.

[23] Elisei, F.; Latterini,L.; Aloisi,G.G.; D'Auria, M. *J. Phys. Chem.* **1995**, *99*, 5365, and references cited therein.

[24] Kim, S.H.; Stair, P. C.; Weitz, E. *Langmuir* **1998**, *14*, 4156.

[25] Meng, H.; Perepichka, D.F.; Bendikov, M.; Wudl, F.; Pan, G. Z.; Yu, W.; Dong, W.; Brown, S. *J. Amer. Chem. Soc.* **2003**, *125*, 15151.

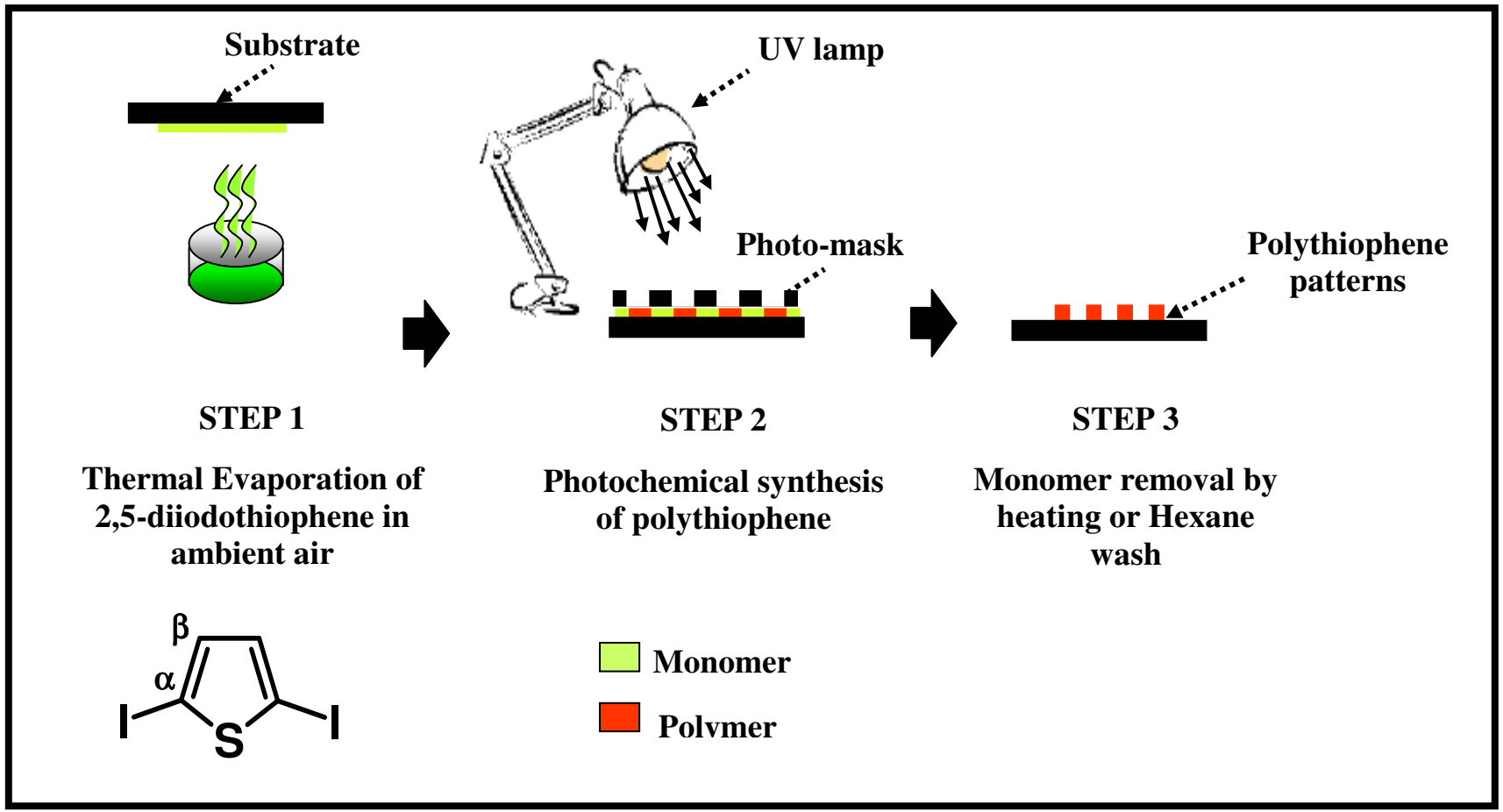

Fig. 2.1 Schematic of the photochemical synthesis of polythiophene patterns on a substrate by deposition of 2,5-diiodothiophene followed by UV irradiation through a photomask. The structure of 2,5-diiodothiophene with the α- and β- position indication is also shown.

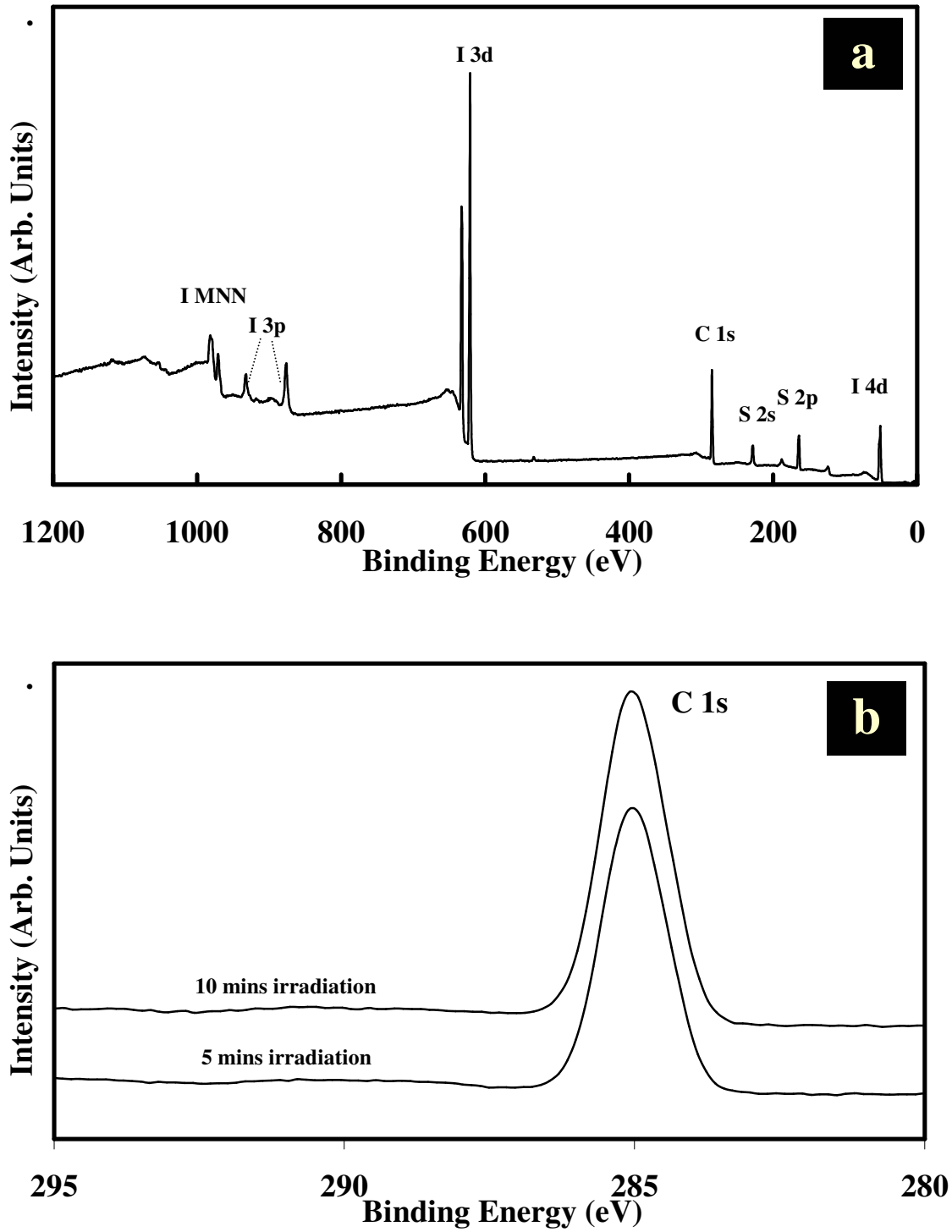

Fig. 2.2 (a) XPS survey spectrum and high resolution spectra of **(b)** C1s, **(c)** S2p, and **(d)** $I3d_{5/2}$ regions of the polythiophene thin film photochemically synthesized on a glass substrate.

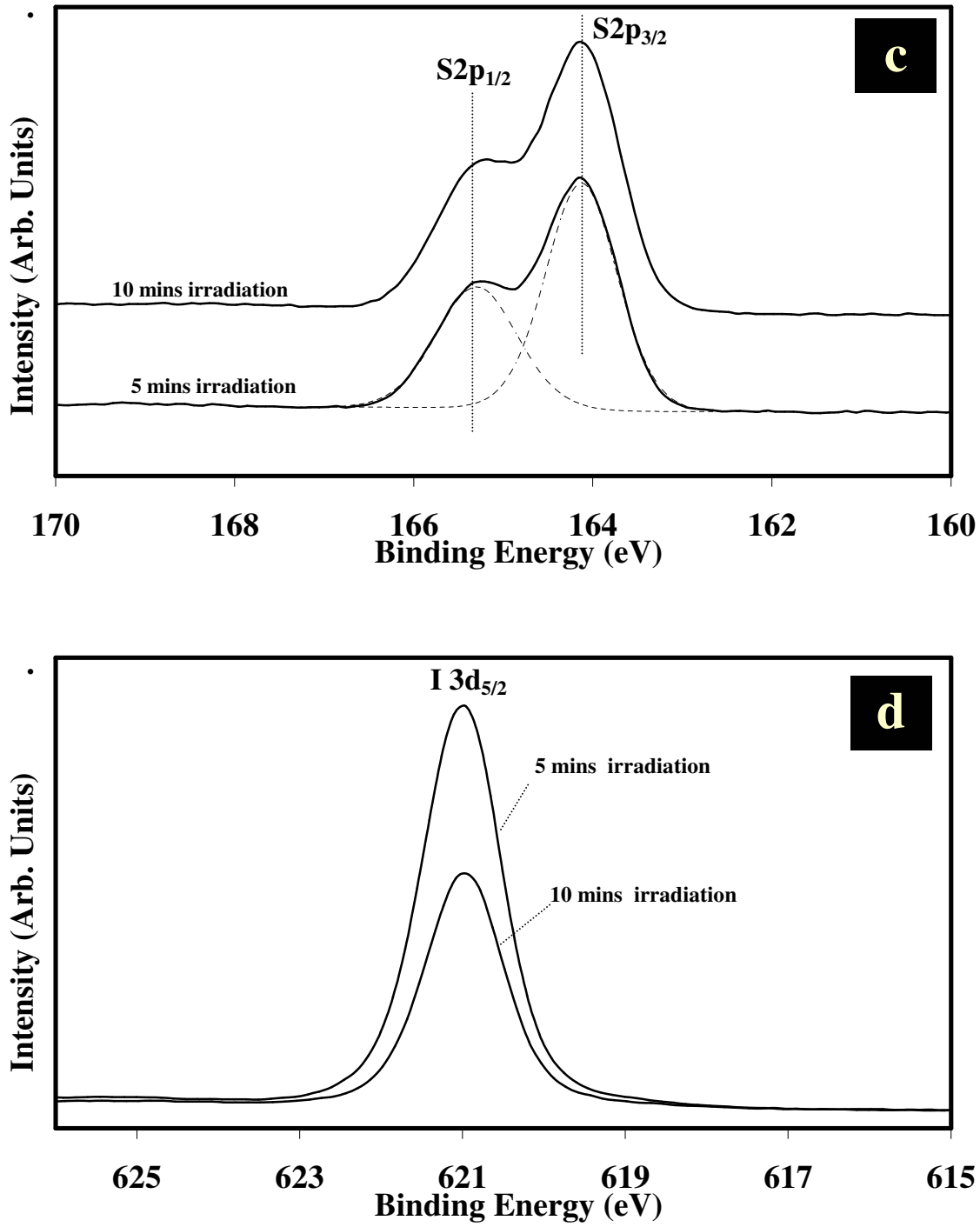

Fig. 2.2 (a) XPS survey spectrum and high resolution spectra of **(b)** C1s, **(c)** S2p, and **(d)** $I3d_{5/2}$ regions of the polythiophene thin film photochemically synthesized on a glass substrate.

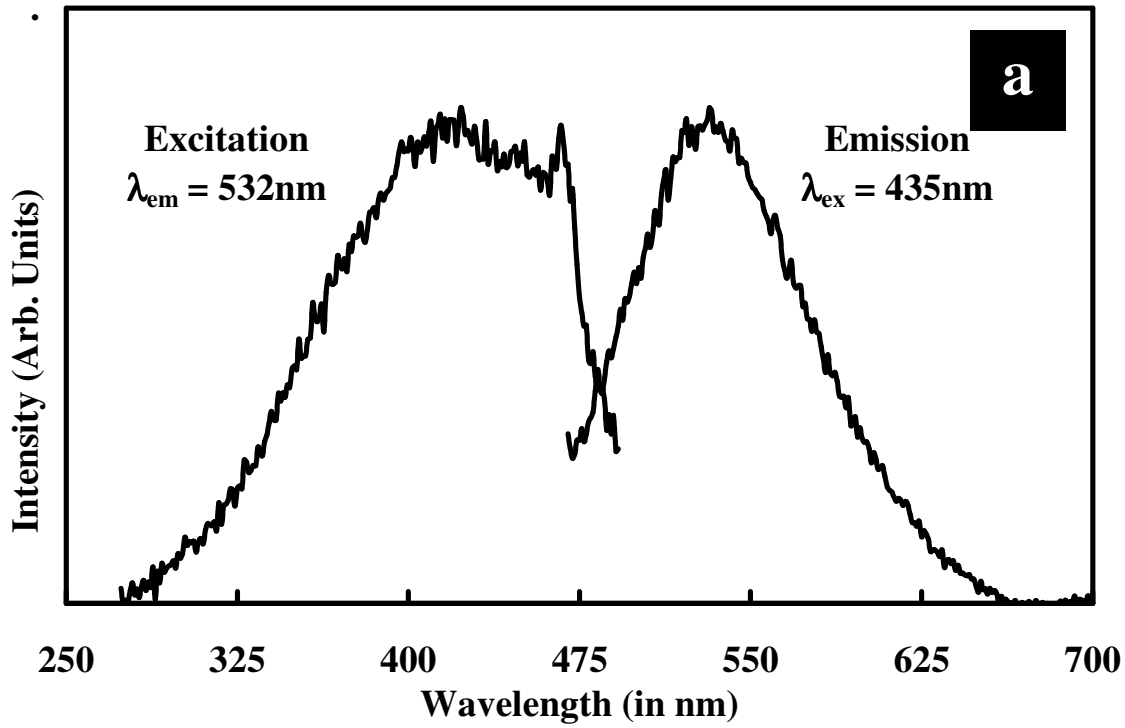

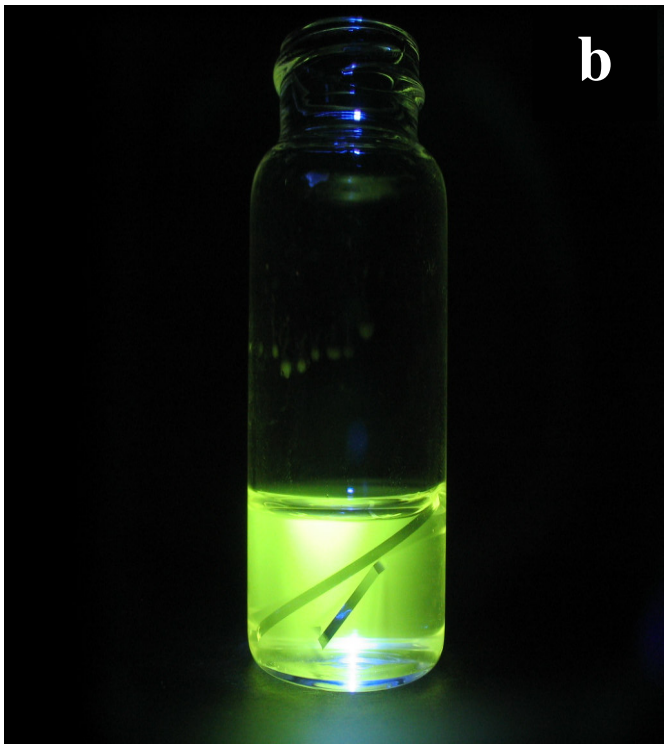

Fig. 2.3 (a) Photoluminescence excitation and emission spectra of the photochemically synthesized polythiophene films on a glass substrate and **(b)** color photograph of the photoluminescence emission from the THF extract of the photochemically synthesized polymer films. (Excitation wavelength is 435nm).

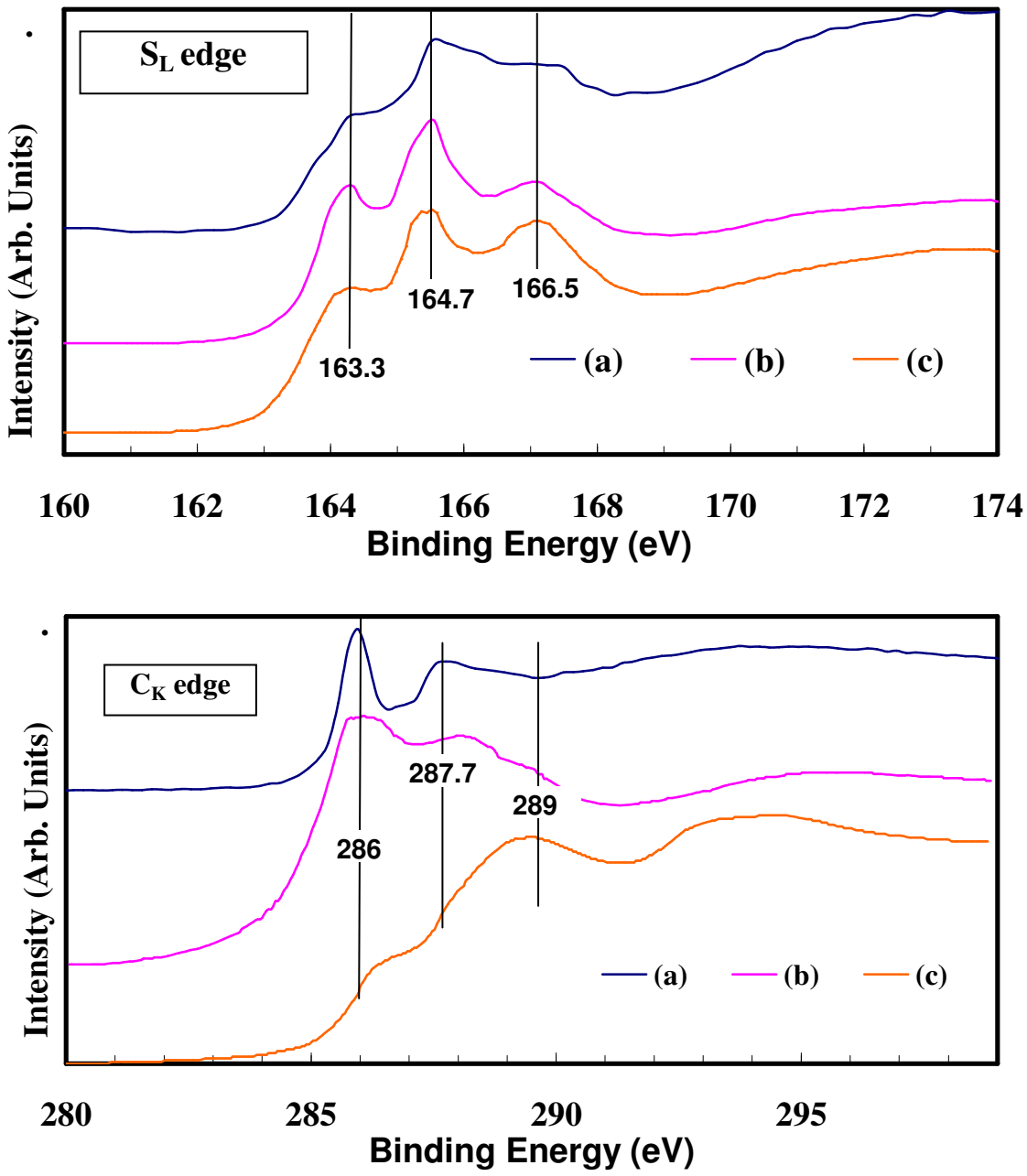

Fig. 2.4 S_L edge and C_K edge of grazing incidence NEXAFS spectra: **(a)** Photochemically synthesized polythiophene film, **(b)** Electrochemically deposited polythiophene film [11], **(c)** Electrochemically deposited poly-3,dodecyl-thiophene film [11].

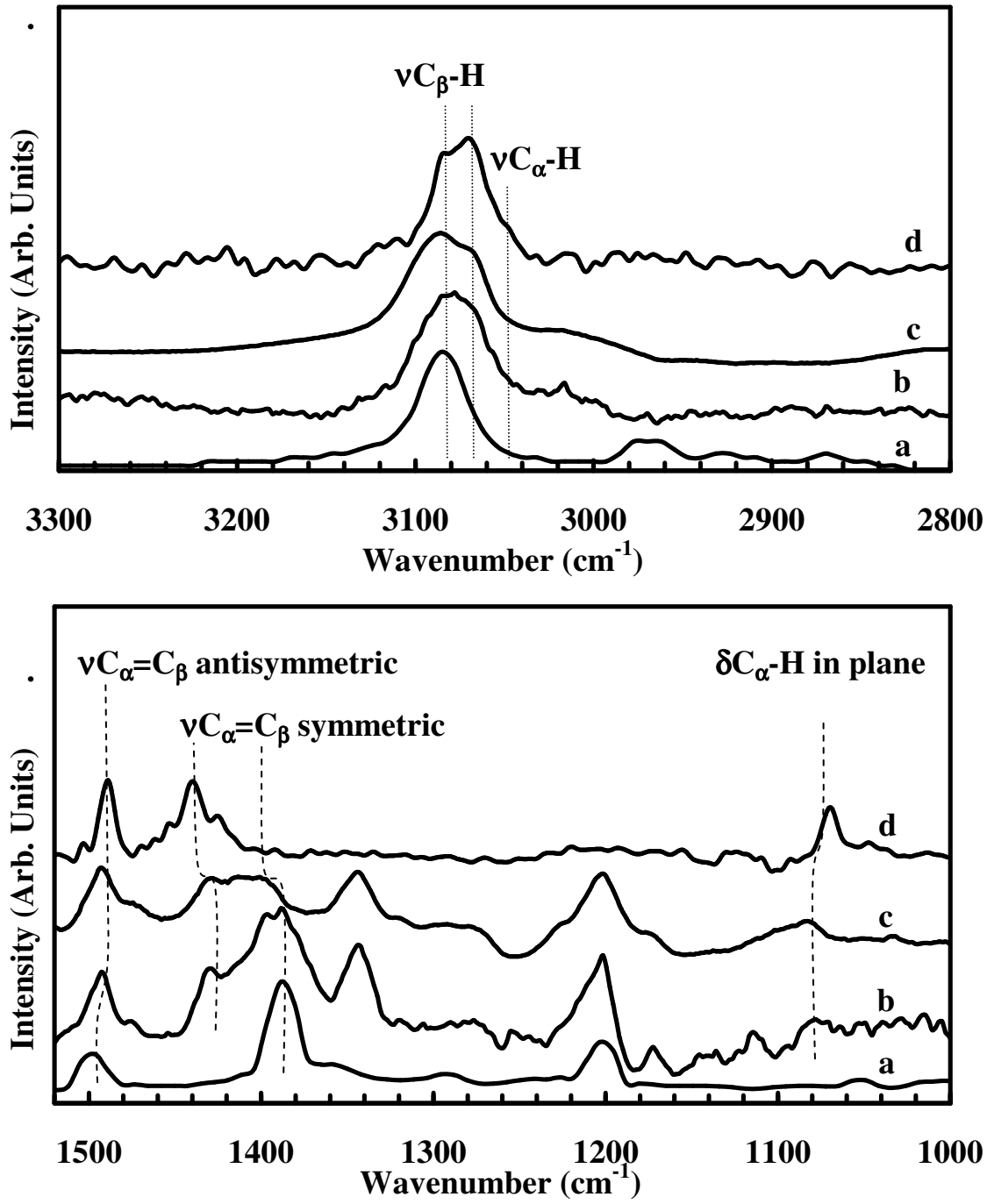

Fig. 2.5 IR spectra of **(a)** 2,5-diiodothiophene, **(b)** polythiophene thin film produced by 2 min UV irradiation, **(c)** polythiophene thin film produced by 5 min UV irradiation, and **(d)** chemically synthesized polythiophene (purchased from Aldrich). The polythiophene thin film shown in **(b)** and **(c)** are produced directly on gold substrates by the photochemical method described in the text. The thin film spectra shown in **(b)** and **(c)** are obtained by the reflection-absorption technique and the powder spectrum shown in **(d)** is obtained by the diffuse-reflection technique. The monomer spectrum shown in **(b)** is from the Aldrich reference library.

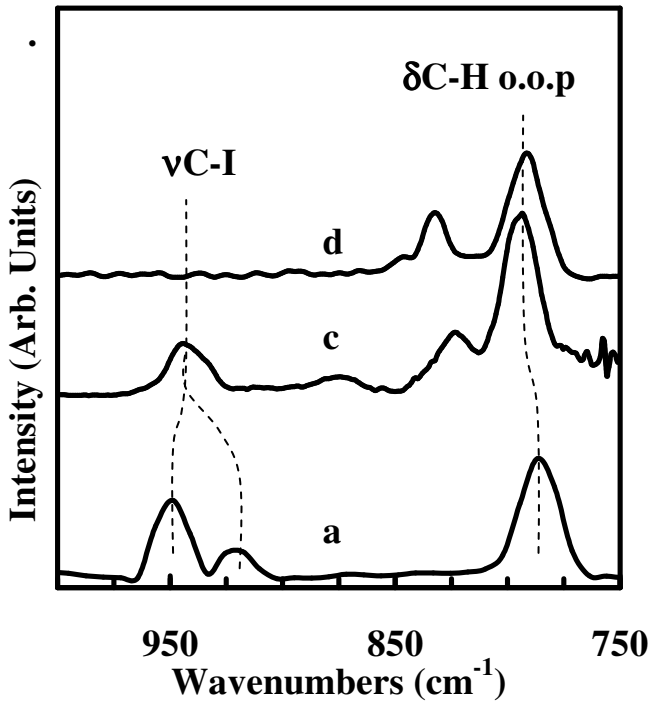

Fig. 2.5 IR spectra of **(a)** 2,5-diiodothiophene, **(b)** polythiophene thin film produced by 2 min UV irradiation, **(c)** polythiophene thin film produced by 5 min UV irradiation, and **(d)** chemically synthesized polythiophene (purchased from Aldrich). The polythiophene thin film shown in **(b)** and **(c)** are produced directly on gold substrates by the photochemical method described in the text. The thin film spectra shown in **(b)** and **(c)** were obtained by the reflection-absorption technique and the powder spectrum shown in **(d)** was obtained by the diffuse-reflection technique. The monomer spectrum shown in **(b)** is from the Aldrich reference library.

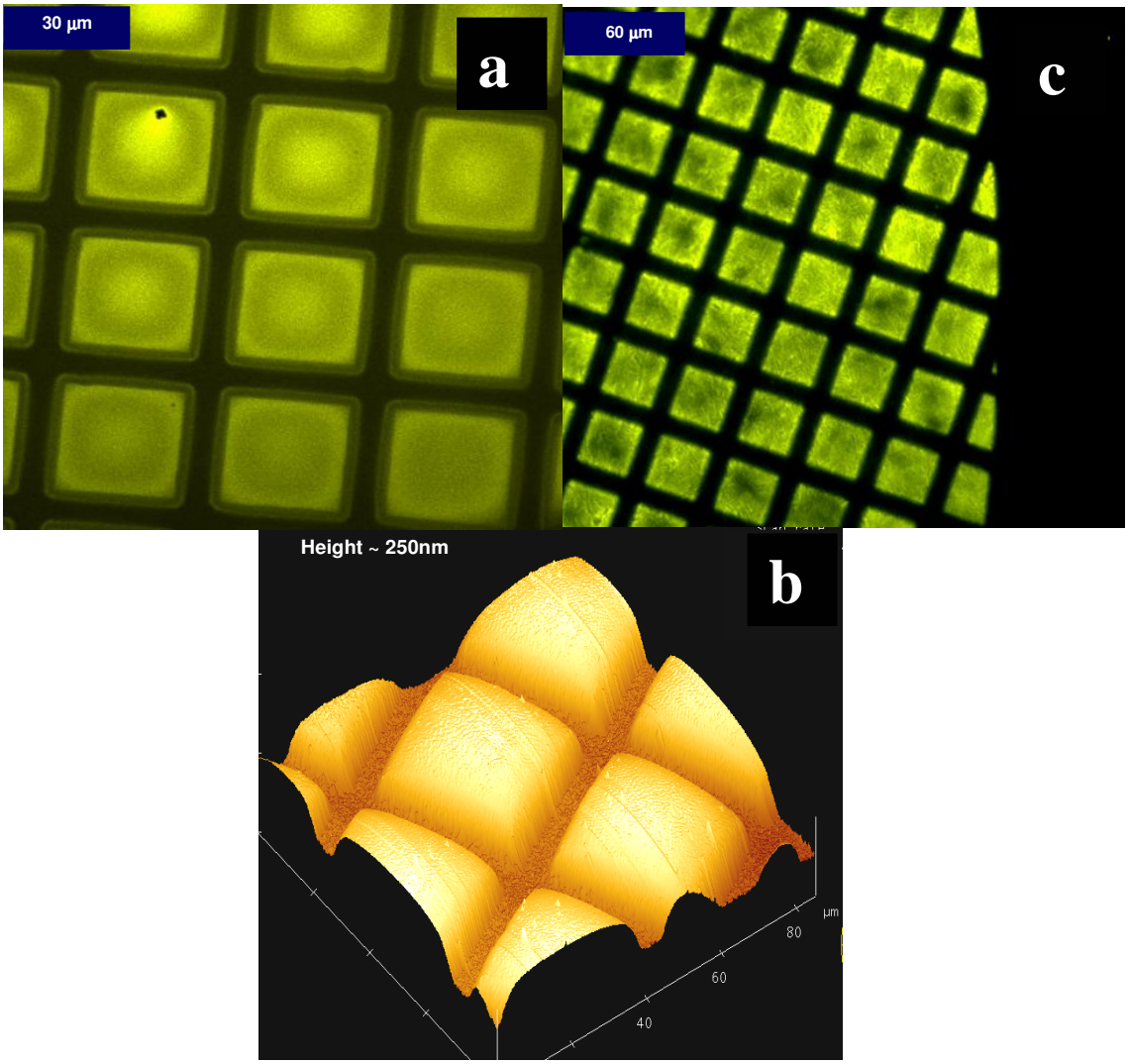

Fig. 2.6 **(a)** Fluorescence microscope and **(b)** tapping-mode AFM images of polythiophene patterns generated on a thiophene thiol terminated gold substrate. **(c)** Fluorescence microscope image of polythiophene patterns on a melt-cast polyethylene film. A 600-mesh TEM grid is used as a photo-mask for making patterns.

Chapter 3

Synthesis of polythiophene films and patterns on copper substrates using photo-activated Ullmann coupling reaction

3.1 Introduction

In 1901, Ullmann first reported homo-coupling of aromatic halides using copper bronze as a reducing agent at elevated temperatures (> 100 °C) as illustrated by the example in Fig. 3.1 [1,2]. In addition to using copper bronze, these reductive homo-coupling have also been carried out using highly activated forms of other metals such as nickel, palladium, zinc and so on [3,4]. These reductive homo-coupling is of particular interest to materials chemists as it can be employed for coupling aromatic molecules into conjugated polymers. Steinkopf et al [5] and Pomerantz et al [6] have reported synthesis of oligothiophene and polythiophene respectively using copper powder as reducing agent at a temperature of about 150 °C. In the former report, 2-iodothiophene and in the latter, carboxylate substituted 2,5-dibromothiophene has been used as the monomer. Traditional thermally activated process is convenient for bulk synthesis of polythiophene but it is not directly applicable to fabrication of polythiophene films and micro-patterns for the following reasons. Thermal activation in solution phase desorbs the monomer and the intermediates formed at the copper surface into the solution phase leading to polymer formation in the bulk. While thermal activation in gas phase will evaporate the monomer film immediately leaving behind just a few monolayers of polythiophene on the copper surface. Thus, the critical disadvantage of thermally activated chemistry is that it cannot

be localized within a thin monomer film and utilized to convert the entire monomer film into polymer film. Also, conventional lithographic techniques cannot be integrated with the thermally activated chemistry to fabricate micro-patterns of polythiophene. These difficulties can be avoided if the thienyl halide monomers are activated photochemically at room temperature.

A photo-activated Ullmann coupling using copper metal is detailed in this chapter and using this chemistry thin films and micro-patterns of polythiophene have been synthesized on copper substrates starting from 2,5-diiodothiophene as the monomer. We utilize selective photodissociation of the C-I bond in 2,5-diiodothiophene to generate thienyl radicals in a thin monomer film (~100nm). These radicals react with the copper substrate producing organo-copper intermediates. Photochemical activation allows us to generate the radicals at room temperature and thus the monomer desorption (or evaporation) are prevented. Presence of stable monomer film contains the organo-copper intermediates within the film thereby localizing the Ullmann chemistry. The organo-copper intermediates contained in the monomer film react with the monomer and convert the monomer into polymer film (~100nm). Photochemical activation also makes it easy to produce micro-patterns of polythiophene films (~100nm) via irradiation of monomer films through a photomask.

3.2 Experimental

Thin films of copper (Cu), gold (Au), platinum (Pt), and palladium (Pd) substrates were prepared on silicon wafers by thermal evaporation just prior to use. In the case of

copper, a thin foil (> 99.99 % purity) was also used after cleaning the surface with nitric acid (1.5N) to remove the oxide layer [4]. Silicon substrate with native oxide (SiO_2) layer is used after it is cleaned with a 5:1:1 mixture of H_2O:NH_4OH:H_2O_2 at 70 °C. 2,5-diiodothiophene (monomer) was thermally evaporated at ~120^oC in ambient conditions and deposited onto the substrate which is held at room temperature. The deposited monomer thickness was kept constant at ~140 nm in this experiment. The monomer film was irradiated with a collimated UV beam from a 200W mercury lamp (Oriel 6283) for 3 minutes in argon. The IR radiation from the UV lamp was removed using a water filter to prevent the sample from heating during UV irradiation. The thickness of the final polymer film was ~100 nm. These thin films of the polythiophene were then analyzed in ambient conditions with Photo-luminescence (PL), X-ray photo-electron spectroscopy (XPS) and Raman spectroscopy (632.8 nm HeNe laser). Monochromatic Aluminium Kα was used as the X-ray source for XPS and the binding energies reported here are referenced to Carbon 1s at 284.6 eV). Copper iodide (CuI), a side product of the Ullmann reaction, is photoluminescent when excited with photons of wavelength lesser than 430 nm [7]. In order to avoid photoluminescence from CuI, the polythiophene film synthesized on Cu was analyzed with two different excitations, λ = 435±1.5 nm and 455±1.5 nm. Both PL emission spectra were found to be identical, confirming that the emission is from polythiophene and not from CuI. Refer appendix C for further discussion on this issue.

3.3 Results and discussion

The goal of this chapter is to confirm the Ullmann coupling reaction during photochemical activation of monomer film on a Cu substrate. But, as discussed in the chapter two, photochemical irradiation of thin film of 2,5-diiodothiophene on any substrate produces polythiophene. So, in order to prove the mediation of Ullmann coupling reaction, the spectroscopic analysis of photohemically synthesized polythiophene on a Cu substrate is compared with that on other substrates.

Fig. 3.2 compares the photoluminescence emission spectrum of the polythiophene film (~ 100nm thick) synthesized on Cu to that synthesized on the other substrates such as SiO_2, Au, and Pd. Emission maximum of the thin polymer film synthesized on SiO_2 or Au or Pd, is at 545 nm (green yellow), while that on Cu is at 605 nm (orange red). These PL results clearly indicate that the polythiophene film synthesized on Cu has a longer conjugation length than those synthesized on other inactive substrates such as SiO_2, Au, and Pd. Comparison of the observed emission maxima with the reported values in literature [8] shows that the average conjugation length of polythiophene on Cu to be ~7, whereas those on the other substrates are ~4.

The polythiophene film (~100nm) synthesized on Cu is further analyzed with surface enhanced Raman spectroscopy (SERS). Fig. 3.3 compares the SERS data of polythiophene synthesized on Cu and Au with the Raman spectrum of a chemically-synthesized polythiophene reference sample (purchased from Aldrich). The peaks at 691 cm^{-1} , 1043 cm^{-1}, and 1215 cm^{-1} are attributed to C-S-C ring deformation, C_β-H bending,

and C_α-$C_{\alpha'}$ inter-ring stretching respectively [9,10]. The presence of these peaks confirms that the thienyl ring structure is preserved during the photochemical reaction. For the polythiophene film synthesized on Cu, the ring C_α=C_β anti-symmetric peak appears as a shoulder at ~1510 cm^{-1}, the symmetric peak is located at ~1450 cm^{-1} and the intensity ratio (I (anti-sym) / I (sym)) is estimated to be 0.3 by fitting the peaks to a Lorentzian distribution. For the polythiophene film synthesized on Au, the anti-symmetric and symmetric peaks are located at ~1440 cm^{-1} and 1520 cm^{-1} respectively and the intensity ratio is estimated to be ~ 1. These peak positions and intensity ratio can be used to estimate the degree of conjugation [9,10]. As the number of thiophene ring units in α-α' oligothiophene increases from 3 to 8, the C_α=C_β anti-symmetric stretching peak location gradually shifts from 1530 cm^{-1} to 1502 cm^{-1} and the intensity ratio decreases gradually from 0.67 to 0.20. Detailed peak locations and the ratio of peak intensities are summarized in table 3.1. From this comparison, the average conjugation length of the polythiophene synthesized on Cu and Au are estimated to be ~7 and ~4 respectively, which is consistent with the photoluminescence data.

Increased conjugation length can be explained by the reaction of Cu from the substrate with the thienyl radicals generated at the interface leading to the formation of 2-thienyl copper intermediates as shown in the reaction 1 of Fig. 3.4 [3,4]. These organo-copper intermediates react with other monomer molecules exclusively at 2 or 5 positions leading to α-α' coupled products and CuI as shown in the reaction 2 of Fig. 3.4 [11]. In the case of other substrates only the direct photochemical pathway is operative and there is no additional mechanism that aid α-α' coupling. Thus only polymer of shorter conjugation length ~ 4 and molecular iodine by-product is formed by the direct

photochemical pathway as shown in the reaction 3 of Fig. 3.4 [12]. But in the presence of Cu, the photochemical pathway is altered by the Ullmann reaction pathway to yield polymer with greater extent of α-α' coupling and CuI as by product. Operation of Ullmann reaction pathway exclusively on Cu substrate is further supported by the formation of CuI indicated by the XPS results.

Fig. 3.5 shows the XPS results of the polythiophene film synthesized on various substrates. It can be seen from Fig 3.5a, iodine $3d_{5/2}$ peak from the polymer film synthesized on Cu is located at 619.7 eV while that on Au (and others) is at 620.5 eV. The former correspond to the iodide anion from the CuI [13] and later from the un-reacted carbon-iodine bond [14]. This supports the operation of Ullmann reaction pathway with the formation of Iodide shown in the reaction 2 of Fig. 3.4. Fig 3.5 b,c shows the Cu 2p3/2 and Cu $L_3M_{4,5}M_{4,5}$ regions from the polymer film synthesized on Cu. Cu $L_3M_{4,5}M_{4,5}$ regions is compared with the standard CuI[13] and Cu metal [15] spectrum. The Cu $L_3M_{4,5}M_{4,5}$ Auger peak from the polymer film is in agreement with CuI (570.5 eV) and not metallic Cu (568.1 eV) [13,15]. Quantification of XPS results reveals that Cu/I ratio is ~ 1 which is consistent with the formation of CuI.

I/C ratio from the polymer film synthesized Cu film is ~ 0.6 and that on Au is ~ 0.1. Theoretical I/C ratio in the 2,5-diiodothiophene monomer is 0.5. Interestingly, I/C ratio of the polymer synthesized on Cu is more than that of the monomer although it would be expected to stay the same or reduce based on the Fig. 3.4. Increase in I/C ratio may be just apparent and it may be due to error in the relative sensitivity factor of iodine used for XPS quantification. More importantly, the marked difference between the I/C ratio of the polymer film synthesized on Cu and on other substrate confirms that on a

non-reactive substrate only the photochemical pathway is operative with the loss of iodine because of the formation of volatile molecular iodine [12], whereas on the Cu substrate the Ullmann reaction pathway is operative with almost all the iodine from the carbon-iodine converted to iodide. Fig 3.6 shows the spectra of sulfur 2p region, carbon 1s region and the survey spectrum. Intactness of the majority of the thiophene units is supported by the well-resolved doublet at 163.8eV and 165eV consistent with the previously reported sulfur 2p peak positions for polythiophene [16]. A lower binding energy doublet is often observed in the sulfur and is attributed to the sulphide species formed by concurrent desulphurization reaction [17]. Also, we observe that amount of sulphide species increases as the irradiation time is increased. Sulphide formation is consistent with the reported sulfur loss by desulphurization reaction in the chemically synthesized polythiophene by the nickel catalyzed Ullmann reaction [18]. A single carbon 1s peak at 284.6eV confirms the absence of oxygenated defects during polymerization.

As discussed in the second chapter, the substrate peaks are not observed in XPS of the films synthesized on other metals and SiO_2. This is because the polythiophene films are much thicker than the escape depth of substrate photoelectrons. In contrast, strong Cu peaks are observed in XPS of polythiophene synthesized on a Cu substrate. This cannot be attributed to the incomplete coverage of polythiophene on Cu because those peaks are due to CuI and not due to metallic Cu. These results indicate that the Cu atoms from the substrate are dissolved into the film in the form of organo-copper intermediates during the photo-chemical reaction. As shown in Fig. 3.7, a liquid phase is observed in the film during UV irradiation. This might be due to the formation of photochemical intermediates with low melting points (such as 2-iodothiophene which is a liquid at room temperature).

This liquid phase formation may facilitate the diffusion of organo-copper intermediates formed at the heterogeneous interface into the monomer film. These organo-copper intermediates present in the film initiate Ullmann coupling reaction through out the thin film aiding in formation of α-α' coupled polythiophene. Sulfur atom in a neighboring thiophene unit may play a role in stabilizing the organo-copper intermediates thereby aiding dissolution of the intermediates into the monomer film. Photolithographic patterning of polythiophene is also demonstrated using a TEM grid as a photo mask. Fig. 3.8 shows the pseudo colored fluorescence microscope image of photo-patterned polythiophene on a Cu substrate.

3.4 Conclusion

In conclusion, the selective photodissociation of the C-I bond in 2,5-diiodothiophene on Cu leads to Ullmann coupling reaction involving substrate atoms and produces polythiophene with an average conjugation length of ~7. This chemistry allows *in-situ* synthesis of thin films and micro-patterns of unsubstituted polythiophene from the monomer film and thus overcomes the intractability issues of polythiophene. Presence of CuI in the synthesized polythiophene thin films may be advantageous in applications such as hybrid solar cell, as CuI is large band gap material that can be used as a hole acceptor [7]. The photo-activated Ullmann coupling reaction may be extended to other conjugated polymers and used to fabricate thin film or micro-pattern devices containing unsubstituted conjugated polymers as a functional component.

3.5 References

[1] Nelson, T.D.; Crouch, R.D. *Organic Reactions* **2004**, *63*, 265.

[2] Fanta, P.E. *Chemical Reviews* **1964**, *64*, 613.

[3] Rieke, R.D. *Science* **1989**, *246*, 1260

[4] Fürstner, A. *Angew. Chem. Int. ed. Engl*. **1993**, *32*, 164.

[5] Steinkopf, W.; Leitsmann, R.; Hofmann, K.H. *Lieb. Ann. Chem.* **1941**, *546*, 180.

[6] Pomerantz, M.; Yang, H.; Cheng, Y. *Macromolecules* **1995**, *28*, 5706.

[7] Sirimanne, P.M.; Shirata, T.; Damodare, L.; Hayashi, Y.; Soga, T.; Jimbo, T. *Solar Energy Materials & Solar Cells* **2003**, *77*, 15.

[8] Fichou, D.; Ziegler, C. In *Handbook of Oligothiophenes and Polythiophenes*; Fichou, D., ed.; Wiley-VCH: Weinheim, Germany, **1999**.

[9] Louarn, G.; Buisson, J.P.; Lefrant, S.; Fichou, D. *J. Phys. Chem.* **1995**, *99*, 11399.

[10] Furukawa, Y.; Akimoto, M.; Harada, I. *Synthetic Metals* **1987**, *18*, 151.

[11] Xi, M.; Bent, B.E. *J. Am. Chem. Soc.* **1993**, *115*, 7426.

[12] Natarajan, S.; Kim, S.H. *Thin Solid Films*, in review.

[13] Vasquez, R.P. *Surface Science Spectra* **1994**, *2*, 149.

[14] Sloan, D.; Sun, Y.M.; Ihm, H.; White, J.M. *J. Phys. Chem. B* **1998**, *102*, 6825.

[15] Miller, A.C.; Simmons, A.C. *Surface Science Spectra* **1993**, *2*, 55.

[16] Jugnet, Y.; Tourillon, G.; Duc, T.M. *Phys. Rev. Lett.* **1986**, *56*, 1862.

[17] Chawla, S.K.; Sankarraman, N.; Payer, J.H. *J. Electron Spectro. Relat. Phenom.* **1992**, *61*, 1.

[18] Kiso, Y.; Yamamoto, K.; Tamao, K.; Kumada, M. *J. Am. Chem. Soc.* **1972**, *94*, 4374.

No of thiophene units in α-α' oligothiophene	$C_\alpha=C_\beta$ symmetric stretch peak location (cm^{-1})	$C_\alpha=C_\beta$ anti-symmetric stretch peak location (cm^{-1})	Ratio of intensity of anti-symmetric to symmetric
3	1461	1530	0.67
4	1458	1514	0.41
6	1457	1504	0.23
8	1456	1502	0.20

Table 3.1 $C_\alpha=C_\beta$ symmetric and anti-symmetric stretching vibration peak positions and the intensity ratio of α-α' oligothiophenes.

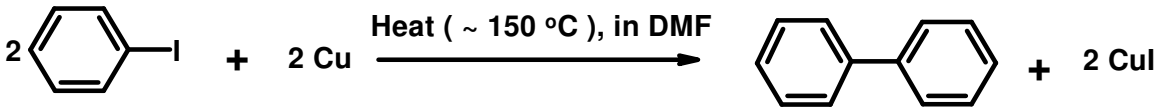

Fig. 3.1 An example of traditional thermally activated Ullmann coupling.

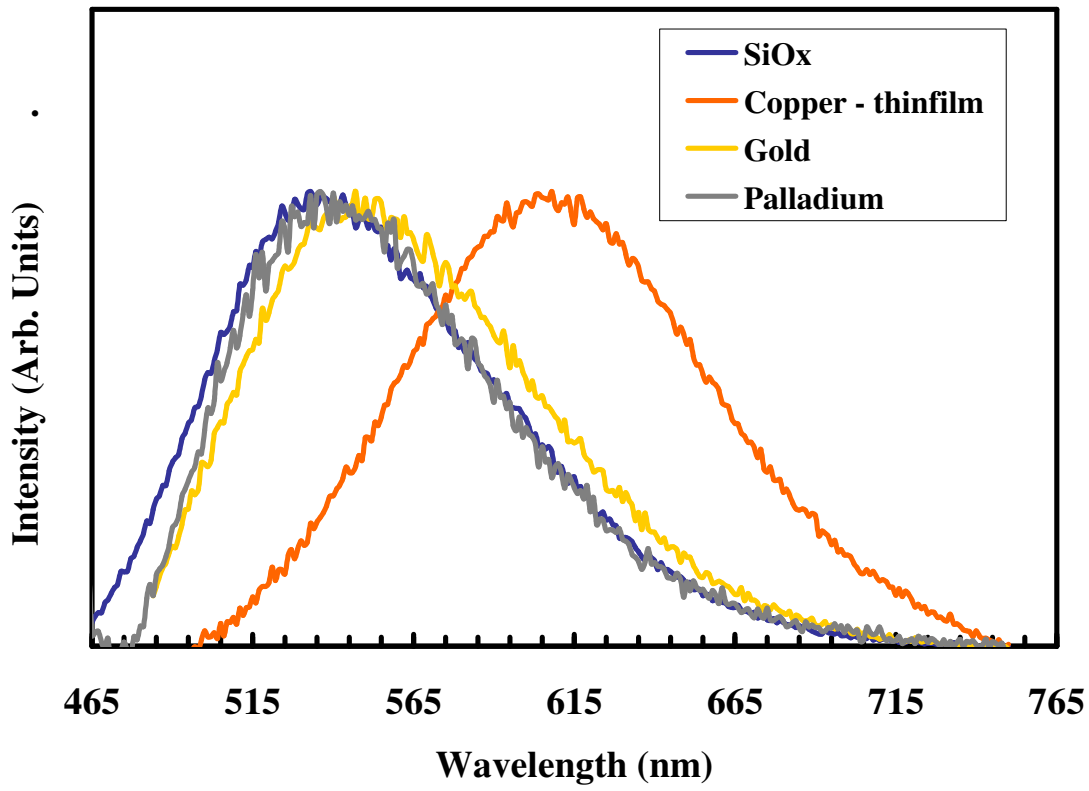

Fig. 3.2 Photoluminescence emission of the polymer film synthesized on copper is compared to that synthesized on other substrates such gold, palladium, and silicon with native oxide.

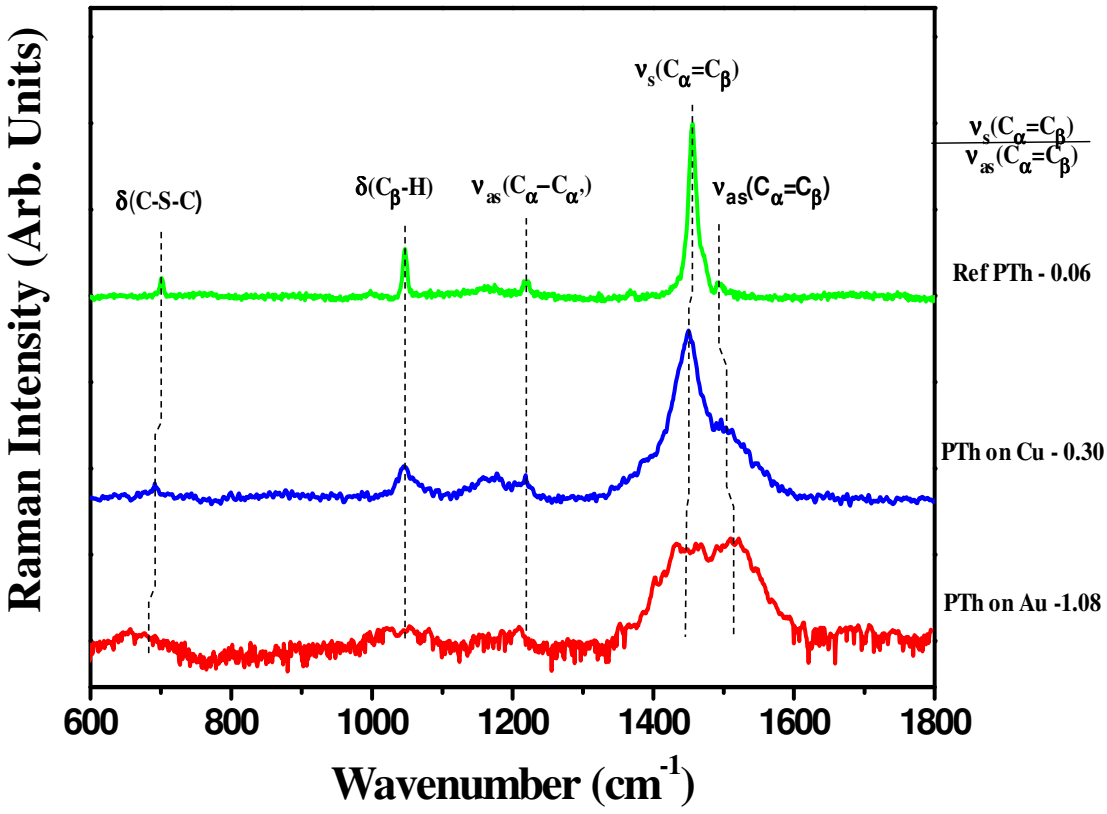

Fig. 3.3 Raman spectrum of chemically synthesized polythiophene powder, surface-enhanced Raman spectrum (SERS) of photochemically synthesized polythiophene film on copper and on gold are compared.

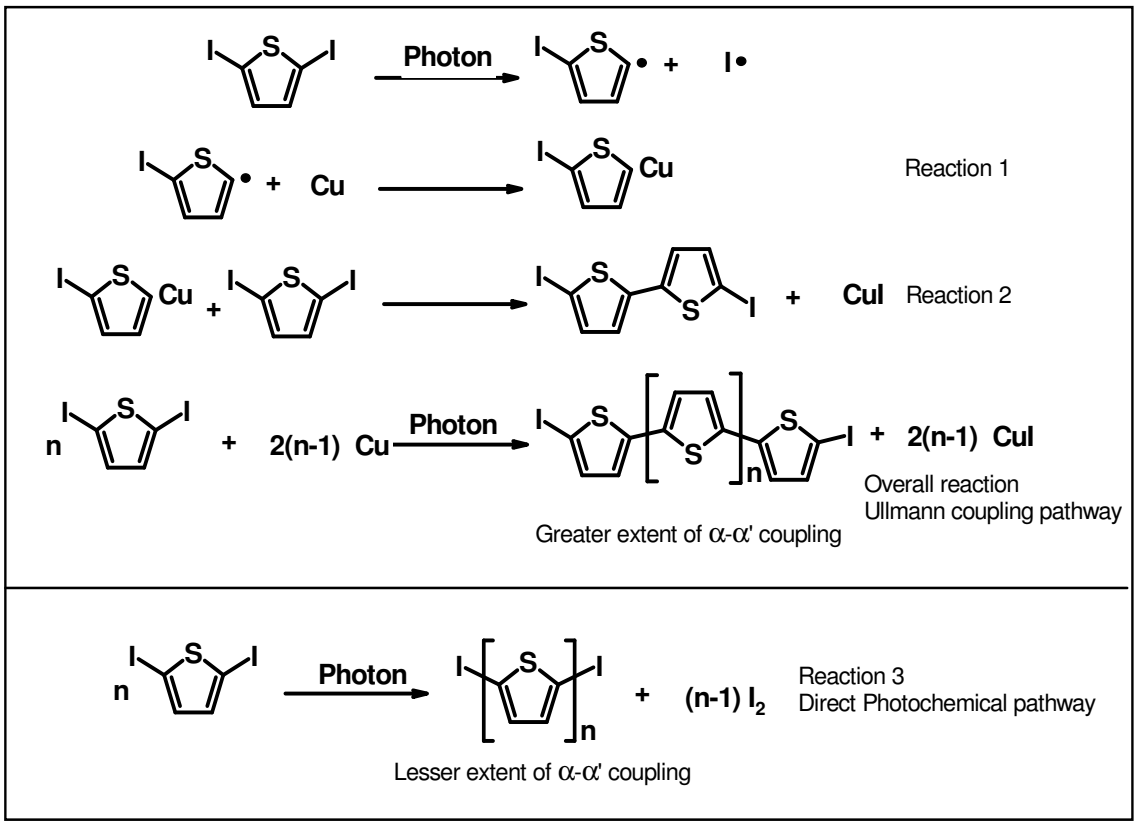

Fig. 3.4 Mechanism of photo-activated Ullmann coupling on a copper substrate.

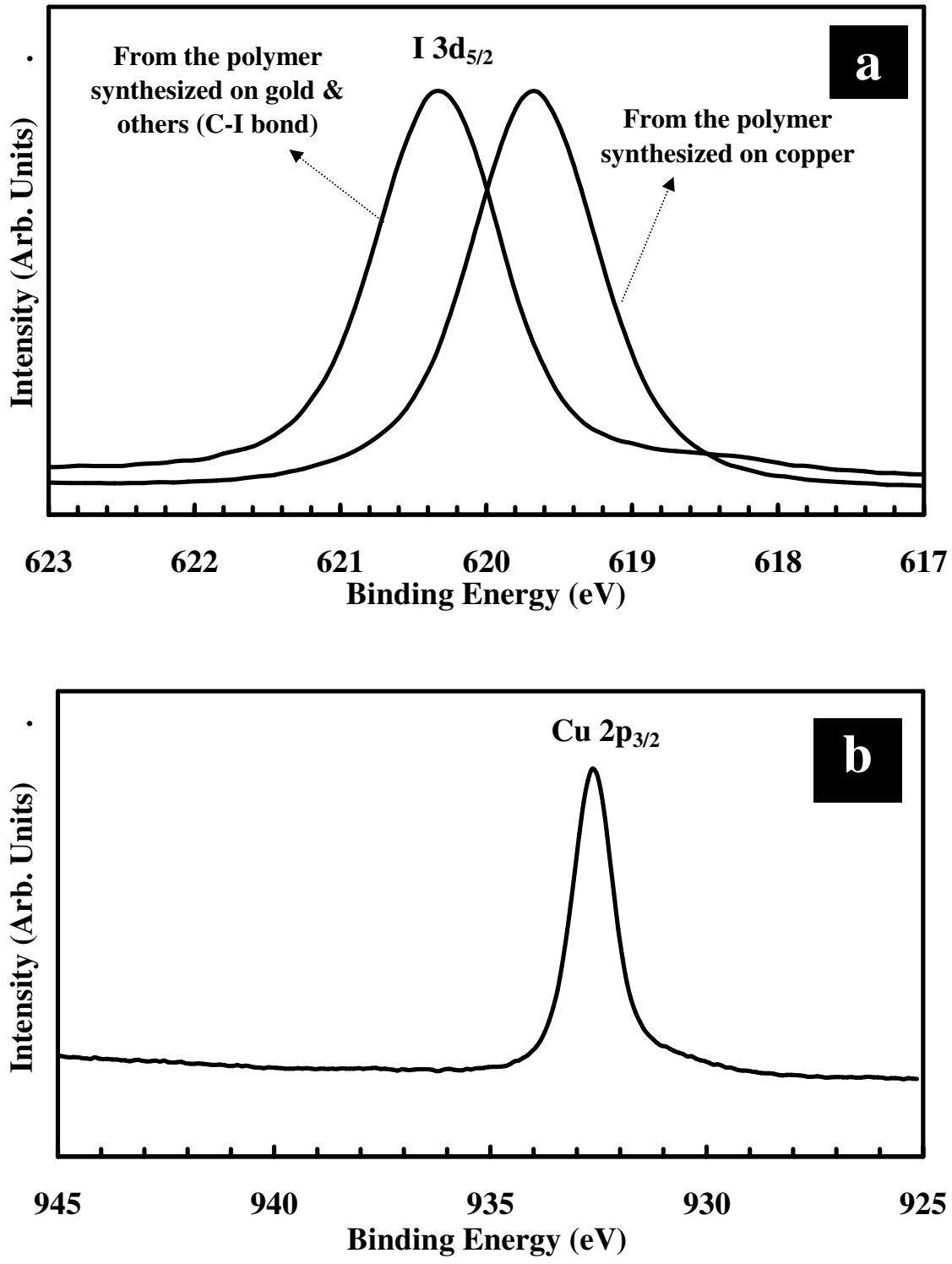

Fig. 3.5 (a) I $3d_{5/2}$ region of the polymer film synthesized on copper is compared to that synthesized on other substrates such gold, palladium, platinum, silicon with native oxide. **(b)** Cu 2p3/2 region of the polymer film synthesized on copper. **(c)** Cu $L_3M_{4,5}M_{4,5}$ region of the polymer film synthesized on copper is compared with the standard CuI[13] and Cu metal [15] spectrum.

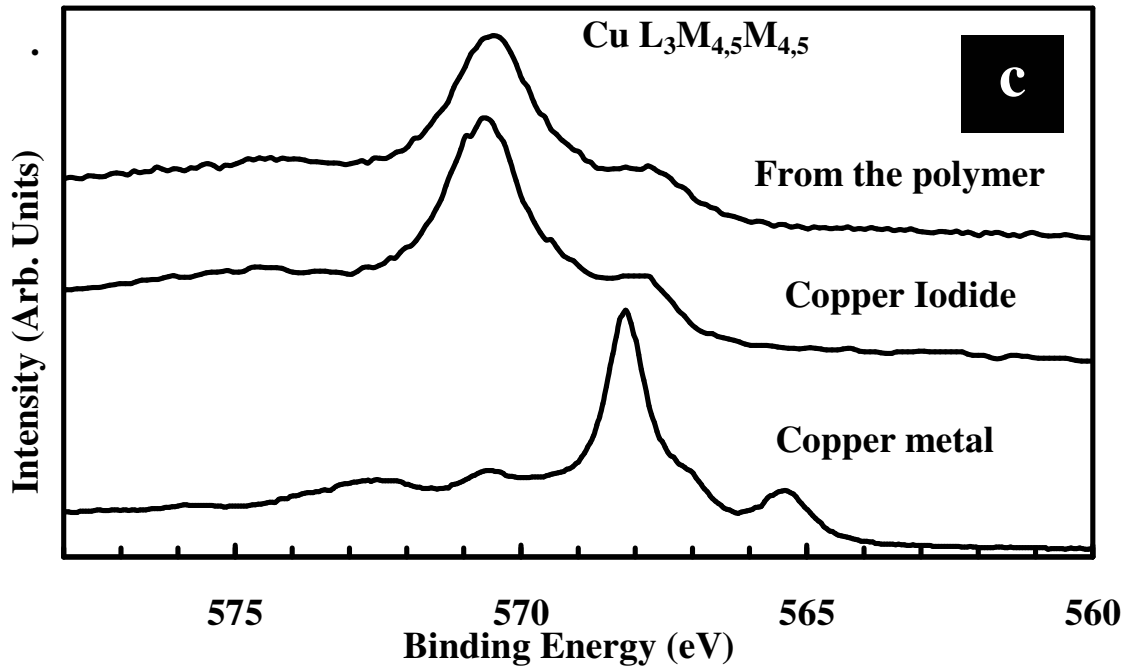

Fig. 3.5 (a) I $3d_{5/2}$ region of the polymer film synthesized on copper is compared to that synthesized on other substrates such gold, palladium, platinum, silicon with native oxide. **(b)** Cu 2p3/2 region of the polymer film synthesized on copper. **(c)** Cu $L_3M_{4,5}M_{4,5}$ region of the polymer film synthesized on copper is compared with the standard CuI[13] and Cu metal [15] spectrum.

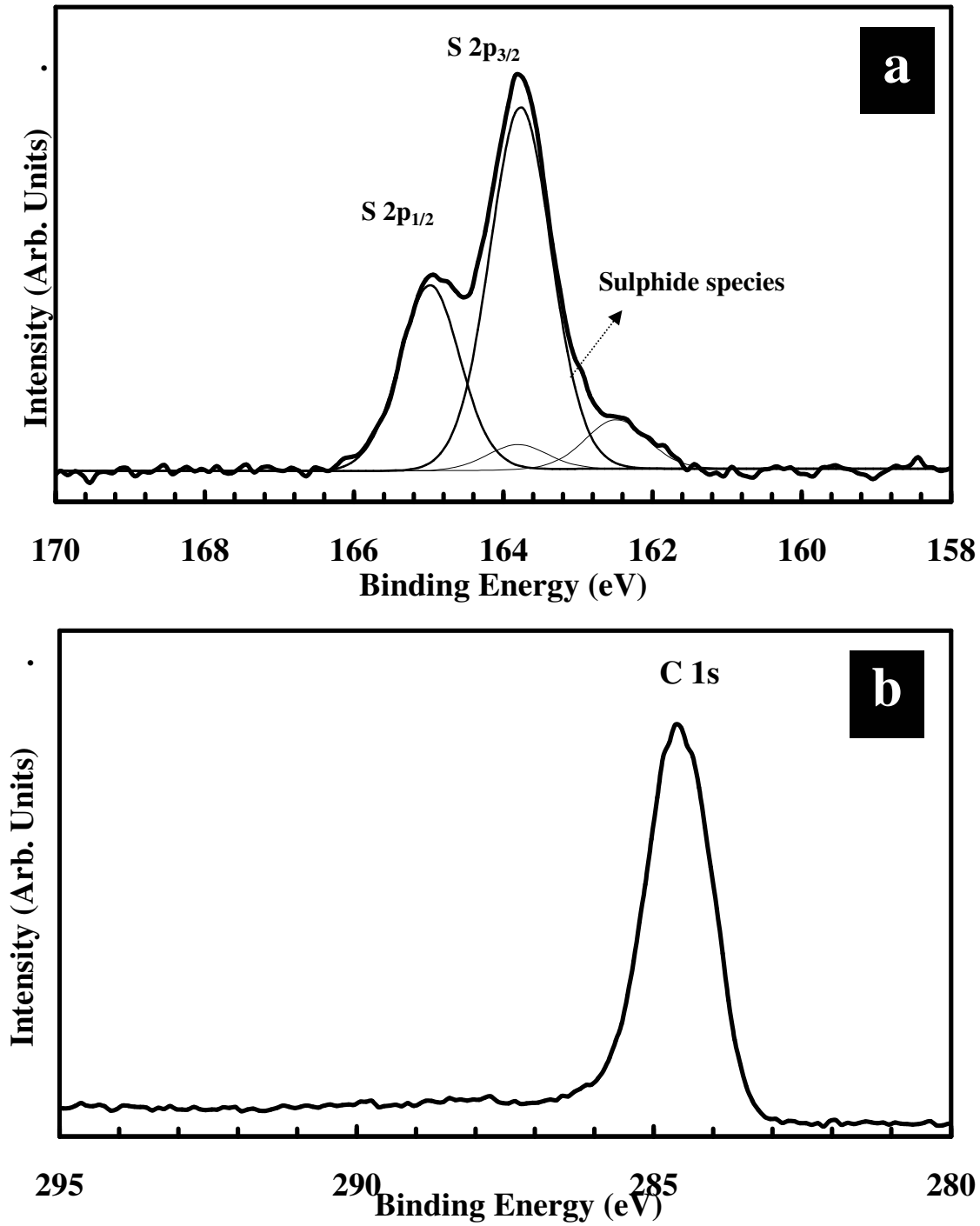

Fig. 3.6 (a) S 2p region **(b)** C 1s region **(c)** Survey spectrum of the polymer film synthesized on copper.

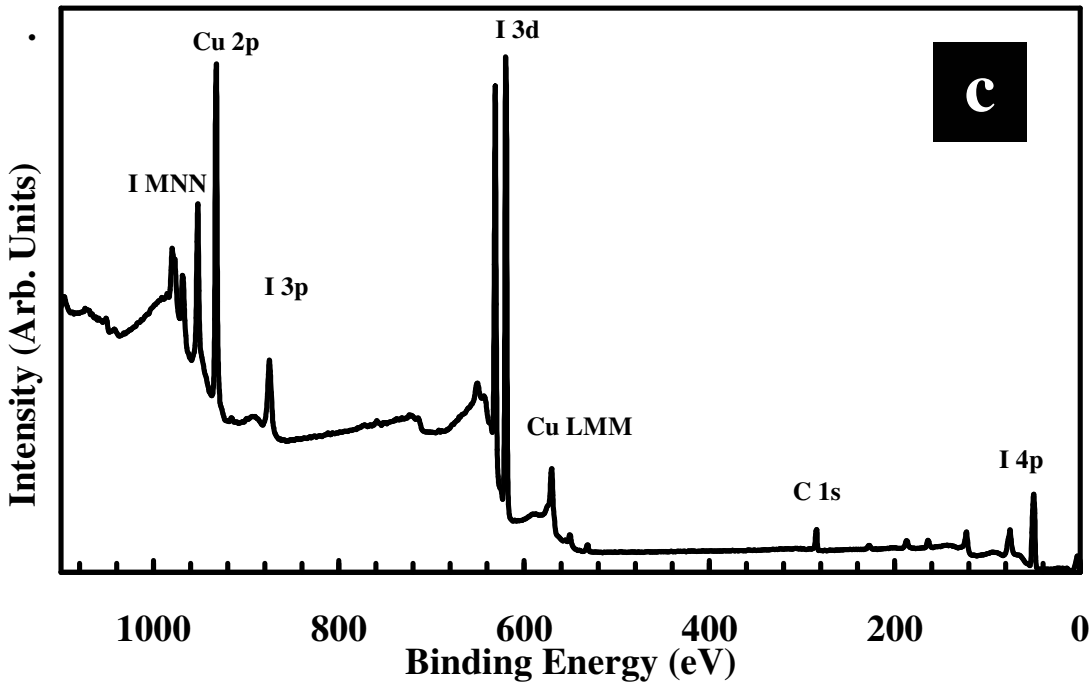

Fig. 3.6 (a) S 2p region **(b)** C 1s region **(c)** Survey spectrum of the polymer film synthesized on copper.

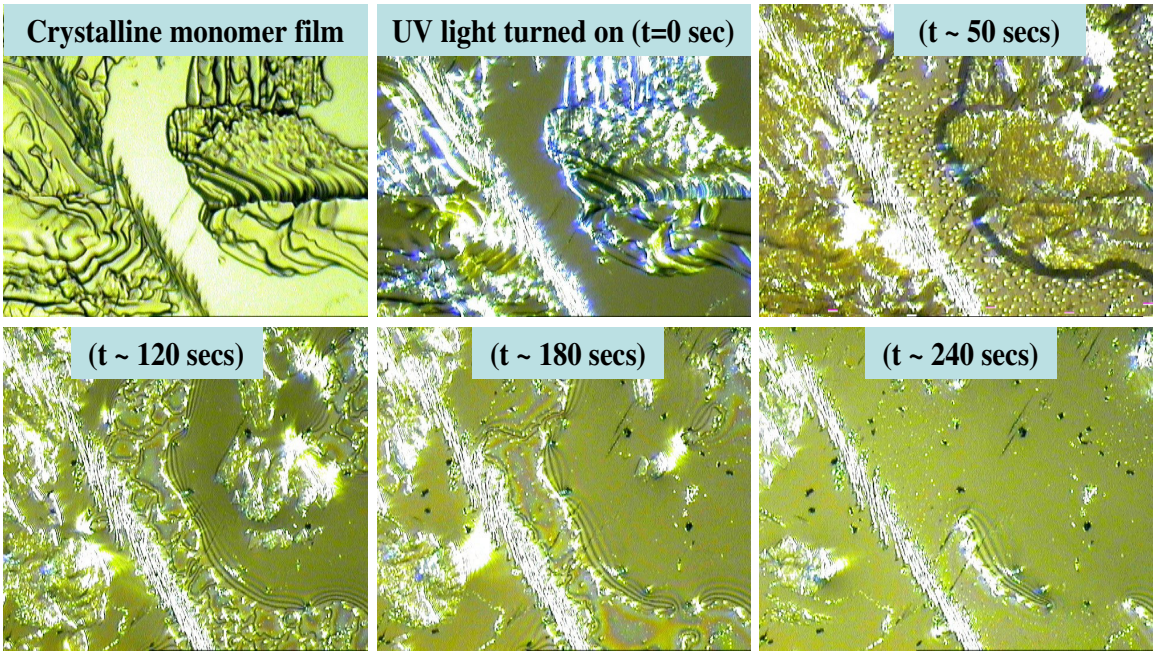

Fig. 3.7 Snapshots of 200x optical microscope video showing liquid formation during irradiation of solid 2,5-diiodothiophene film.

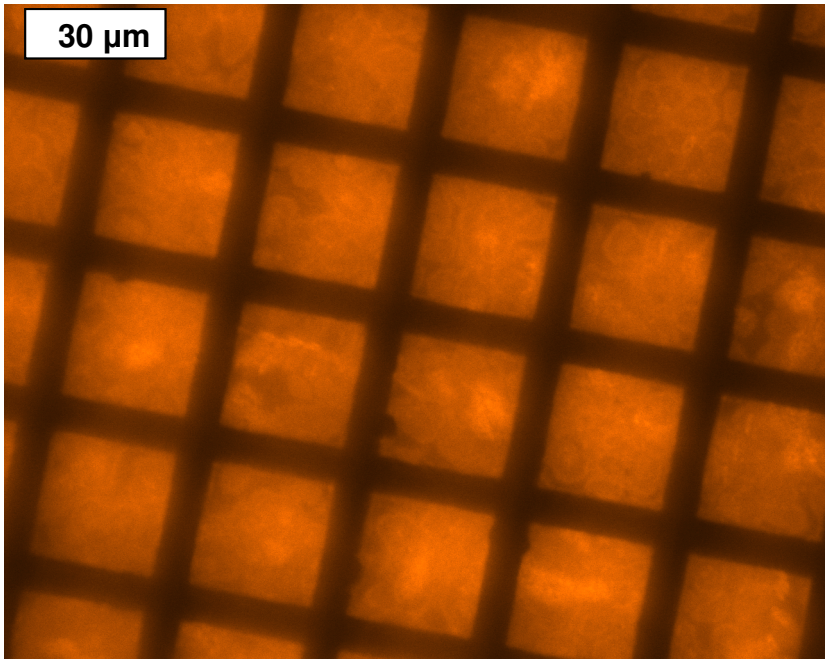

Fig. 3.8 Pseudo colored fluorescence microscope image of photo-patterned polythiophene on a copper substrate.

Chapter 4

Insights on the mechanism of the photochemical and the photo-activated Ullmann coupling processes

4.1 Introduction

In the first half of this chapter mass spectrum, mechanism and kinetics of the photochemical process are discussed. The mass spectrum of the photochemically synthesized polymer is obtained using MALDI-MS (Matrix Assisted Laser Desorption Ionization Mass Spectrometry). Details of the MALDI-MS experiments are provided in the appendix C. Based of the speculated mechanism and the mass spectrum, a stochastic model is developed to explain the trends in the mass spectrum of the photochemically synthesized polythiophene. Further, degree of polymerization and some stochastic parameters representing the mechanism of the polymerization are estimated by comparing the model with the actual mass spectrum

As hypothesized in the third chapter, the copper from the substrate reacts with the photogenerated radicals producing organo-copper intermediates at the interface and these intermediates diffuse from the interface into the monomer film initiating the Ullmann coupling reaction. In the second half of the chapter, experimental evidences supporting this hypothesis are presented and a diffusion-reaction model is developed to explain the extent of mediation of Ullmann coupling reaction as a function of initial monomer thickness.

4.2 Mass spectrum of the photochemically synthesized polymer

Mass spectrum of the photochemically synthesized polythiophene by the process described in Chapter 2 is as shown in Fig. 4.1. The presence of the sharp peaks in the mass spectrum suggests that the polymers are not cross linked. This is consistent with the observation described in Chapter 2 that the photochemically synthesized polymers are soluble in THF. Results below 500 amu are not analyzed because of excessive fragmentation of the polymer during the laser desorption process. A detailed and careful analysis of the mass spectrum results with the help of the molecular mass spreadsheet shown in Fig. 4.2 reveal that the final product consists of distributions of series of polymers. This spreadsheet is calculated considering the average atomic mass, as the mass spectrum results lack the resolution to distinguish between the isotopes of an element. As indicated in Fig. 4.1 the polymer sample consists of series of oligothiophenes with number of iodine substitutions ranging from 1 to ~5 and no of thiophene repeat units ranging from 4 to ~ 11. As shown in Fig. 4.1a, the separation between two peaks within a series of same number of iodine substitution is ~ 82 amu which represents the thiophene repeat unit and as shown in Fig. 4.1b, the separation between two peaks within a series of same number of thiophene repeat units is ~ 125.9 which represents the iodine substitution of hydrogen.

4.3 Mechanism and kinetics of polymerization

The presence of complex series of oligothiophene clearly conveys the fact that there are more than one polymerization pathways. Fig. 4.3 shows the various possible reactions for the formation of dimers from the monomer. Formation of thienyl and iodine

radical on photodissociation of carbon-iodine bond as shown in R1 is well established [1]. These photogenerated radicals will have very high kinetic energy (~ 1eV) and may be quenched by collisions with neighboring molecules. This high kinetic energy may aide reactions with high activation barriers. The photogenerated radicals may undergo substitution reactions and abstraction reactions as shown in R2, R3 and R4, R5 respectively [2-8]. R2 and R3 represent the substitution of iodine and hydrogen, respectively, in a neighboring molecule by the photogenerated thienyl radical. Similarly R4 and R5 represent the abstraction hydrogen and iodine, respectively, by the photogenerated thienyl radical.

Reaction R2 will be highly exothermic as it involves breaking of week carbon-iodine bond (~200KJ/mol) to form strong carbon-carbon bond (~600KJ/mol). Although it is a highly exothermic reaction, the rate of the reaction may not be high if the activation energy of the reaction is high. It may have high activation energy as a repulsive interaction is expected between approaching electron rich thienyl radical and the iodine atom during the process of substitution [9]. Even if this reaction has high activation energy, it cannot be entirely discounted, as some of photogenerated radicals will have a kinetic energy high enough to overcome the activation barrier posed by the repulsive interaction. Compared to R2, R3 will be less exothermic as it involves breaking of carbon-hydrogen bond (~300KJ/mol) to form carbon-carbon bond (~600KJ/mol). R3 may have lower activation energy than R2 as the repulsive interaction from a hydrogen atom will be lesser than an iodine atom. R4 is a well established hydrogen abstraction reaction and may be highly probable. R5 is a null reaction as the reactants and the products are same. Based on Fig. 4.3, only R2 and R3 forms dimers and R4 is just a

radical exchange reaction. But the iodothiophene product of R4 can react with the photogenerated thienyl radical forming α-α' coupled dimers as shown in R6; this reaction has been proven to readily occur in solution-phase studies [10]. α-α' coupled dimers may also be produced by radical-radical recombination reactions shown in R7 [11]. In addition to the reactions of thienyl radical, the photogenerated iodine atom can be involved in various reactions producing dimers as shown in Fig. 4.4. Although the reactions shown in Fig 4.3 and 4.4 describe formation of dimers from the monomer, similar reactions can be used to explain the formation trimers, tetramers, so on. Essentially the overall photochemical process can be considered as a step polymerization reaction, with every step initiated by the photogenerated radicals. Assuming that hydrogen substitution (R3) and abstraction (R4 & R6) are the dominant reactions for polymerization, it can be said that for every carbon-iodine bond broken, one carbon-carbon bond will be formed along with one hydrogen iodide molecule. (Note: this assumption may not be always valid because sometimes two carbon-iodine bonds will be broken to form one carbon-carbon bond and one iodine molecule, as in the reactions R2 and R7 of Fig. 4.3) Number average degree of polymerization ($\overline{X}_n$) is given as the total number of monomers molecules initially present (N_o) divided by the total number of molecules present at time t (N_t) [12]. So,

$$\overline{X}_n = \frac{N_o}{N_t}$$

If, M is the concentration of carbon-iodine bond at any time t, M_o is the initial concentration of carbon-iodine bond and V is the total volume of the reactor, then by

assuming that one carbon-carbon bond is formed for every carbon-iodine bond broken, we get,

$$N_o = \frac{M_o * V}{2}; N_t = \left[\frac{M_o}{2} - (M_o - M_t)\right] * V$$

$$\overline{X_n} = \frac{M_o/2}{\left[\frac{M_o}{2} - (M_o - M_t)\right]} = \frac{M_o}{[2 * M_t - M_o]} = \frac{1}{\left[2 * M_t/M_o - 1\right]}$$

If, p is the extent of reaction based on carbon-iodine bond then,

$$\overline{X_n} = \frac{1}{[2 * (1-p) - 1]} = \frac{1}{[1 - 2p]} \qquad \text{Eqn 4.1}$$

From R1 of Fig. 4.3, the rate of carbon-iodine bond dissociation will be directly proportional to the intensity of the photons. Assuming that the rate of radical (thienyl and iodine) recombination is nearly zero, the rate of carbon-iodine bond consumption will be directly proportional to the intensity of light. Accumulation of the radicals and the recombination of these radicals will be negligible, if radicals are consumed immediately by the subsequent polymerization reactions (R2, R3, and R6 of Fig. 4.3). If *M* is the concentration of carbon-iodine bond at any time, then,

$$\frac{-dM}{dt} = K_1[Intensity]$$

Integrating from time t = 0 to t,

$$M_o - M = K_1[Intensity]t$$

So the relation between the extent of reaction *p* of carbon-iodine bond and time is,

$$p = \frac{K_1[Intensity]t}{M_o}$$

Usually, as the extent of reaction increases, the polymerization kinetics is slowed down because of limited mobility (diffusion limited kinetics due to increase in viscosity). Once this stage is reached, the rate of carbon-iodine consumption is determined by the rate of loss of radicals by the polymerization steps (R2, R3, and R6 of Fig. 4.3).

4.4 Stochastic model for the mass spectrum

In this section, a stochastic model is developed to explain the mass spectrum or the number average distribution of the photochemically synthesized polythiophene. This derivation is just an extension of the Flory's work on the number average distribution of linear step polymerization [13]. Flory's derivation is shown pictorially in Fig. 4.5 and the explanation is as follows,

If p is the extent of reaction based on carbon-carbon bond formation, then the probability of finding a reacted monomer is *p* and the probability of finding an unreacted monomer is 1-*p*. A reacted monomer can be defined as a monomer that formed a carbon-carbon with another monomer or in other words, a monomer that is linked to another monomer. An X-mer is formed when X-1 monomers react consecutively and terminates with an unreacted monomer. So the probability of forming an X-mer (P_x) is given by,

$$P_X = p^{X-1}(1-p) \qquad \text{Eqn 4.2}$$

Structural characterization techniques used so far cannot reveal the presence of branching in the photochemically synthesized polythiophene, so as a first approximation it is assumed that all the polymer chains are linear. On this assumption, Eqn. 4.2 can be used to describe the number average distribution of the photochemically synthesized polythiophene.

As can be seen from the mechanism shown in Fig. 4.3 and 4.4 , the monomer unit of the polymer can be one of the following – thiophene with two iodine units (ThI_2) or thiophene with one iodine (ThI) or just thiophene (Th). An X-mer from the sample can be made out of any of the three monomeric units. For example, a 3-mer can be Th-Th-Th or Th-Th-ThI or Th-Th-ThI_2 or ThI-ThI-ThI or ThI-ThI-ThI_2 and so on. So just the X-mer will have a distribution of molecular masses depending on the number of iodines it carries. Lets say at some point during the polymerization, the probability of finding a ThI_2, ThI and Th in the polymer sample are *a*, *b*, and *c* respectively. Number of species of X-mer will be equal to total number of terms in the trinomial expansion of $(a+b+c)^X$, which is equal to $\frac{(X+1)(X+2)}{2}$.

Probability of an X-mer having *n* ThI groups and *m* Th groups is given by,

$$M_{n,m} = \frac{X!}{(X-n-m)!n!m!} a^{(X-n-m)} b^n c^m \qquad \text{Eqn 4.3}$$

Where, n and m can vary from 0 to X.

In summary, Eqn 4.2 gives the probability of finding an X-mer and Eqn 4.3 gives the probability of that X-mer having *n* ThI monomeric units and *m* Th monomeric units. So, the overall probability of finding a polymer chain with *n* ThI monomeric units, *m* Th monomeric units and *X-n-m* ThI_2 monomeric is given by the product of Eqn 4.2 and Eqn 4.3.

$$P_{X-n-m,n,m} = p^{(X-1)}(1-p)\frac{X!}{(X-n-m)!n!m!} a^{(X-n-m)} b^n c^m \qquad \text{Eqn 4.4}$$

The polymerization may start from thiophene with two iodine units (as in R3 of Fig. 4.3), but the chain elongation steps mainly consists of either an addition of an iodothiophene or

thiophene unit. So, as the chain gets longer the probability of finding a ThI_2 in the chain drops very quickly. In other words, probability of finding a ThI_2 monomeric unit is a sharply decreasing function of X. For X=1, that is in a pure monomer all the units are just ThI_2, so a = 1, b + c = 0. For X > 5, it can be assumed that a = 0, b + c = 1. Thus for X>5, Eqn 4.4 becomes,

$$P_{X-k,k} = p^{(X-1)}(1-p)\frac{X!}{k!(X-k)!}b^k c^{(X-k)} \qquad \text{Eqn 4.5}$$

Where *k* is the number of ThI units and *X*-*k* is the number of Th units.

Eqn 4.5 is fitted to the experimental mass spectrum and the results are shown in Fig. 4.6. The extent of reaction based on carbon-carbon formation is found to be 0.66 and probability of finding a Th and ThI in the chain are 0.63 and 0.37 respectively. Assuming that one carbon-carbon bond is formed for every carbon-iodine bond broken, we can say that the extent of reaction based on carbon-iodine bond is 0.33. For p = 0.33, the number average degree of polymerization ($\overline{X}_n$) is calculated to be ~3 based on Eqn. 4.1. Mass spectrum of the polymers irradiated longer are shown in appendix C. Increasing the irradiation time doesn't change the extent of reaction significantly indicating a diffusion limited kinetics. As the polymerization progresses, the concentration of polymer increases, hence the viscosity increases and so the mobility of radicals (and other reacting species) decreases. As the mobility of the radicals decreases, the rate of polymerization drops and the rate eventually becomes zero when the diffusion constant of radicals become too low compared to experimental time frame. When the rate of polymerization becomes zero, the extent of polymerization will reach a saturation value as indicated by the mass spectrum results.

4.5 Diffusion-reaction model to predict the extent of copper mediation

As hypothesized in the third chapter, the copper from the substrate reacts with the photogenerated radicals producing organo-copper intermediates at the interface and these intermediates diffuse from the interface into the monomer film initiating the Ullmann coupling reaction. Based on this hypothesis, we expect the extent of mediation of Ullmann coupling reaction in the bulk photochemical reaction to decrease with an increase in the thickness of the monomer film. Also, we know that the thickness of the final polymer film is directly dependant on the initial monomer film thickness. Thus, as the polymer film becomes thinner, the extent of mediation of Ullmann coupling reaction should be greater.

The following experimental observations show an increase in the extent of mediation of Ullmann coupling reaction with a decrease in the polymer thickness thus lending a strong support to the above mentioned hypothesis. Firstly, we observe that PL (photoluminescence) emission maximum red shifts as the thickness of polymer film decreases, as shown in the Fig 4.7. This observation is consistent with our expectation that the extent of mediation of Ullmann coupling reaction should be greater in thinner polymer films. As the extent of Ullmann coupling reaction increases the extent of α-α' coupling in the final polymer product increases, thus the emission maximum from the final polymer product is red shifted. PL emission maximum of the polythiophene film (photochemically synthesized on a copper substarte) of thickness ~100nm, ~250nm and ~550nm are found to be ~ 610nm (Orange red), ~575nm (yellow), ~ 540nm (greenish yellow) respectively. The second experimental evidence comes from the surface

elemental composition analysis of the polythiophene films of varying thickness using XPS. Consistent with the expectation, Cu/C atomic ratio decreases with the increase in the polymer thickness. Surface Cu/C ratio of the polythiophene film of thickness ~ 100nm, 250nm and 550nm are found to be 0.8, 0.15, and 0.02 respectively. Again, the third experimental evidence comes from the high resolution XPS of I $3d_{5/2}$ region from the polymer of varying thickness. As discussed in the third chapter, the byproduct of Ullmann coupling reaction is copper iodide and as the extent of mediation of Ullmann coupling reaction increases the presence of iodide increases. As shown in the Fig. 4.8, in the 100nm film most of the iodine left behind is in the form of iodide, in the 250nm film the ratio of iodine as C-I bond to the iodine as iodide is about 0.6:0.4 and in the 550nm film most of iodine left behind is in the form C-I bond.

Diffusion reaction model to explain the mediation of Ullmann coupling in the bulk photochemical reaction is as follows. As mentioned previously, the copper from the substrate reacts with the photogenerated radicals producing organo-copper intermediates at the interface and these intermediates diffuse from the interface into the monomer film initiating the Ullmann coupling reaction. The schematic of the process is shown in Fig. 4.9. This process is modeled by the one dimensional diffusion reaction model [14]:

$$D_{l,t}\frac{\partial^2 C_{l,t}}{\partial l^2} = \frac{\partial C_{l,t}}{\partial t} + KC_{l,t} \qquad \text{Eqn. 4.6}$$

Where $C_{l,t}$ is the concentration of the organo-copper intermediates in the monomer film, D is the diffusion constant of the intermediates in the monomer film, K is the rate constant for the reaction between the organo-copper intermediate and the monomer (or any n-mer). The boundary conditions are that the concentration of organo-copper intermediates is constant at l = 0 (i.e. copper surface) and there is no loss or flux of the

intermediates at l = L (surface of the monomer). The initial condition is that the concentration of the intermediates is zero through out the monomer film.

$$B.C's$$

$$C_{l=0,t} = C*$$

$$\left(\frac{\partial C}{\partial l}\right)_{l=L,t} = 0$$

$$I.C's$$

$$C_{l,t=0} = 0$$

Dimensionless form of Eqn. 4.6 and the boundary and initial conditions are,

$$x = \frac{l}{L}; t' = \frac{Dt}{L^2}; K' = \frac{KL^2}{D}; C_{x,t} = \frac{C_{l,t}}{C*}$$

$$\frac{\partial^2 C_{x,t'}}{\partial x^2} = \frac{\partial C_{x,t'}}{\partial t'} + K' C_{x,t'}$$

$$B.C's$$

$$C_{x=0,t'} = 1$$

$$\left(\frac{\partial C}{\partial l}\right)_{x=1,t'} = 0$$

$$I.C's$$

$$C_{x,t'=0} = 0$$

Monomer thickness (L) has effect on the extent of mediation of Ullmann coupling reaction for the following reasons. First the boundary condition at the copper interface i.e., concentration of the organo-copper intermediates depends on the thickness of the monomer film. Second the average diffusion constant of the intermediates in the monomer film depends on the monomer film thickness. These aspects are discussed in detail and captured mathematically in the following paragraphs.

Assuming that all the radicals near the surface react with the copper, the concentration of organo-copper intermediates produced at the surface is directly proportional to the radical concentration near the surface of copper. The radical

concentration at the copper surface depends on the intensity of photons at the surface of copper. The intensity of photons at the surface of copper can be found using the Lambert-Beer's law and the intensity of photons at the copper surface depends on the intensity of the photons at the surface of the monomer (I_o), monomer thickness (L), concentration of monomer (c) and extinction coefficient of the monomer (e). Photons reflected from the substrate are neglected in this model. Decrease in the intensity of photon is schematically shown Fig. 4.9. The extinction coefficient is estimated from UV-Vis measurements and the details are discussed in appendix C. One of the important assumptions in determining the concentration of organo-copper species is that radicals generated in the bulk of the monomer reacts immediately with other monomers rather than diffusing towards the copper surface. So the dimensionless concentration of organo-copper is related to the monomer thickness (l) by the following relation.

$$C_{organo-copper} = C^* = \frac{I_o 10^{-ecL}}{I_o}$$

Substituting the numerical values for extinction coefficient (e = 7.8 * 10^6 cm^2/mol) and concentration of solid film of monomer (c = 0.00253 mol/cm^3), we get

$$C^* = 10^{-19734L} \qquad \text{Eqn 4.7}$$

where L is the thickness of the monomer in cm.

As mentioned briefly in Chapter 3, the diffusion of organo-copper species is facilitated by liquid formation during the UV irradiation of monomer. This liquid formation has been experimentally observed using an optical microscope. This liquid formation may be due to photodissociation reaction (R1 and R4 of Fig. 4.3) that generates iodothiophene which is a liquid at room temperature. Thus, the diffusion constant of the intermediates in the monomer film will depend on the concentration of iodothiophene in

the film. The concentration of iodothiophene at any point depends on the intensity of photons at that point. As discussed in the previous paragraph, the intensity of photon at the surface of copper decreases exponentially with increase in the monomer film thickness. Thus, as the monomer film thickness increases, the local diffusion constant at the surface of copper decreases exponentially.

$$D_{coppersurface} = D_0 10^{-19734L}$$

As soon as the UV light is shined, a gradient in the concentration of iodothiophene will be created. But, this concentration gradient will be evened out as the iodothiophene diffuses. Thus in order to capture more realistic picture an averaged diffusion constant is used. This average value varies with film thickness (L) as,

$$D_{avg} = \frac{\int_0^L D_o 10^{-19734l}\, dl}{\int_0^L dl} \qquad \text{Eqn 4.8}$$

$$D_{avg} = \frac{D_o[1-10^{-19734L}]}{19734L\ln 10}$$

For the numerical solution D_o is assumed to be 10^{-6} cm^2/sec which is at lower end of typical diffusion constant in liquids.

In the model developed, the diffusion constant is assumed to be independent of time, but in reality this may not be the case for a polymerization reaction. In general, as polymerization reaction progresses, the viscosity of the system increases hence the diffusion constant decreases with time. In the particular case of conducting polymers, these effects may be more drastic than in conventional polymers due very high intermolecular packing forces. One of the important parameters in the model that determine the rate of polymerization is K′; if K′ is very high then the polymer will form

immediately in the vicinity of the copper preventing further diffusion of the intermediates. We experimentally observe that copper effect is significant even in 200nm thick monomer films. So, the K' should be comparable to the D/L^2. For numerical solution purpose, K′ is assumed to be 1 for the monomer thickness of 100nm. Also the rate of polymerization in the bulk is probably slow, because if it is not slow, diffusion of organo-copper intermediates would have been prevented by increase in viscosity. Bulk polymerization step may involve series of reactions such as R4 and R6, and the initial rate of polymerization will be slow in this case because initial concentration of iodothiophene is zero.

For any monomer thickness L, boundary condition at copper surface is calculated using Eqn. 4.7 and the average diffusion constant is calculated using Eqn. 4.8. Fig. 4.10 shows the plot of dimensionless average diffusion constant (D_{avg}/D_o) and concentration of organo-copper intermediates at the surface of copper (C*) versus monomer film thickness (L). Using these values, equation 4.1 is numerically solved employing the implicit finite difference with a time and space discretization of 0.001 and 0.01 [15] and total time of 0.1 sec. For the D ~10^{-6} cm^2/sec and L ~ 10^{-5} cm, steady state will be reached on the order of 10^{-3} sec. So, total time of 0.1sec is enough to capture the steady state observations. The monomer thickness was varied (L = 100nm, 150nm, 250nm, 550nm) and the concentration of reacted organo-copper species at each point along the polymer thickness for each L during the total time of 0.1 sec is calculated. Concentration of reacted organo-copper species at any point x is given by $\int_o^{t'} K' C_{x,t} dt'$. Table 4.1 summarizes the boundary conditions, diffusion and reaction constants used for various L.

Concentration of reacted organo-species quantitatively represents the extent of mediation of Ullmann coupling reaction. The results of numerical solution showing the concentration profile for various initial monomer thicknesses is shown in Fig. 4.11. The results are qualitatively consistent with the experimental observations showing that the extent of mediation of Ullmann coupling reaction is greater as the polymer film is thinner.

4.6 References

[1] Elisei, F.; Latterini,L.; Aloisi,G.G.; D'Auria, M. *J. Phys. Chem.* **1995**, *99*, 5365, and references cited therein.

[2] Martelli, G.; Spagnolo, P; Tiecco, M. *J. Chem. Soc. B* **1968**, 901.

[3] Dermer, O.C; Edmison, M.T *Chem. Rev.* **1957**, *57*, 77.

[4] Bunnett, J.F.; Wamser, C.C. *J. Amer Chem. Soc.* **1966**, *88*, 5534.

[5] Dannley, R.L.; Gregg, Jr. E.C.; Phelps, R.E.; Coleman, C.B. J. Amer. Chem. Soc. **1954**, *76*, 445.

[6] Danen,W.C.; Saunders, D.G.; Rose, K.A *J. Amer Chem. Soc* **1973**, *95*, 1612.

[7] Burkey, T.J.; Griller, D.; Lunazzi, L.; Nazran, A.S. *J. Org. Chem.* **1983**, *48*, 3704.

[8] Lunazzi, L.; Placucci, G. J. Chem. Soc. Perkin. Trans. II **1982**, 875.

[9] Fox, R.J; Evans, F.W.; Szwarc, M. *Transactions of the Faraday Soc.* **1961**, *57*, 1915

[10] D'Auria, M. *Gazzetta Chimica Italiana* **1989**, *119*, 419

[11] Park, J.; Lin, M.C. *J. Phys. Chem.* **1997**, *101*, 14.

[12] Odian, G.G. *Principles of Polymerization* **2004**, 4th edition, Wiley, New York.

[13] Flory, P.J. *Principles of Polymer Chemistry*; Cornell University Press **1953**.

[14] Bird, R.B.; Stewart, W.E.; Lightfoot E.N. *Transport Phenomena*; Wiley, Singapore **1994**.

[15] Duda, J.L. *Penn State ChE 546 course notes* **2001.**

Monomer Thickness (L) (* 10^{-7} cm)	Concentration of organo-copper intermediates at the interface (C*)	D_{avg}/D_o ($D_0 = 10^{-6}$ cm^2/sec)	Dimensionless time (for t = 0.1secs)	Dimensionless reaction constant (K′)
100	0.65	0.8	800	1
150	0.5	0.7	311	2.6
250	0.35	0.6	96	8.3
550	0.1	0.35	12	69

Table 4.1 Parameters used for various monomer thickness (L).

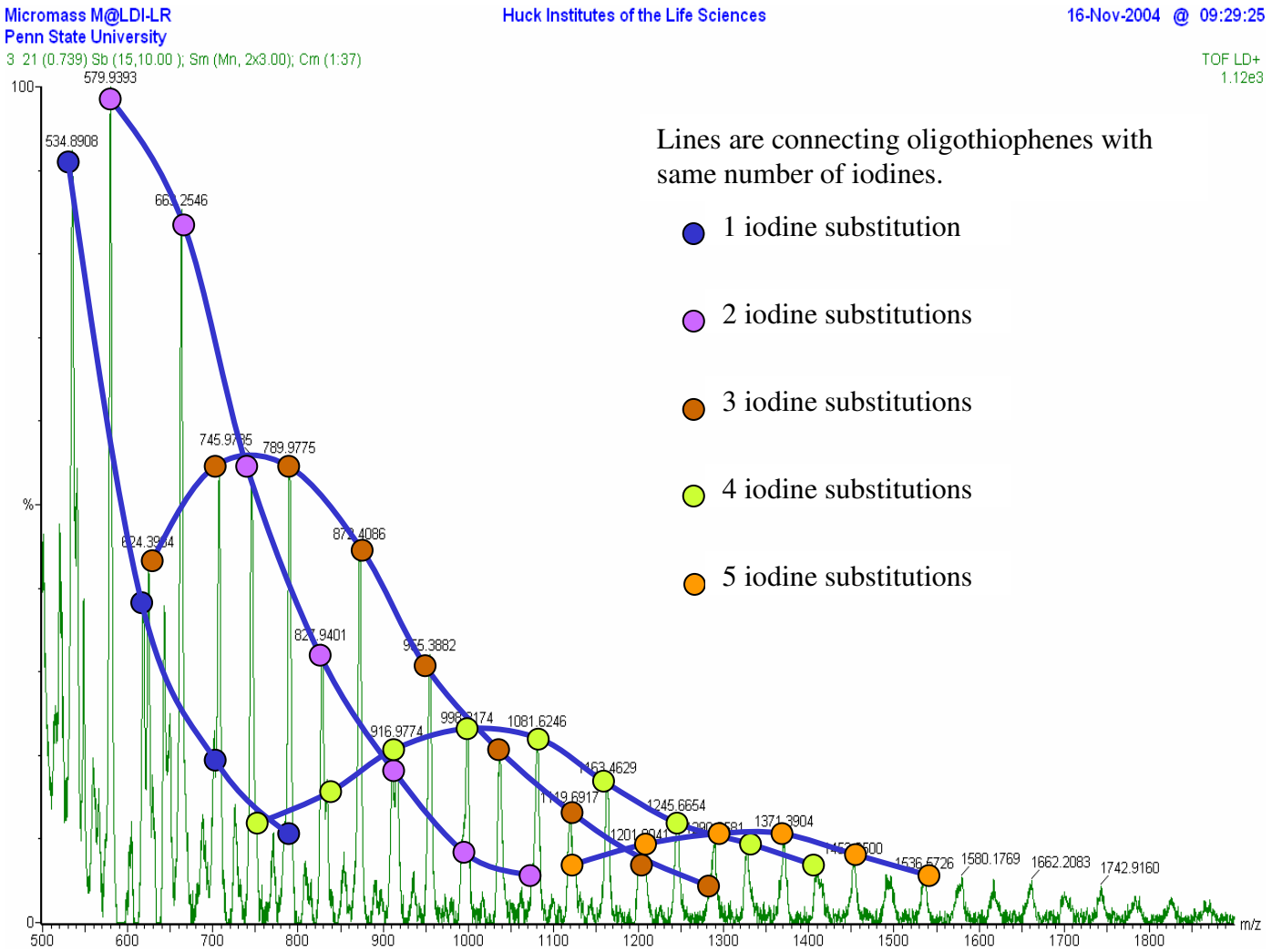

Fig. 4.1 a) MALDI-MS of photochemically synthesized polythiophene film (Lines are connecting oligothiophenes with same number of iodines).

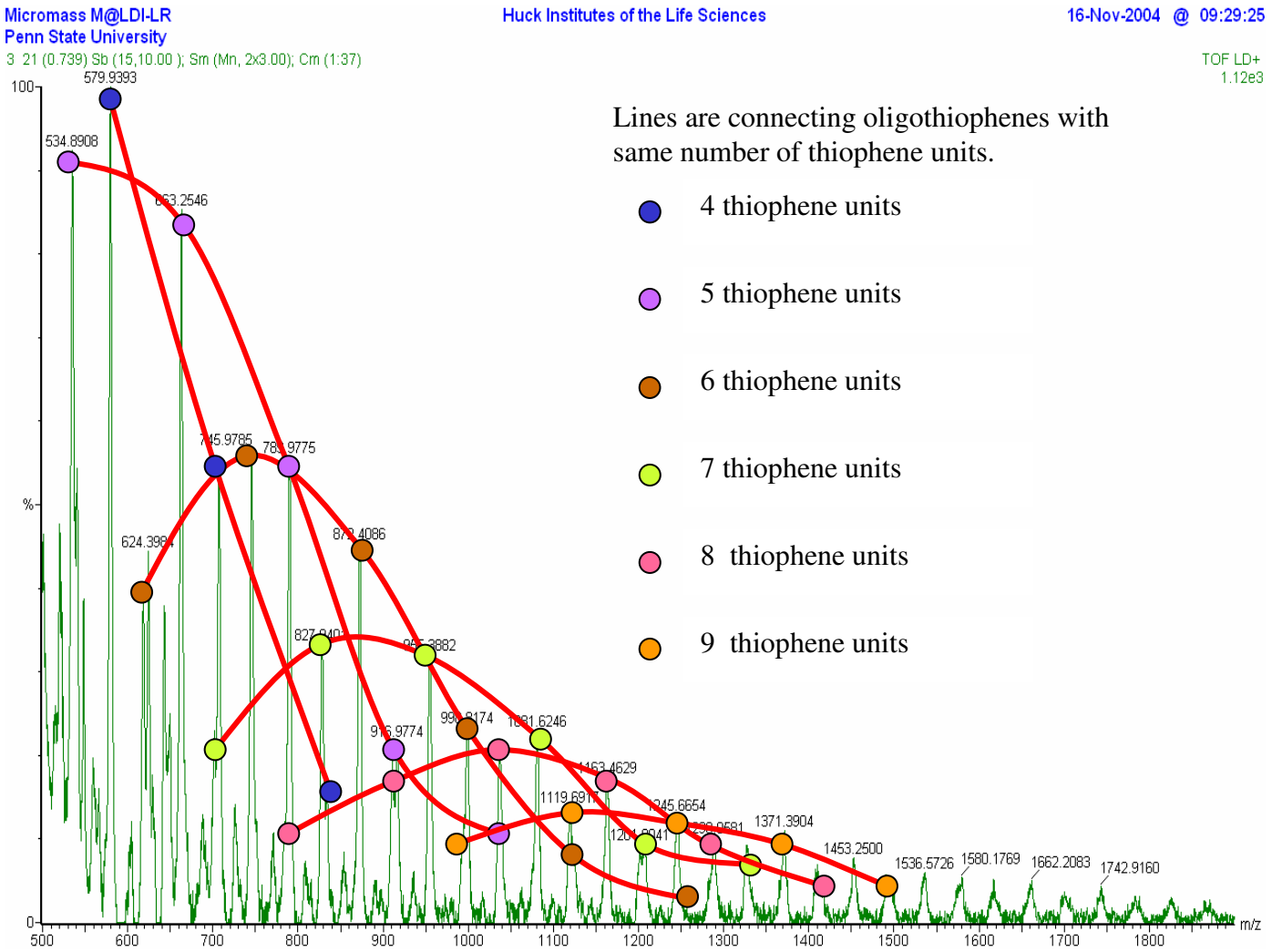

Fig. 4.1 b) MALDI-MS of photochemically synthesized polythiophene film. (Lines are connecting oligothiophenes with same number of thiophene repeat units)

Iodine atoms	0.0	1.0	2.0	3.0	4.0	5.0	6.0	7.0	8.0	9.0	10.0
Thienyl units											
1	84.1	210.0	335.9	461.8	587.7						
2	166.3	292.2	418.1	544.0	669.8	795.7	921.6				
3	248.4	374.3	500.2	626.1	752.0	877.9	1003.8	1129.7	1255.6		
4	330.5	456.4	582.3	708.2	834.1	960.0	1085.9	1211.8	1337.7	1463.6	1589.5
5	412.6	538.5	664.4	790.3	916.2	1042.1	1168.0	1293.9	1419.8	1545.7	1671.6
6	494.8	620.7	746.6	872.4	998.3	1124.2	1250.1	1376.0	1501.9	1627.8	1753.7
7	576.9	702.8	828.7	954.6	1080.5	1206.4	1332.3	1458.2	1584.1	1709.9	1835.8
8	659.0	784.9	910.8	1036.7	1162.6	1288.5	1414.4	1540.3	1666.2	1792.1	1918.0
9	741.1	867.0	992.9	1118.8	1244.7	1370.6	1496.5	1622.4	1748.3	1874.2	2000.1
10	823.3	949.2	1075.0	1200.9	1326.8	1452.7	1578.6	1704.5	1830.4	1956.3	2082.2
11	905.4	1031.3	1157.2	1283.1	1409.0	1534.9	1660.8	1786.6	1912.5	2038.4	2164.3
12	987.5	1113.4	1239.3	1365.2	1491.1	1617.0	1742.9	1868.8	1994.7	2120.6	2246.5
13	1069.6	1195.5	1321.4	1447.3	1573.2	1699.1	1825.0	1950.9	2076.8	2202.7	2328.6
14	1151.7	1277.6	1403.5	1529.4	1655.3	1781.2	1907.1	2033.0	2158.9	2284.8	2410.7
15	1233.9	1359.8	1485.7	1611.6	1737.5	1863.4	1989.2	2115.1	2241.0	2366.9	2492.8
16	1316.0	1441.9	1567.8	1693.7	1819.6	1945.5	2071.4	2197.3	2323.2	2449.1	2575.0

Fig. 4.2 Spreadsheet to calculate the molecular mass of the oligothiophenes with varying number of iodine substitutions. Highlighted molecular masses represent the locations of the prominent peaks in the experimental result shown in Fig. 4.1.

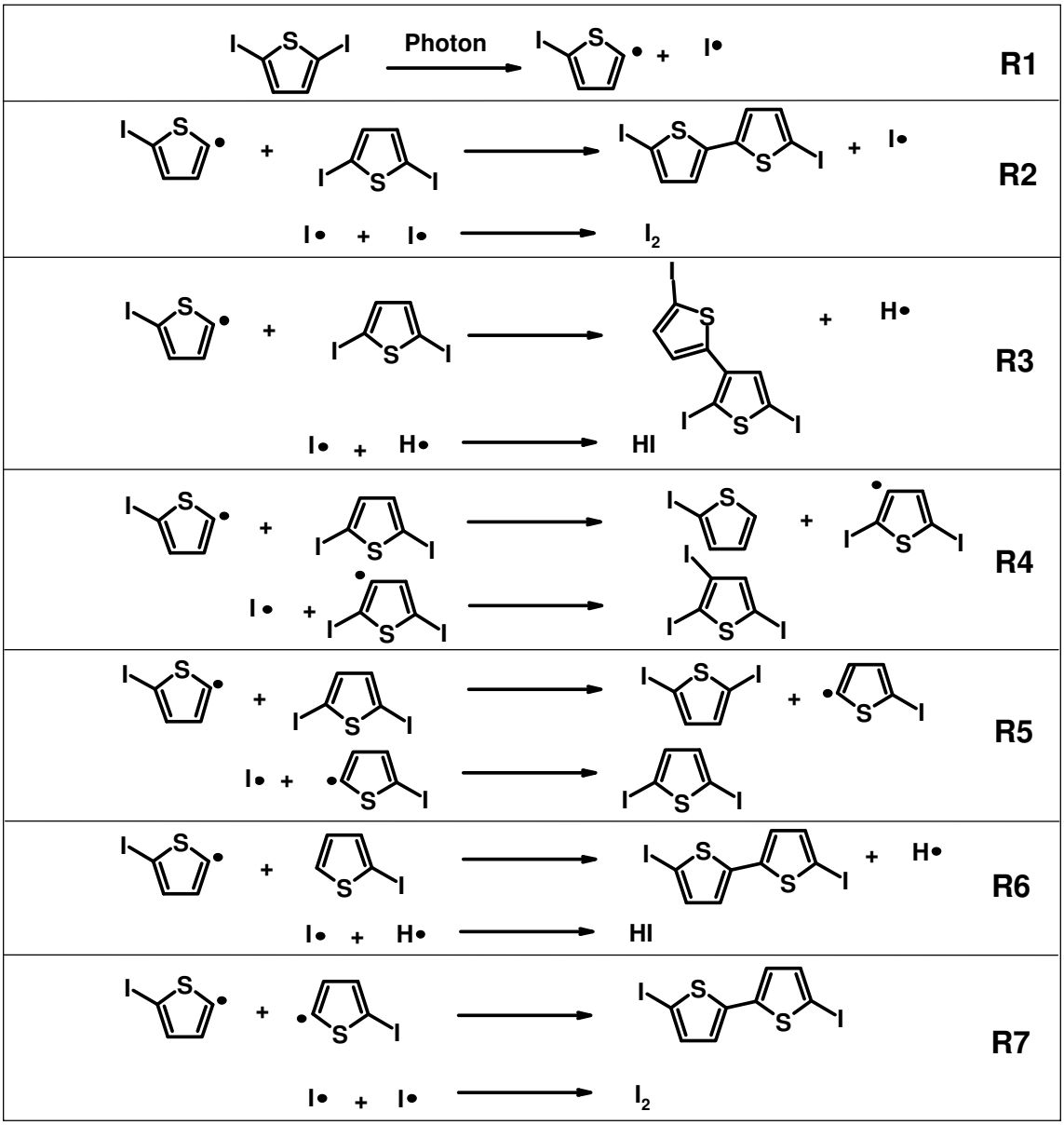

Fig. 4.3 Reactions of photo-generated thienyl radical.

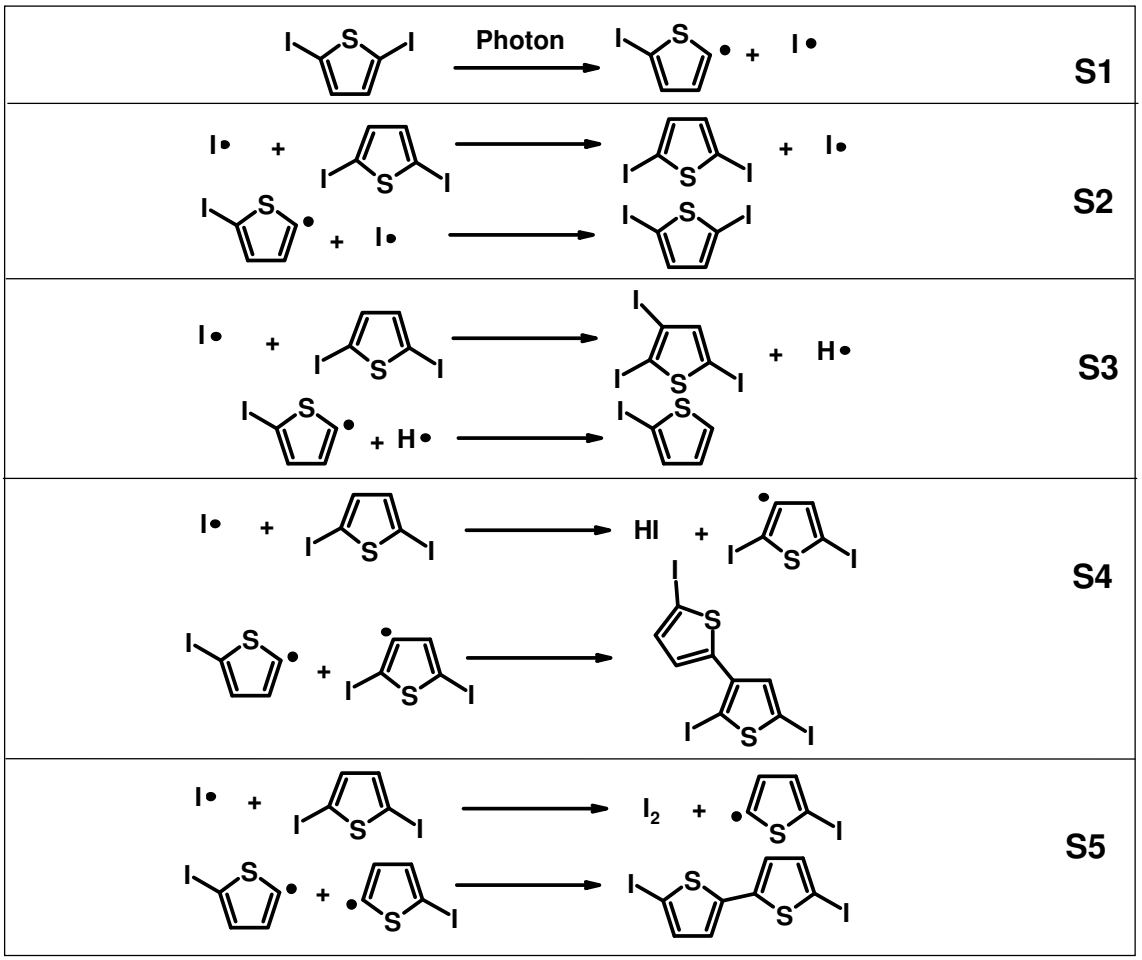

Fig. 4.4 Reactions of photo-generated iodine radical.

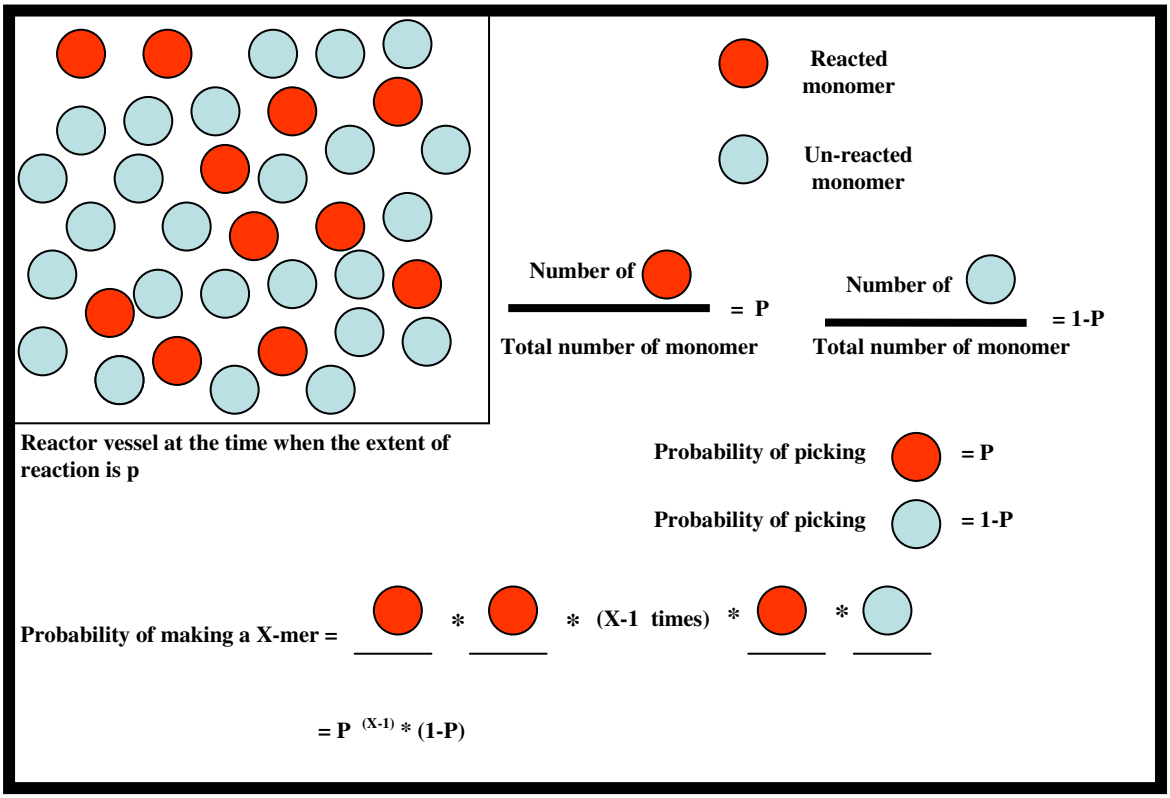

Fig. 4.5 Flory's derivation for number average distribution in a linear condensation (or step) polymer

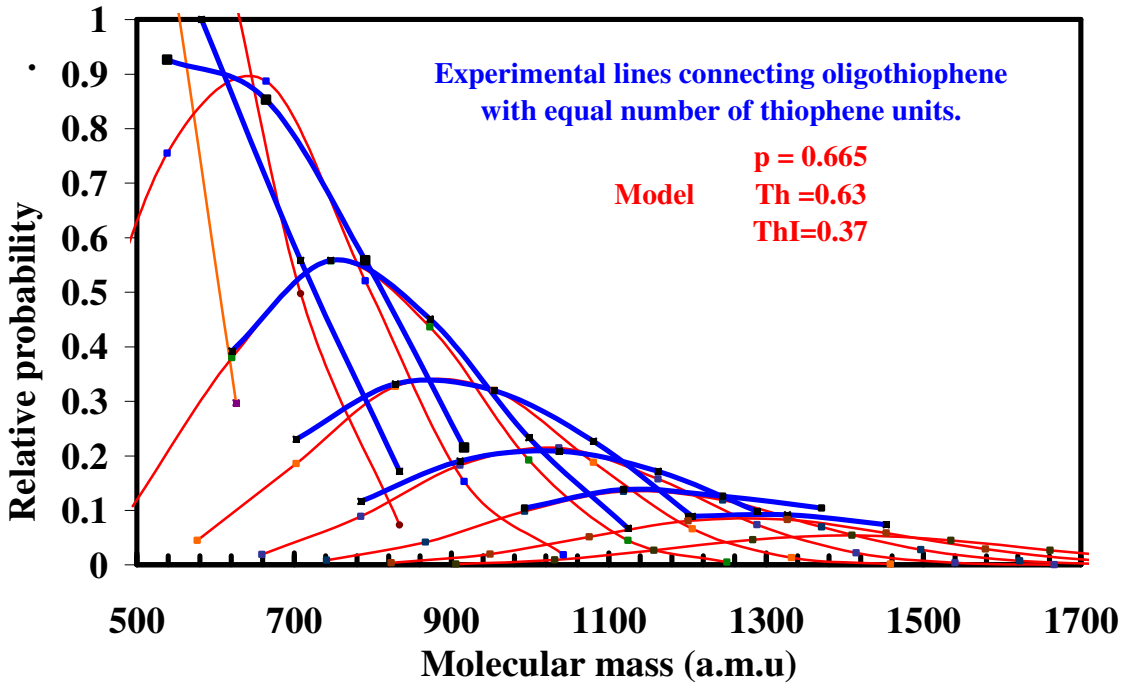

Fig. 4.6 Plot showing the experimental mass spectrum of the polythiophene sample and the prediction based on equation 4.4. Extent of reaction is 0.665 and the probability of finding a Th and ThI are 0.63 and 0.37 respectively.

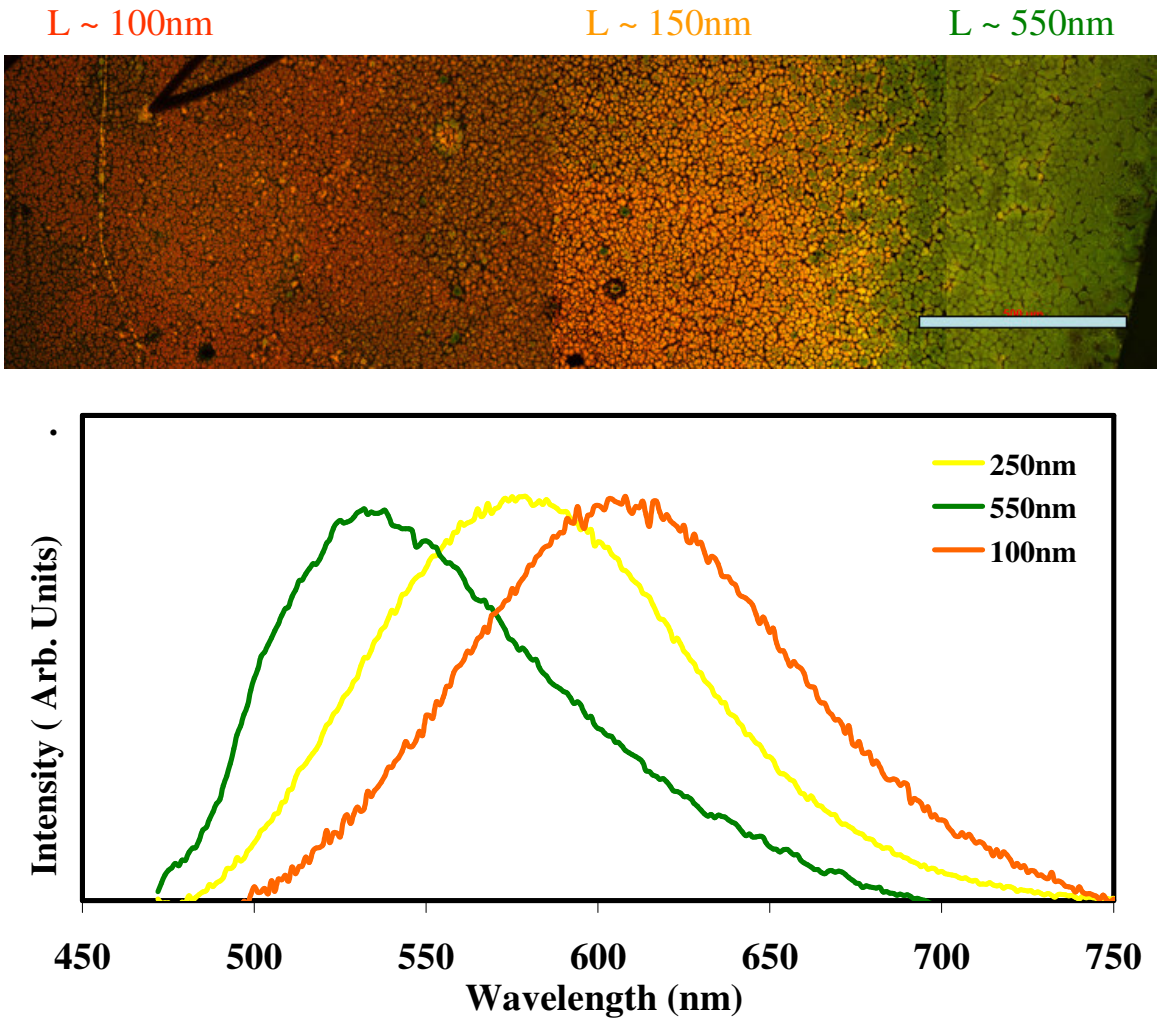

Fig. 4.7 Photoluminescence (PL) emission redshifts with the decrease in the thickness of the polythiophene film synthesized on copper. Top – Pseudo colored PL image showing the redshift. Bottom – Spectroscopic data confirming the redshift.

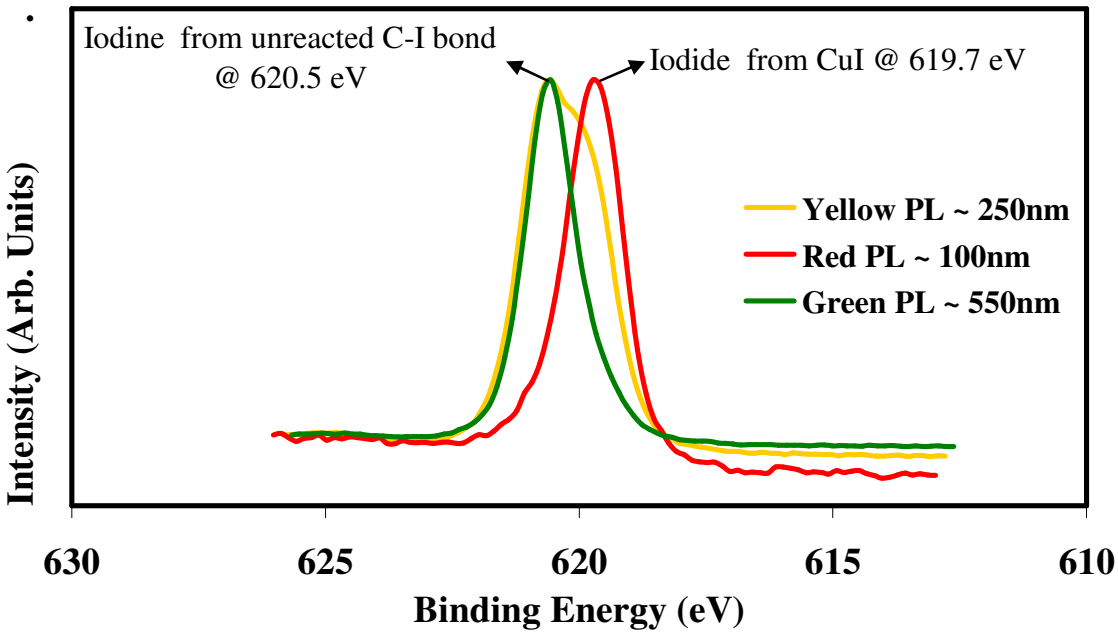

Fig. 4.8 High resolution XPS of I $3d_{5/2}$ region showing the increase in the iodide content with the decrease in the polythiophene film thickness. Iodide content is a representative of the extent of mediation of Ullmann coupling reaction.

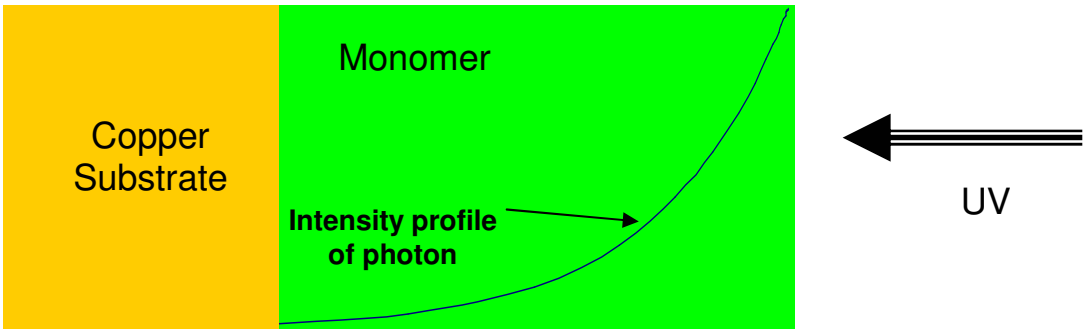

Fig. 4.9 Schematics of the photo-activated Ullmann coupling. Concentration of organo-copper intermediates depends on the intensity of photons reaching the surface of copper.

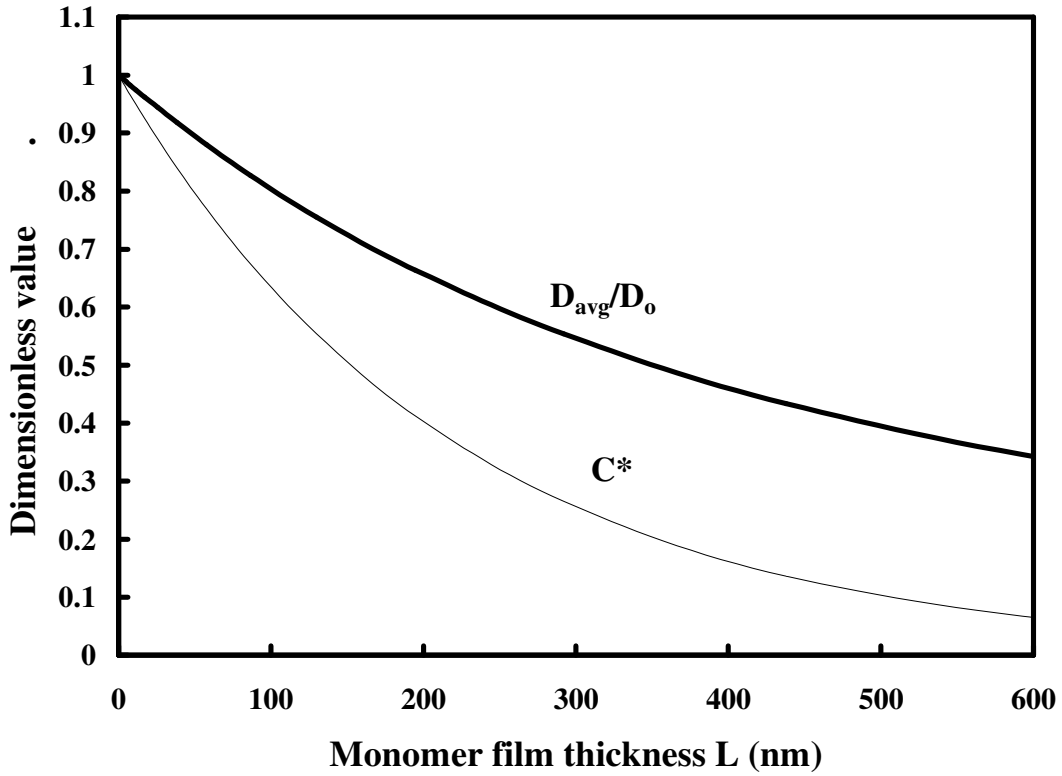

Fig. 4.10 Dimensionless average diffusion constant (D_{avg}/D_o) and concentration of organo-copper intermediates at the surface of copper (C*) versus monomer film thickness (L).

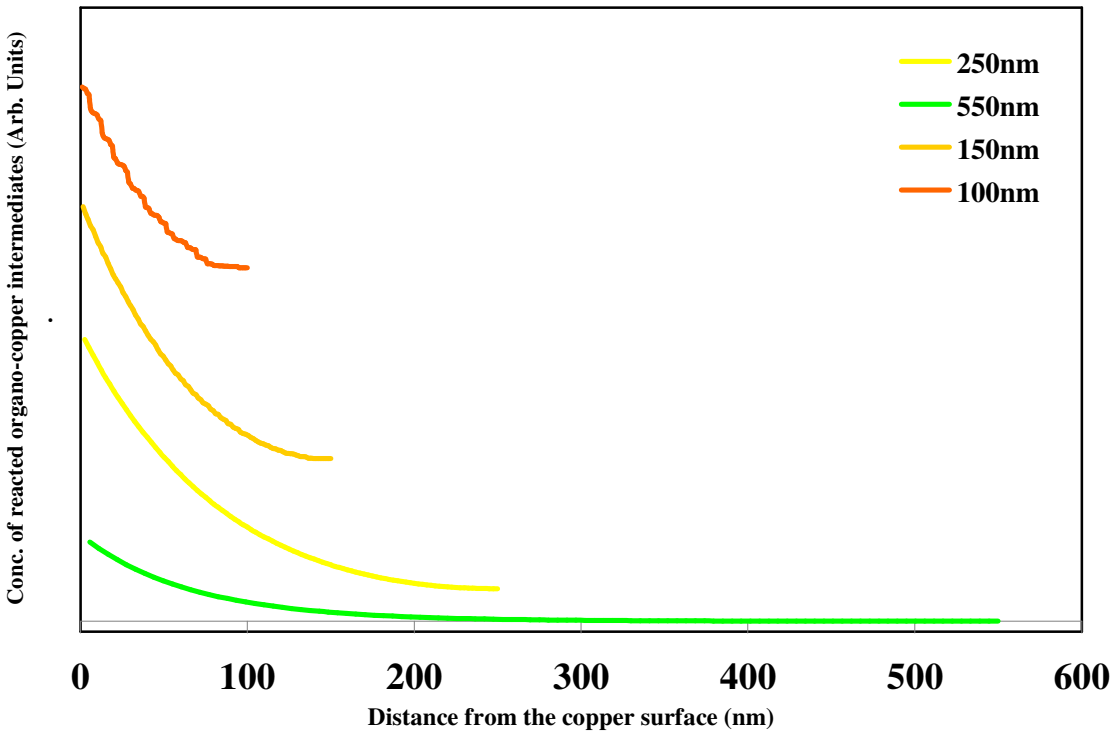

Fig. 4.11 Results of numerical solution of diffusion-reaction model capturing the effect of thickness on the extent of mediation of Ullmann coupling reaction. As the thickness decreases, the concentration of reacted organo-copper intermediates or the extent of mediation of Ullmann coupling increases.

Chapter 5

Mask-less fabrication of polythiophene patterns by photochemical conversion of the regio-selectively condensed 2,5-diiodothiophene

5.1 Introduction

In this chapter, a mask-less technique for the fabrication of periodic patterns of polythiophene is described. This mask-less approach utilizes regio-selective condensation of monomer on the chemically patterned substrate surfaces containing periodic arrays of wettable regions surrounded by non-wettable regions. This condensed monomer pattern is then irradiated with UV light to convert them into polythiophene by the process described in the second chapter. Since the monomer is confined in specific regions on the substrate, the polymer patterns can be produced at those locations by blanket irradiation of UV light without a mask. Effects of wettability contrast and the dimension of the periodicity on pattern recognition during the monomer deposition are discussed.

The wettability patterned substrates have been utilized for selective condensation of liquids or selective dewetting of polymer thin films on the wettability-patterned substrate surfaces [1-13]. The same process can be employed for production of conjugated polymer patterns. General procedure for regio-selective synthesis of polythiophene is as follows. The first step is the generation of wettability patterns on the substrate using the self-assembled monolayer (SAM) chemistry. Then the monomer is vapor deposited on the patterned substrate, leading to selective condensation of the monomer at the more wettable regions. Finally, these monomer patterns are

photochemically converted into polymer patterns by the process described in the second chapter.

Two conditions should be met for this approach to be successful. First, the monomer molecules deposited on the substrate should have enough mobility so they can migrate until they find the minimum energy regions or in other words, more wettable regions. Secondly, there should be proper surface modifiers that will generate a high enough wettability contrast for selective aggregation of monomers on the substrate. 2,5-diiodothiophene is used for regio-selective growth of polythiophene on a gold surface as it satisfies these two criteria. 2,5-diiodothiophene is a solid with a melting temperature of 34 ^{o}C. Since the difference between the substrate temperature (room temperature ~ 35 ^{o}C) and the bulk melting temperature is only ~10^{o}C, molecules that land on the substrate surface will have sufficient mobility until they find regions with minimum free energy. As it will be discussed, wettability of 2,5-diiodothiophene is found to be greater on a thiophene terminated surface than on a OH/CH_3 terminated surface. So, a combination of thiophene and OH/CH_3 terminated SAM is used to generate the wettability contrast.

5.2 Experimental

The wettability patterns on the gold substrate were made in two different methods – (a) via polydimethysiloxane (PDMS) stamping of thiols on a homogenous gold substrate [1,2] and (b) via substrate specific SAM chemistry on a heterogeneous substrate composed of an array of square gold pads on a native silicon oxide layer. The wettability patterning procedures for both homogenous and heterogeneous substrates are summarized

in Fig. 5.1. In both cases, arrays of completely wettable square regions are surrounded by less wettable lines.

The PDMS stamp was prepared using a Sylgard 184 elastomer and commercially available optical grating (120 lines/mm) as a master mold. For stamping CH_3 terminated thiol (1-hexadecanethiol) PDMS stamp was used as it is and for stamping OH terminated thiol (11-mercapto-1-undecanol) UV ozoned PDMS stamp was used. In order to generate arrays of completely wettable square regions on a less wettable matrix, the following procedure was used. Crisscrossing lines of the OH- or CH_3-terminated SAM were first generated by stamping ethanol solutions of these thiol compounds twice in orthogonal directions. Then, the thiophene-terminated SAM was produced in the unstamped square regions by immersing the entire substrate in a dichloromethane solution of 2-mercaptothiophene.

The heterogeneous substrate consisting of 100 nm thick gold pads on a native silicon oxide surface was made using photolithography (TEM grid was used as photomask) and thermal evaporation of gold. The dimension of the gold pads is 7.5 μm × 7.5 μm and the pads are separated by 5 μm silicon oxide regions. The gold surface was first coated with the thiophene-terminated SAM by immersing the substrate in the dichloromethane of 2-mercaptothiophene. The substrate was removed from the thiol solution, rinsed with dichloromethane, dried under nitrogen flow, and then immersed in a hexane solution of hexamethyldisilazane (HMDS) to cover the silicon oxide surface with CH_3 functional groups [15].

2,5-diiodothiophene was thermally evaporated and deposited onto these substrate surfaces. The monomer deposition rate was ~14 nm/sec. The deposited monomer layer was then irradiated with a 200W mercury lamp. The final thickness of polymer patterns is around ~ 100 nm. Fluorescence microscopy was used to analyze the polythiophene patterns. The contact angle of 2,5-diiodothiophene liquid droplet was measured on surface-modified substrates at 50 ^{o}C.

5.3 Results and discussion

Fig. 5.2 shows fluorescence microscopic images of polythiophene patterns produced with two difference SAM combinations on gold substrates. In the first combination, square patterns of the thiophene-terminated SAM are separated by the lines of the OH-terminated SAM. In the second combination, the CH_3-terminated SAM lines are used in place of the OH-terminated SAM lines to separate the thiophene-terminated SAM squares. The periodicity of the square patterns is same in both the combinations because they are produced using the same process (Fig. 5.1a). Fluorescence microscope images clearly show that the combination of thiophene-/CH_3-terminated SAMs exhibits better pattern recognition than that of thiophene-/OH-terminated SAMs. The edges of the polymer square patterns on the thiophene/OH combination are not as straight as those on the thiophene/CH_3 combination. Moreover, the corners of the polymer square patterns are more rounded in the case of the thiophene/OH combination.

The differences in the shapes of final polymer patterns grown on these two test surfaces clearly indicate the importance of the wettability contrast of the initial patterns

on the substrate in generating good quality polythiophene patterns [11,16]. The wettability of monomer can be inferred from the contact angle of the monomer liquid droplet on these surfaces. Table 5.1 compares the contact angles of the monomer liquid on surfaces with different functional groups. A lower contact angle means a better wettability. The 2,5-diiodothiophene liquid completely wets the thiophene-terminated SAM surface. Its wettability is intermediate on the OH terminated surface and the lowest on the hydrophobic CH_3-terminated surface. Therefore, the thiophene/CH_3 combination gives the largest wettability contrast.

The large wettability contrast requirement can be qualitatively understood from the free energy minimization point of view [16]. In order to minimize the solid-liquid interfacial free energy, monomer molecules selectively aggregate or pinned within the more wettable region. Once formed, the monomer droplets in this region try to avoid sharp edges as these sharp edges will increase vapor-liquid interfacial free energy. Therefore, there will a competition between these two phenomena, especially at the corner of the square pattern. In the case of thiophene/CH_3 combination, the high vapor/liquid interfacial free energy due to sharp corners is tolerated as the wettability contrast is large. However, in the case of thiophene/OH combination, the wettability contrast is not large enough to compensate the free energy increase due to formation of sharp edges. This leads to poor pattern recognition in the case of thiophene/OH combination with the rounded edges and corners. Since the final shape of the produced polymer patterns are exclusively determined by these monomer droplet shapes, it is very important to utilize the highest wettability contrast to obtain a good recognition of the underlying wettability patterns.

Amount of the monomer that can be pinned inside the more wettable region for a given dimension of underlying pattern is another governing factor [16]. Bridging defects are often observed in the case of thiophene/OH combination as shown in Fig. 5.3, while they are not formed in the case of thiophene/CH_3 combination for the same monomer dose. The bridging defect formation also results from the low wettability contrast for the thiophene/OH combination. The maximum amount of monomer that can be contained in each pattern is determined by the contact angle difference at the boundary as illustrated in Fig. 5.2c [16]. If the amount of monomer exceeds this value, the monomer floods into the less wettable regions lines. On the substrate patterned with thiophene-/CH_3-therminated SAMs, the large contact angle difference allows pinning of a large quantity of monomers within the thiophene-terminated square region without flooding into the CH_3 region. If the same amount of monomers is deposited on the thiophene/OH combination structure that has a smaller contact angle difference, the excess monomers overflow across the OH lines into a neighboring thiophene terminated region.

The regio-selective growth can also be accomplished on the heterogeneous substrates with periodic arrays of square gold patches on a silicon oxide substrate. In this case, a wettability contrast large enough for good pattern recognition can be generated by covering the gold surface selectively with the thiophene thiol and reacting the hydroxyl groups on the silicon oxide surface with the HMDS. This process produces thiophene terminated gold regions surrounded by CH_3 terminated silicon oxide surface. Fluorescence microscope image of polymer patterns generated with the heterogeneous substrate is shown in Fig. 5.4. Strong photoluminescence from the polythiophene is seen on the thiophene-SAM covered gold regions. The polymer patterns closely follow the

underlying gold patterns. The corners of the square patterns are slightly rounded as the corners of the underlying square gold pads are rounded.

An additional feature that can be found in Fig. 5.4 is the presence of small dots at the intersection of the less wettable silicon oxide lines. These island-like secondary spots are very reproducibly observed for the gold/silicon oxide test structure. Although the contact angle of the HMDS-treated silicon oxide (44^o) is not as high as the CH_3-terminated SAM surface on the gold (60^o), we do not think the reduced wettability contrast is the main cause. In the case of thiophene/OH combination which has only 20^o contact angle difference, the island-like secondary structures at the intersection of the OH-terminated SAM lines are absent. The formation of these secondary structures appears to be the consequence of the increased separation distance between the completely wettable patches. The spacing between completely wettable regions are increased from ~1.5 μm in the case of PDMS stamping on the gold surface to ~5 μm in the case of gold square patches surrounded by silicon oxide regions.

The secondary structure formation with increased spacing of the less wettable region has been theoretically predicted in other systems such as dewetting of polymer thin films on wettability patterned substrate surfaces [10-13]. Sharma and coworkers reported the instability and dynamics of thin film of Newtonian liquid on top of a chemically heterogeneous surface using a hydrodynamic model. Their simulation results show that good pattern recognition can be achieved when the width of less wettable region that separates more wettable region is smaller than the spinodal wavelength (characteristic length scale of dewetting) on a homogenous substrate. When the width of the less wettable region is less than the spinodal wavelength, single rupture of the film is initiated

at the center. This rupture widens along the width of the stripe, dewetting the liquid from the less wettable region to more wettable region. If the width of the less wettable region is larger than the spinodal wavelength, two ruptures are initiated in the less wettable region near the wettability contrast boundaries. As the liquid fronts connected to the more wettable regions move toward the wettability contrast boundaries, a thin cylinder of the liquid is left at the center of the less wettable region. These thin cylindrical liquid lines located along the center of the less wettable stripes eventually disintegrate due to Rayleigh instability and form droplets at the intersection of the less wettable stripes.

From the comparison of Fig. 5.2 and 5.4, it can be said that the spinodal wavelength of 2,5-diiodothiophene film is between 1.5 μm and 5 μm. In other words, the separation of the preferentially wettable regions should be smaller than 5μm to attain good pattern recognition in the region-selective deposition of 2,5-diiodothiophene.

5.4 Conclusion

Polythiophene patterning is accomplished by regio-selective condensation of 2,5-diiodothiophene on the wettability patterned substrate surface followed by in-situ photochemical conversion of the monomer patterns into polymer patterns. Key factors controlling the quality of the patterns are the wettability contrast and the dimension of the periodicity. Wettability contrast between the more and less wettable region should be as large as possible and the width of the less wettable should be less than the spinodal wavelength. A combination of 2-mercaptothiophene thiol SAM and CH_3-terminated SAM gives the wettability contrast large enough for good pattern recognition by the

monomer. The width of the less wettable region must be smaller than 5 μm to prevent secondary island structures between the more wettable regions.

5.5 References

[1] Kumar, A.; Whitesides, G.M. *Science* **1994**, *263*, 60.

[2] Biebuyck H.A.; Whitesides, G.M. *Langmuir* **1994**, *10*, 2790.

[3] Gau, H.; Herminghaus, S.; Lenz, P.; Lipowsky, R. *Science* **1999**, *283*, 5398.

[4] Kataoka, D.E.; Troian, S.M. *Nature* **1999**, *402*, 794.

[5] Higgins, A.M.; Jones, R.A.L. *Nature* **2000**, *404*, 476.

[6] Herminghaus, S.; Jacobs, K.; Mecke, K.; Bischof, J.; Fery, A.; Ibn-Elhaj, M.; Schlagowski, S. *Science* **2000**, *282*, 916.

[7] Boltau, M.; Walheim, S.; Mlynek, J.; Krausch, G.; Steiner, U. *Nature* **1998**, *391*, 877.

[8] Nisato, G.; Ermi, B.D.; Douglas, J.F.; Karim, A. *Macromolecules* **1999**, *32*, 2356.

[9] Delongchamp, D.; Hammond, P.T. *Adv. Mater.* **2001**, *13*, 1455.

[10] Sehgal, A.; Ferreiro, V.; Douglas, J.F.; Amis, E.J.; Karim, A. *Langmuir* **2002**, *18*, 7041.

[11] Kargupta, K.; Sharma, A. *Phys. Rev. Lett*. **2001**, *86*, 4536.

[12] Kargupta, K.; Sharma, A. *Langmuir* **2002**, *18*, 1893.

[13] Kargupta, K.; Sharma, A. *Langmuir* **2003**, *19,* 5153.

[14] Natarajan, S.; Kim, S.H. *Thin Solid Films*, in review.

[15] Anwander, R.; Nagl, I.; Widenmeyer, M.; Engelhardt, G.; Groeger, O.; Palm, C.; Röser, T. *J. Phys. Chem. B* **2000**, *104*, 3532.

[16] Lenz, P.; Lipowsky, P. *Phys. Rev. Lett.* **1998**, *80*, 1920.

OH-terminated surface		**CH_3-terminated surface**		**Thiophene-terminated surface**	
11-mercaptoundecanol SAM on Au	**24˚**	16-hexadecanethiol SAM on Au	**60˚**	2-mercaptothiophene SAM on Au	**0˚**
UV-ozone cleaned silicon oxide surface	**25˚**	HMDS treated silicon oxide surface	**44˚**		

Table 5.1 Surface chemistry dependence of the contact angle of 2,5-diiodothiophene liquid on various substrates at ~50 ˚C.

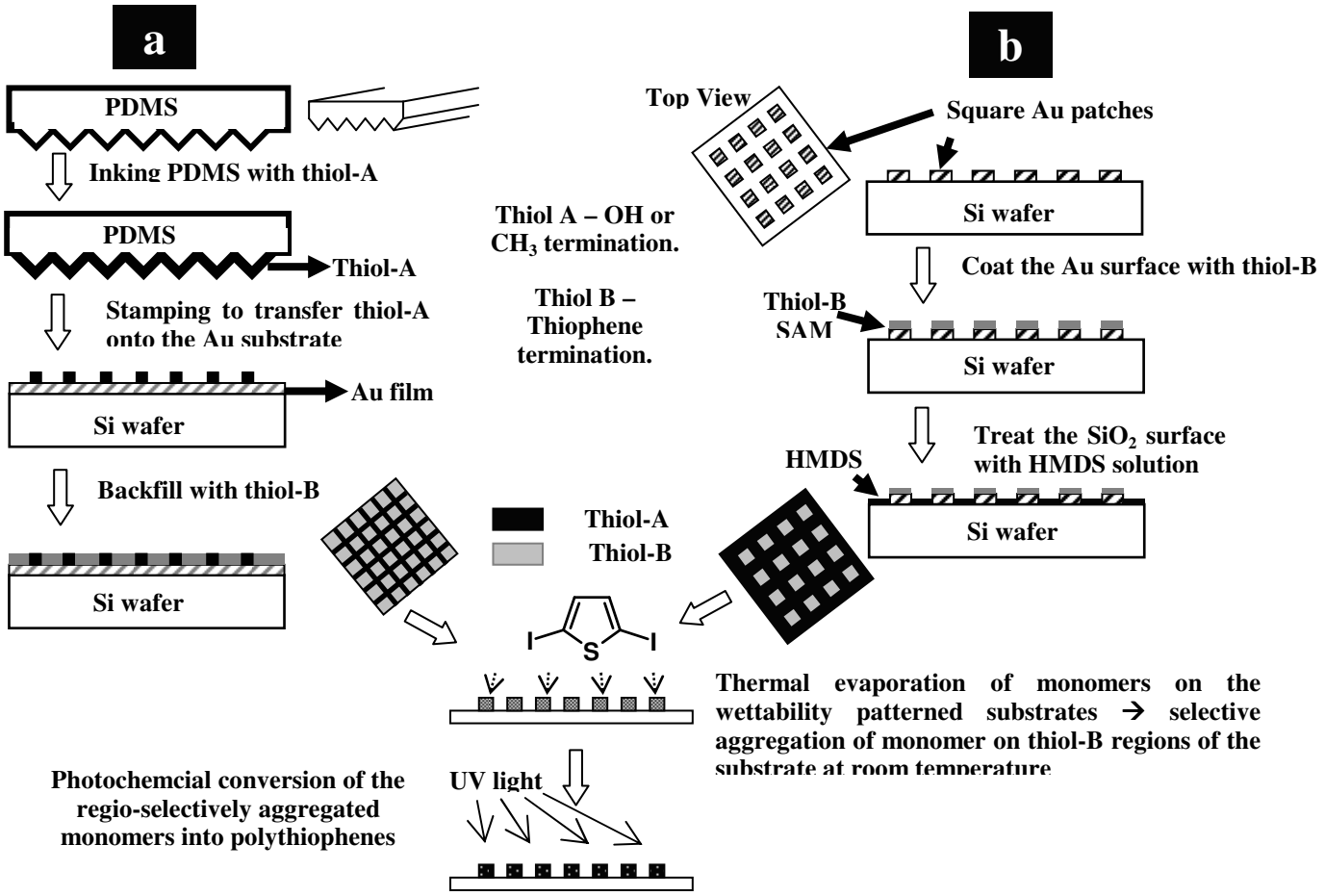

Fig. 5.1 Schematics of wettability patterning of the substrate, regio-selective deposition of 2,5-diiodothiophene, and photochemical conversion of the adsorbed monomer patterns to polythiophene patterns **(a)** PDMS stamping approach is used to generate wettability contrast patterns on gold substrates. **(b)** On Au/SiO_2 substrates, selective formation of thiol SAM on gold followed by hexamethyldisilazane treatment of SiO_2 surface is used.

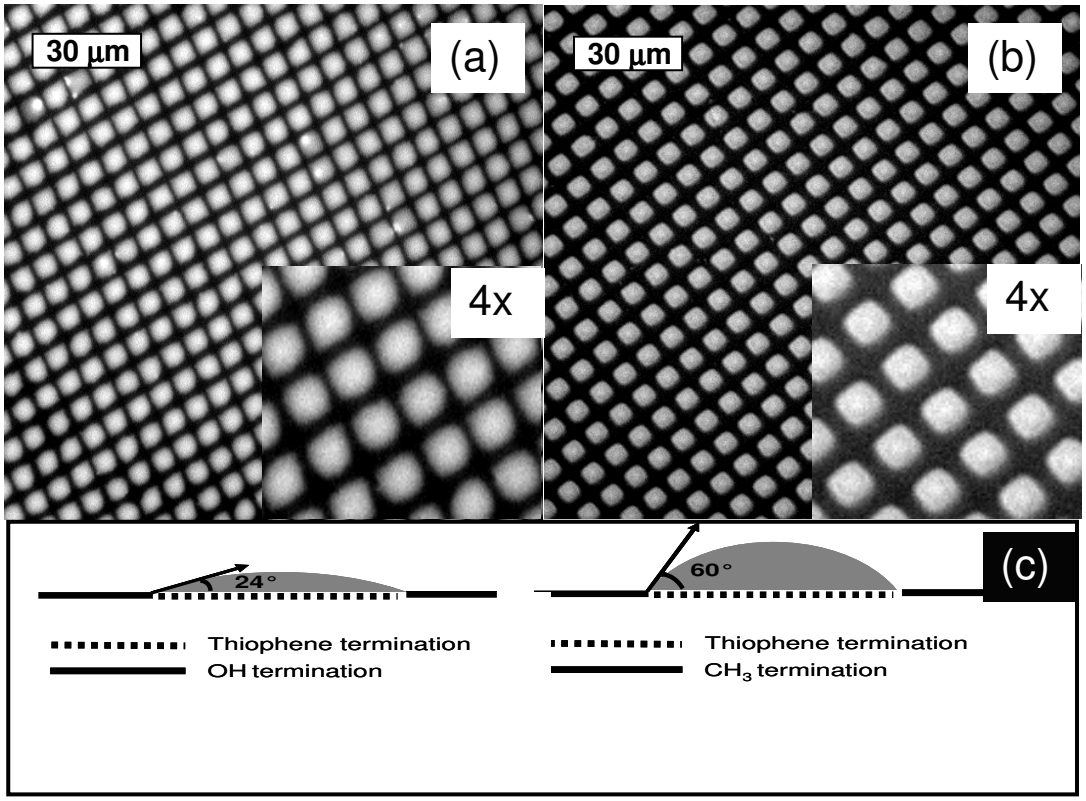

Fig. 5.2 Fluorescence microscope images of the polymer patterns produced on the gold substrates periodically patterned with the thiophene-terminated SAM square regions surrounded by **(a)** OH-terminated and **(b)** CH_3-terminated SAM lines. Image (b) is pseudo colored to show the readers an idea of photoluminescence emission. **(c)** Schematics to show the maximum amount of monomer that can be pinned inside the more wettable region. Insets in **(a)** and **(b)** are digitally magnified by ×4 to show individual patterns.

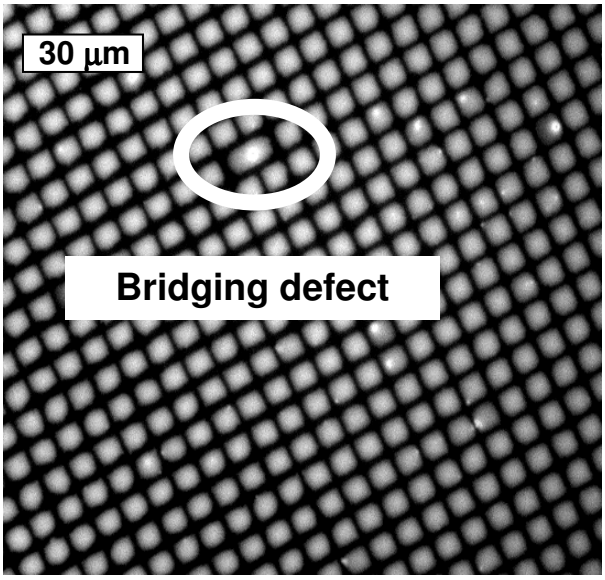

Fig. 5.3 Bridging defect often formed in thiophene/OH combination due to poor wettability contrast.

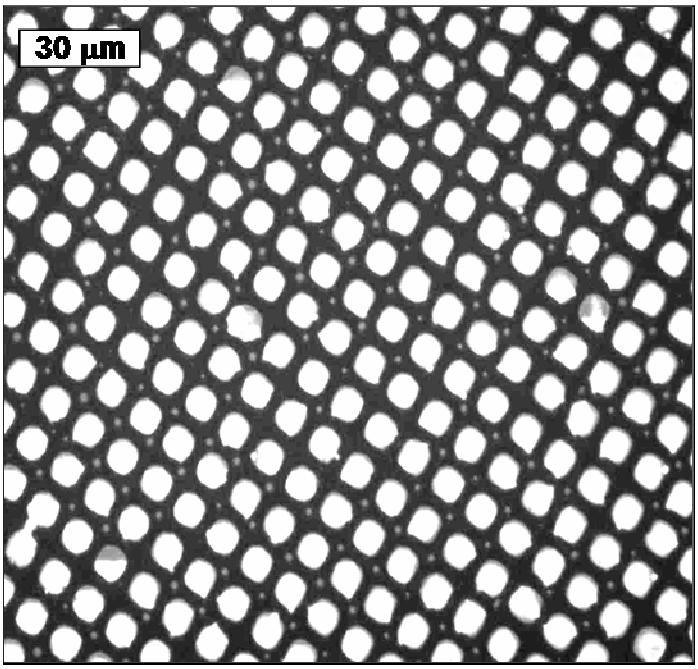

Fig. 5.4 Fluorescence microscope image of the polymer patterns produced on the thiophene-terminated SAM covered Au square patches surrounded by HMDS-treated SiO_2 regions.

Appendix – A

Additional notes on chapter 2

A1. Experimental setup

Experimental setup for polymerizing 2,5-diiodothiophene is as shown in Fig. A1. The setup is purged with argon continuously to displace the air in the chamber with argon. A sponge disperser is used to avoid the convective mixing of the argon with the air on the top of the chamber. The whole setup (dispenser and purge chamber) is enclosed in another box (~ 1ft*1ft*1ft) to avoid convection due to hood's exhaust fan.

A2. Monomer vapor deposition

Evaporation of the monomer is carried out using the conventional hot plate (White color top, Fisher Scientific, Cat No. 11-500-49SH) at the setting of 1¾ and the temperature of the crucible placed at the center is found to be ~160 °C. Crucible is just a 2 cm tall glass vial made by cutting the conventional scintillation vial. For a monomer deposition time of ~ 10 secs, the final polymer thickness is found to be ~ 120nm by tapping mode AFM measurements. The monomer film is usually irradiated immediately after vapor deposition. The polymer film formed on a thiophene or OH terminated surface is extremely smooth (RMS roughness < 1nm) due to complete spreading of the monomer and the intermediates on these surfaces. On a dirty or CH_3 terminated surface, the polymer film formed is not uniform and it appears as small de-wetted droplets. Also, it is found that the monomer deposition on rough edges is more compared to smoother regions, which is probably due to enhanced nucleation on the rougher edges.

A quartz crystal microbalance (QCM) is used to estimate the rate of monomer deposition versus temperature of crucible. In these experiments, the glass crucible is rapidly heated using a nichrome coil and the temperature is measured using a thermocouple closely held to the crucible. At first, the rate of heating that is, the temperature of the crucible (room temperature to ~ 200 °C) versus time is measured. Then, the crucible is filled with ~ 0.5 gm of 2,5-diiodothiophene, heated rapidly and the rate of monomer deposition versus time is measured. Monomer deposition rate is measured using a QCM closely held to the mouth of the crucible. From these two data, rate of deposition for various temperatures are estimated. Fig. A2 shows the plot between the rate of monomer deposition and the temperature of the crucible. The rate of monomer deposition increases with the temperature as the vapor pressure of the monomer increases with the temperature. Based on Clausius-Clayperon equation, the vapor pressure of an ideal liquid increases exponentially with the increase in temperature, so the rate of monomer deposition versus temperature is fitted to an exponential line. The fit is poor probably because of non-ideality of the monomer or heat transfer delays during evaporation or heating of QCM substrate. Further experiments are required to elucidate the reason.

A3. XPS analysis

Samples for XPS analysis are usually prepared ~ 12 hours before the analysis and stored in the absence of light. In the presence of light (UV and blue) and oxygen, the surface of the polymer film formed may get oxidized due to the process of photo-oxidation. Survey spectrums are usually obtained at pass energy of 80eV and high

resolution spectrums at 40eV. Photo-oxidation can be deduced by observing the high resolution carbon 1s region. Oxidative defects such as O=C-O and =C-O show up at 288.9 and 287.3 eV relative to C 1s at 285eV as shown in Fig. A3.

The ratio of Iodine to carbon XPS signal decreases with increase in irradiation time as shown in Fig. A4. This data must be interpreted with caution as this conversion doesn't directly translate into degree of polymerization. As shown in the Fig. A5, it is observed that the decrease in intensity of iodine signal is accompanied by increase in oxygen signal even when the irradiation is carried out in argon environment. This observation indicates as irradiation time is increased, trapped radicals are formed which react with oxygen in air when the polymer films are taken out of the argon environment. These radicals are not able to react with other radials or monomer during the irradiation, because of their decreased mobility. Thus this observation clearly supports the diffusion limited rate mechanism during latter stages of polymerization. During the early stages of polymerization the concentration of polymer is low, hence the viscosity of the film will be low, and so the mobility of radicals and monomer will be high. As the polymerization progresses, the concentration of polymer increases, hence the viscosity increases and so the mobility of radicals (and other reacting species) decreases. If the rate of polymerization is diffusion controlled, the rate of polymerization during the initial stages will be higher compared to latter stages. In fact during latter stages rate of polymerization will become zero almost, when the diffusion constant of radicals become too low compared to experimental time frame. When the rate of polymerization becomes zero, the degree of polymerization will reach a saturation value. Continued irradiation after this point doesn't increase the degree of polymerization, but generates trapped (or immobile)

radicals. These trapped radicals in the polymer film react with oxygen in the air forming oxygenated defects. So the degree of polymerization will be lesser than what is predicted from the conversion data.

A4. Photoluminescence analysis

Photoluminescence analyses are carried out at Prof. Pishko's lab using PTI (Photon Technologies Incorporated, www.pti-nj.com) QM4-2000SE spectrometer. Thin film samples are mounted on a solid state sample holder as shown in Fig. A6. In the case of rough films, light scattering is significant and the intensity of the scattered light is comparable or more than the photoluminescence intensity. A 435 nm interference filter is used in the excitation side to cut out the scattered light intensity and improve the signal to noise ratio. Presence of scattered light is characterized by sharp peaks as shown in Fig. A7. As shown in the figure, most of the scattered light peaks move with the excitation wavelength. 435 nm interference filter is mounted on small square (2" * 2") holder provided with the instrument. UV-Vis characteristics of the 435 nm interference filter are shown in Fig. A8. In the case of smooth films (example – films synthesized on a hydrophilic glass or thiophene terminated gold) scattering is not an issue, hence we are able to get both emission and excitation without using any filters.

A5. AFM Analysis

AFM analysis is done at Prof. Mallouk's lab using DI's multi-mode instrument on tapping mode. Images of the pattern and surface roughness are measured using 110

micron scanner in tapping mode. Roughness analysis of photochemically synthesized polythiophene sample is shown in Fig. A9.

Thickness measurements of the conductivity samples (poly-3-hexylthiophene and photochemical synthesized polythiophene doped with Iodine) were done using MRI's AFM by Mr. Vince Bojan. To estimate the thickness we went to the areas with scratches and scanned over the edge. The results are as shown in Fig. A10 & A11.

A6. Fluorescence microscope analysis

Characteristics of the filter cube used in the fluorescence microscope are shown in Fig. A12. While analyzing the rough samples it is better to turn off the room light (even the computer monitor).

A7. Conductivity measurement

Photolithographic procedure for making conductivity probe

1) Clean glass slide by RCA-1 etch (refer Appendix – C). Take necessary safety precautions while etching.
2) Dry them in argon completely.
3) Spin coat HMDS @ 4000RPM until dry.
4) Bake the slides for 15 secs at 110 °C.
5) Cool the slides and turn off all the lights except a incandescent light.
6) Spin coat Shipley 1827 at 4000RPM for 40 secs.
7) Softbake the slides for 90 secs at 110 °C (as accurate as possible).

8) Press the mask against photoresist using two book clips (Chrome side towards photoresist). Dimensions of the conductivity probe mask are in the lab notebook - 1.

9) Irradiate for ~ 14 secs with the 1.5" dia collimated beam from the lamp (UV lamp should have the deflector and water cooler).

10) Develop with Shipley CD-26 developer for 40 secs.

11) Thermally evaporate or sputter chrome (10nm) & gold (100nm) and make sure the samples don't get heated.

12) Lift off using acetone and dispose the waste properly.

Once the probe is ready attach leads using silver paste. PT films are made directly on a RCA-1 etched glass by the photochemical process and PHT films are spin coated on a RCA-1 etched glass. Both the samples are iodine doped by exposing the samples to iodine vapors in a glass bottle at room temperature for 12-24 hrs. As soon as they are taken out of the doping bottle, they are pressed firmly against the four gold lines and the conductivity is measured using the HP 3468A multimeter. Don't expose the gold fingers directly to iodine for a long time as it forms gold iodide.

A8. RAIRS analysis

RAIRS analysis is carried out at our lab using the right hand side bench. Detection is using the MCT (Mercury Cadium Telluride)-A detector and focusing lens is made of Barium fluoride. The angle between the incidence and the surface normal of the thin film sample is 85 degrees. Remove the photon modulation setup for doing this experiment.

A9. 1,4-Diiodobenzene polymerization

Long UV irradiation (10 min) of thin films (~ 200nm) of 1,4-diiodobenzene in argon environment produces fluorescent material with greenish yellow emission. Photoluminescence excitation and emission of the THF extract of the material is shown in Fig A13. Fluorescence is probably due to formation of conjugated oligo and poly-phenylenes as in photochemical polymerization of 2,5-diiodothiophene.

A10. UV-Vis of photo-polymerized 2,5-diiodthiophene

Fig. A14 shows the UV-Vis of photochemically synthesized polythiophene on a slide glass substrate. Only data above 320nm is shown because the slide glass starts absorbing strongly below 320nm. Strong absorbance of the polymer below 350nm may be due to presence of short oligomers (2 -3 mers) or trapped unreacted monomer or mislinked polymer.

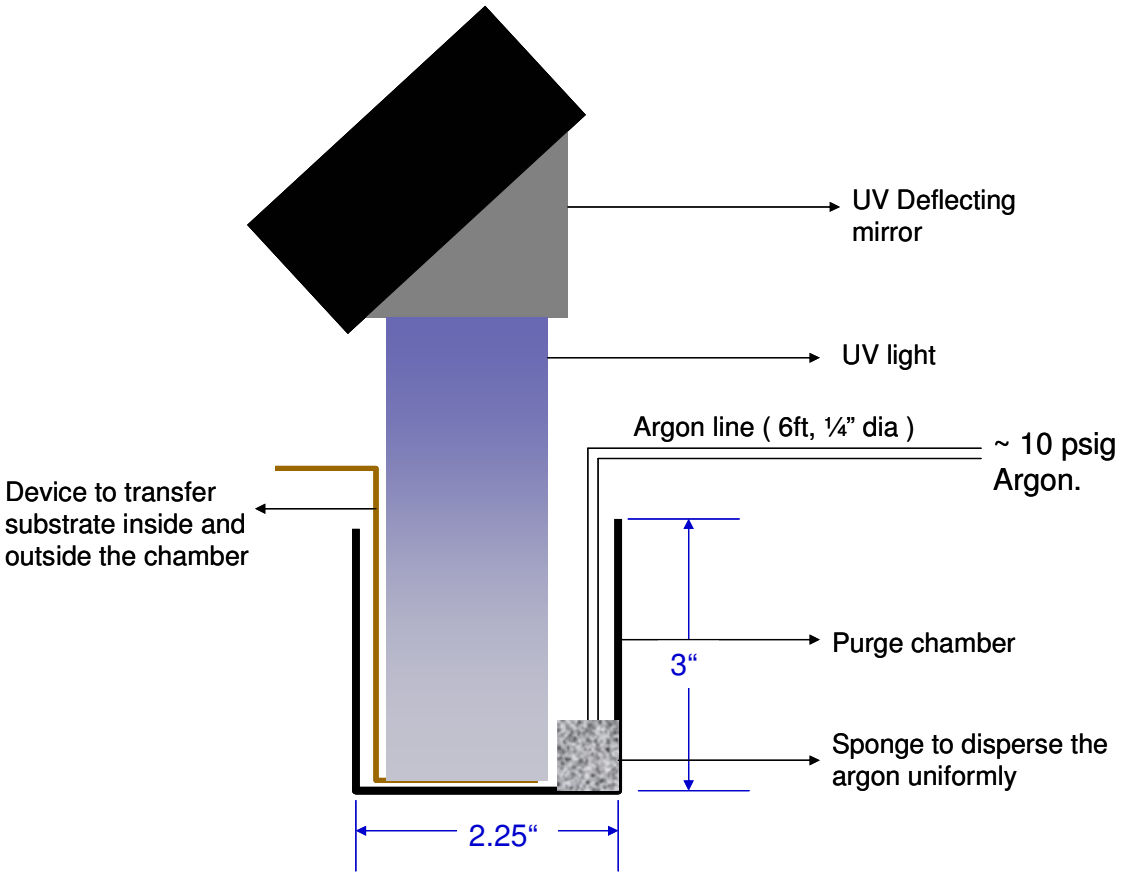

Fig. A1 Schematic of the experimental setup.

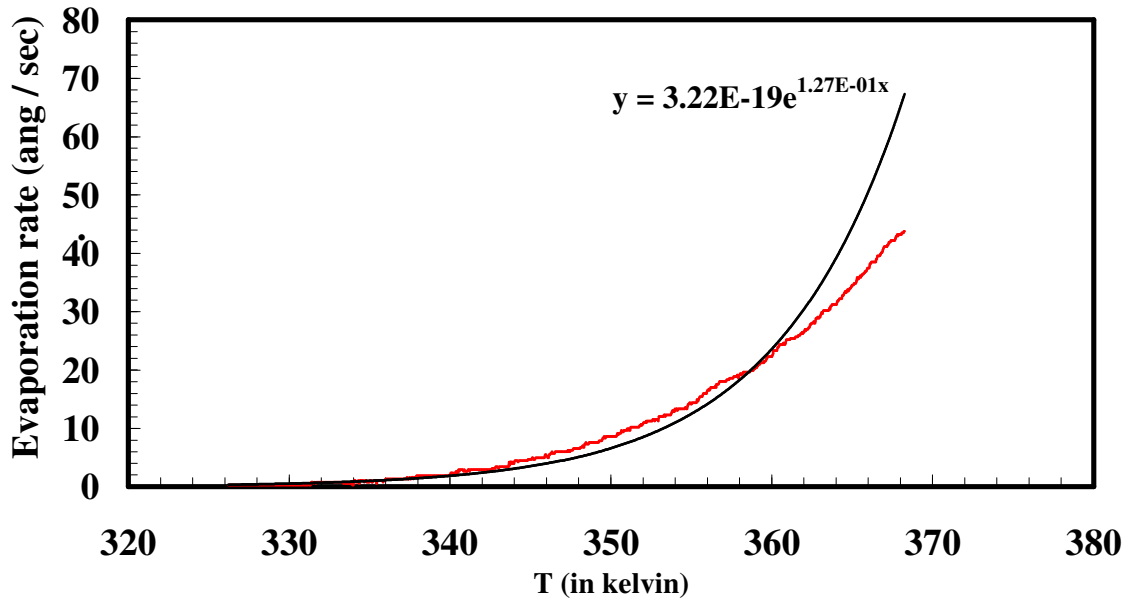

Fig. A2 QCM results showing variation in evaporation rate versus temperature.

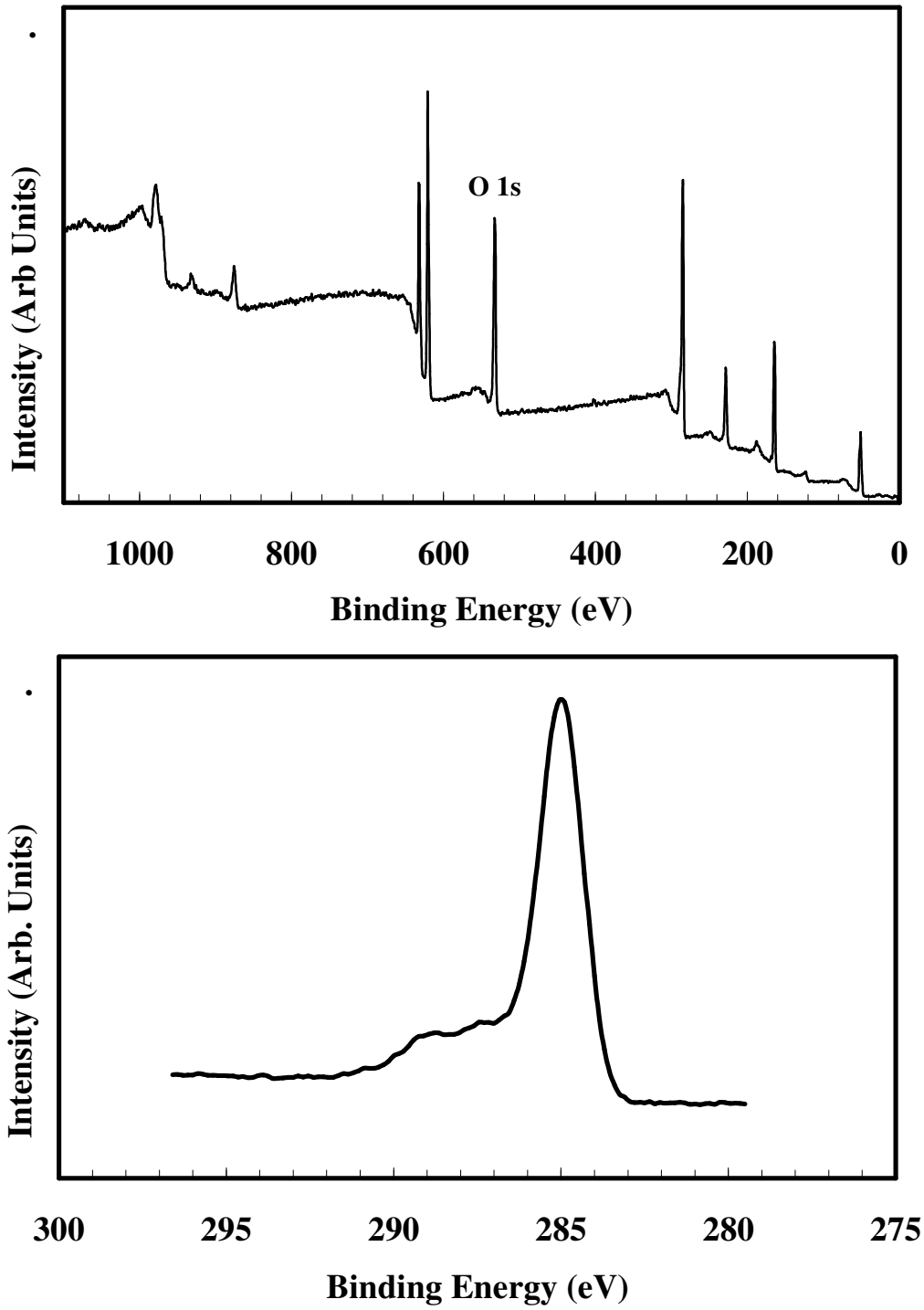

Fig. A3 XPS signature of oxidative defects.

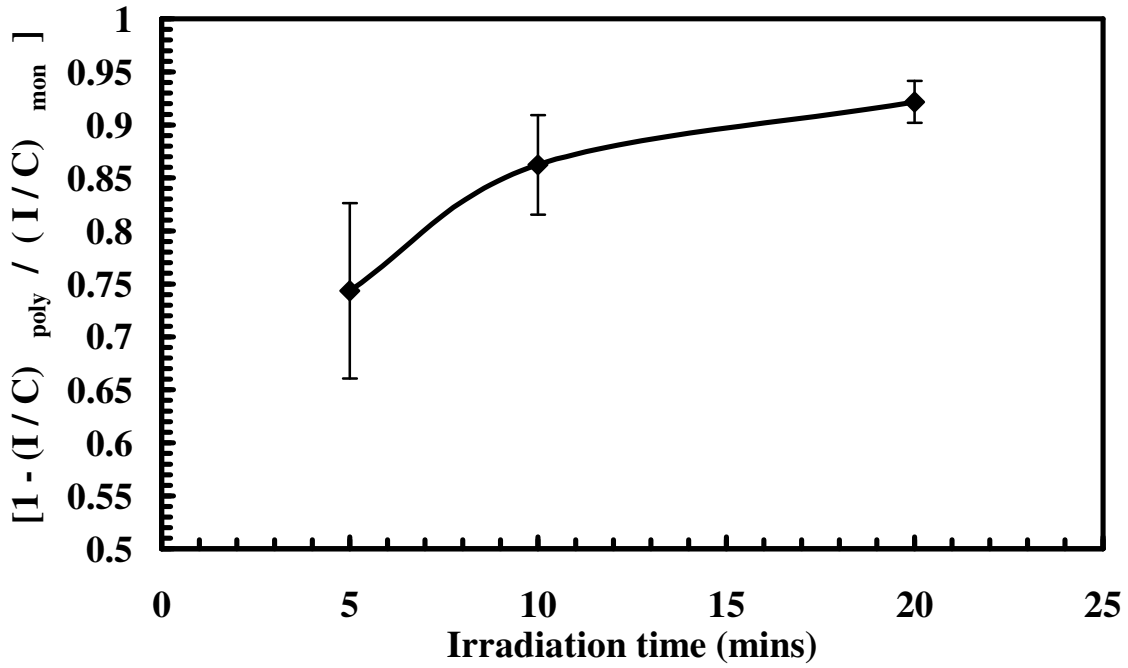

Fig. A4 Conversion vs. Irradiation time based Iodine to carbon ratio from XPS data.

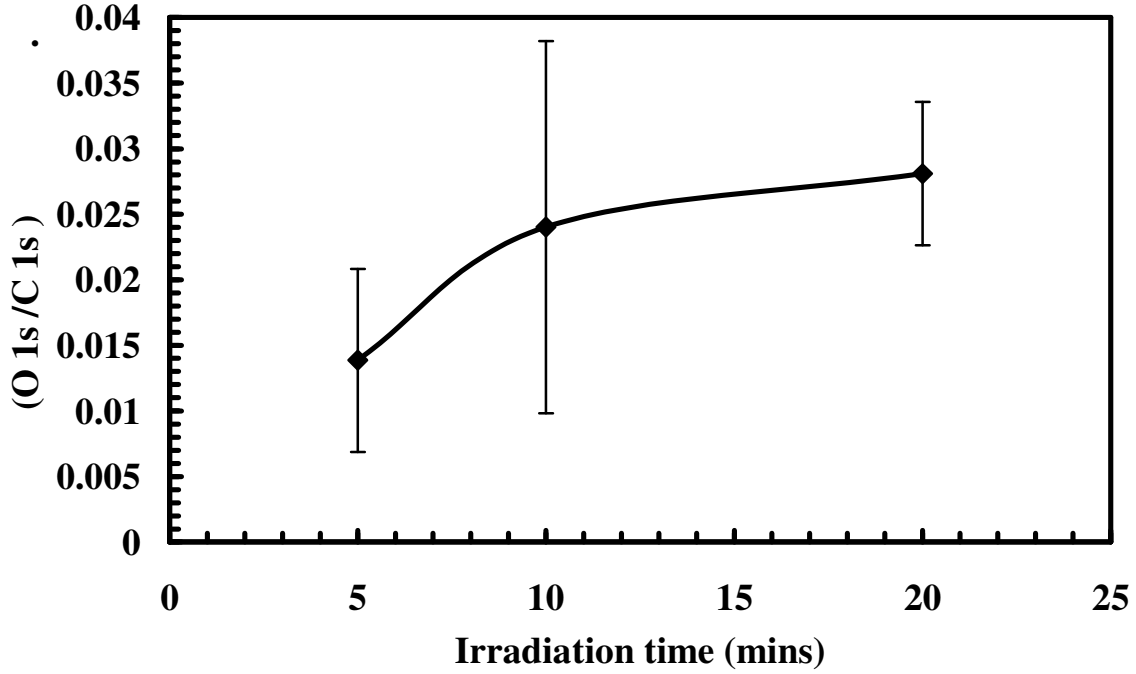

Fig. A5 Oxygen incorporation vs. Irradiation time from XPS data.

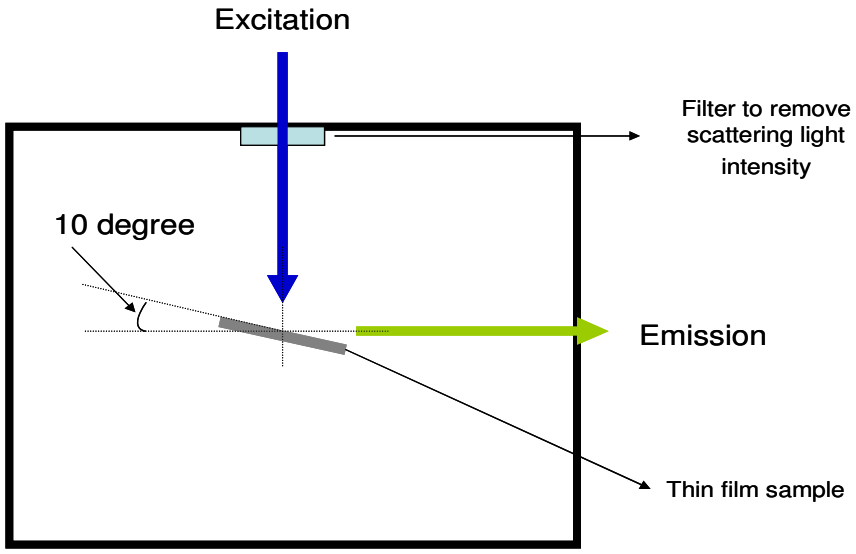

Fig. A6 Sample mounting details for photoluminescence measurements.

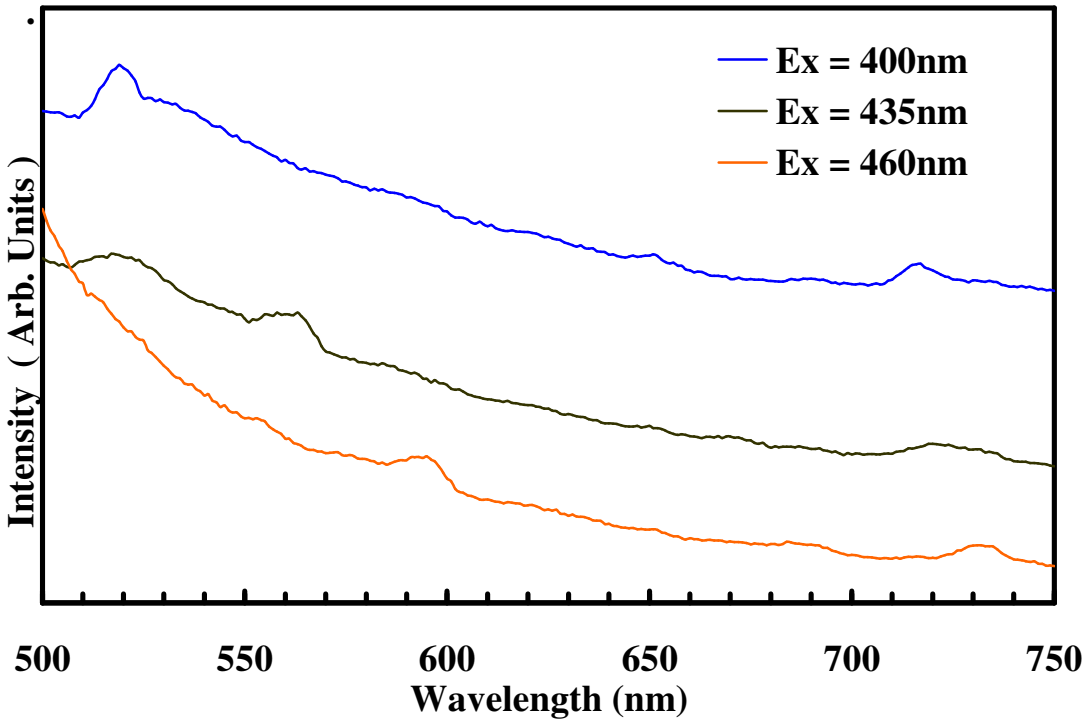

Fig. A7 Scatter light characteristics for various excitations captured using unpolished Silicon wafer.

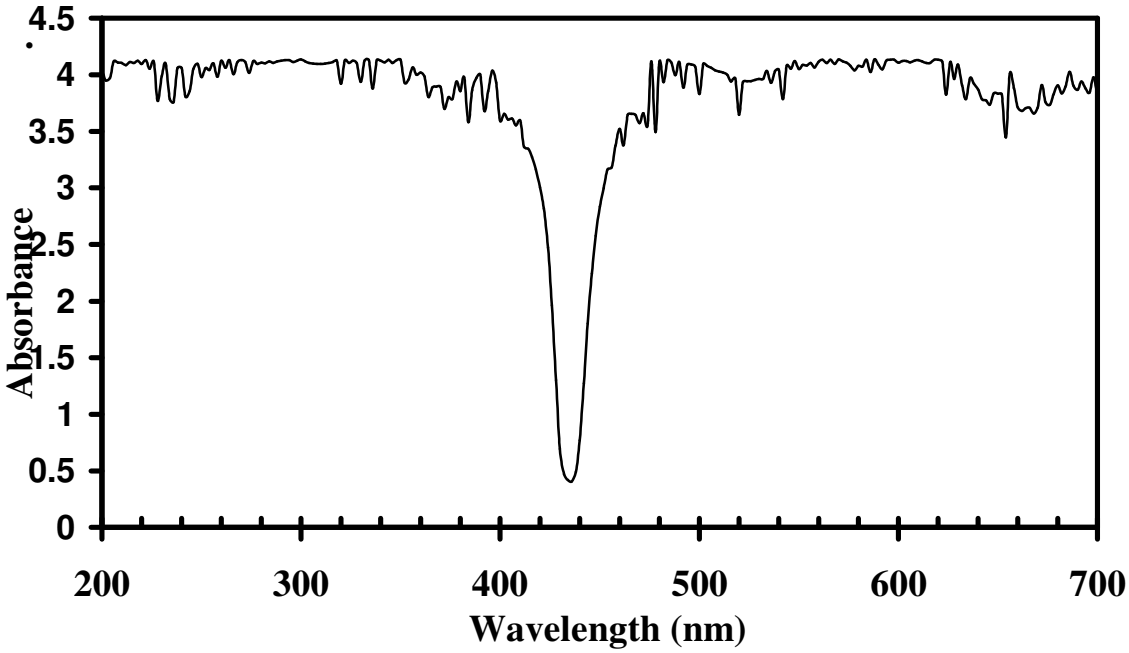

Fig. A8 UV-Vis characteristics of the 435 nm interference filter.

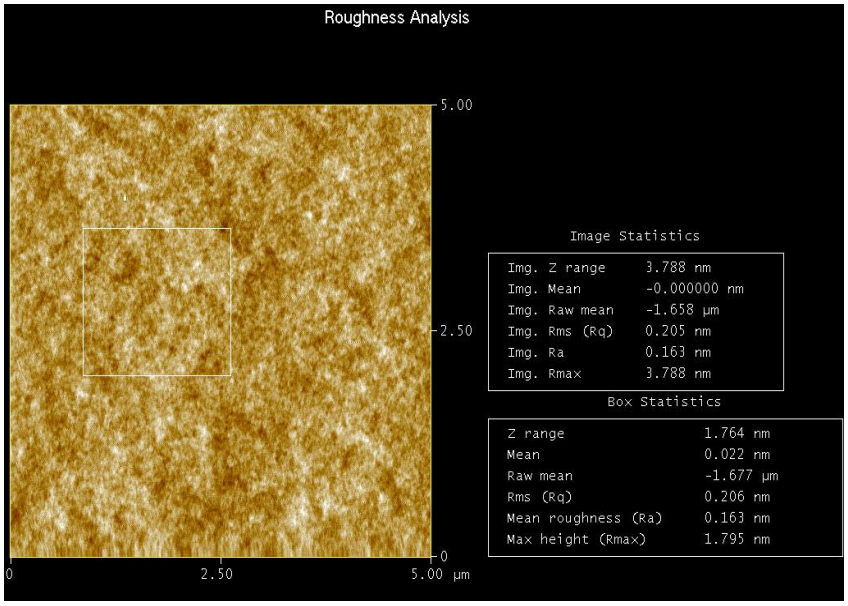

Fig. A9 Roughness analysis of the photochemically synthesized sample.

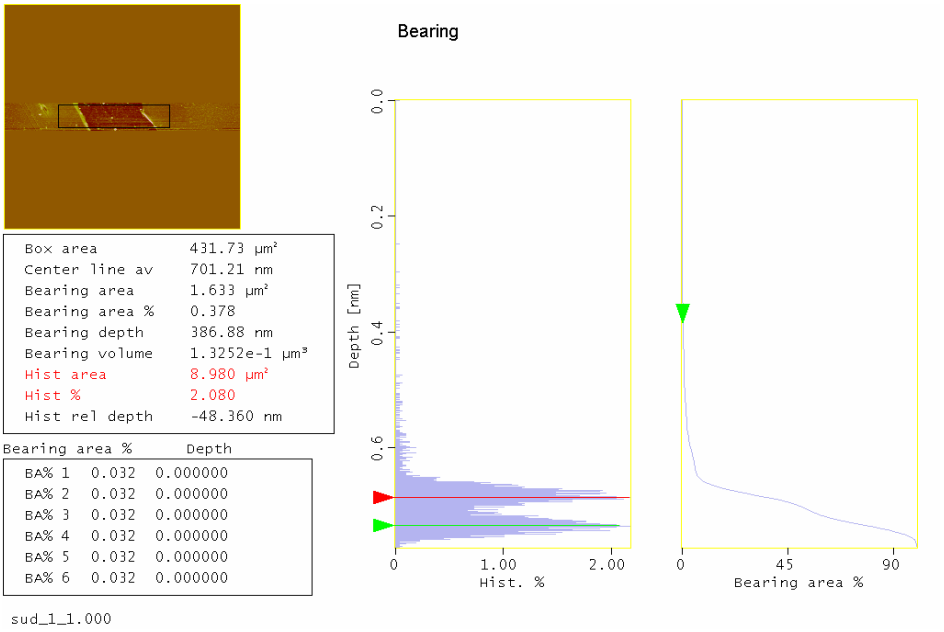

Fig. A10 Thickness measurement data of PHT film. (Thickness ~ 50nm)

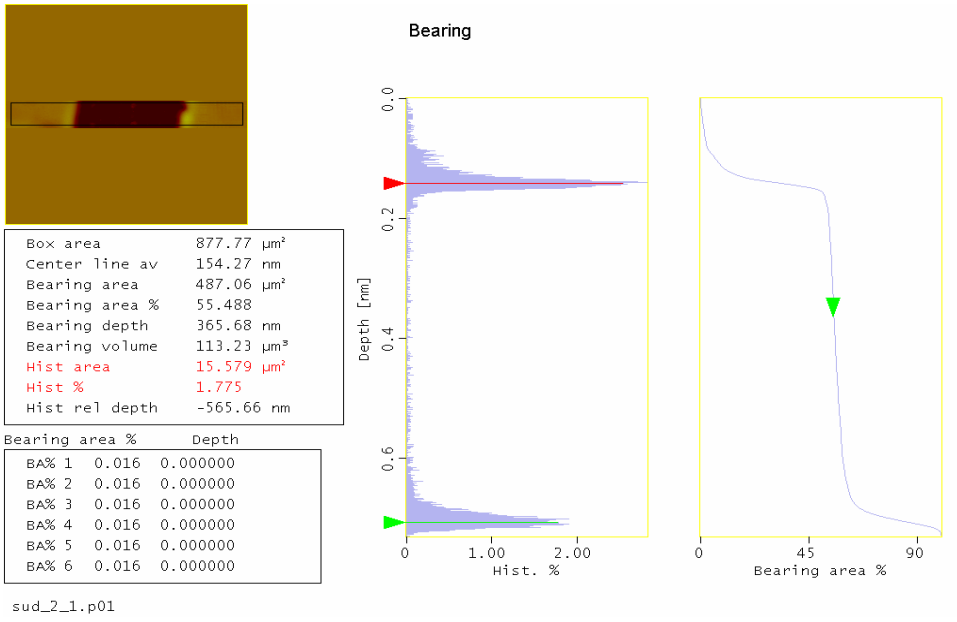

Fig. A11 Thickness measurement data of photochemically synthesized PT film. (Thickness ~ 550nm)

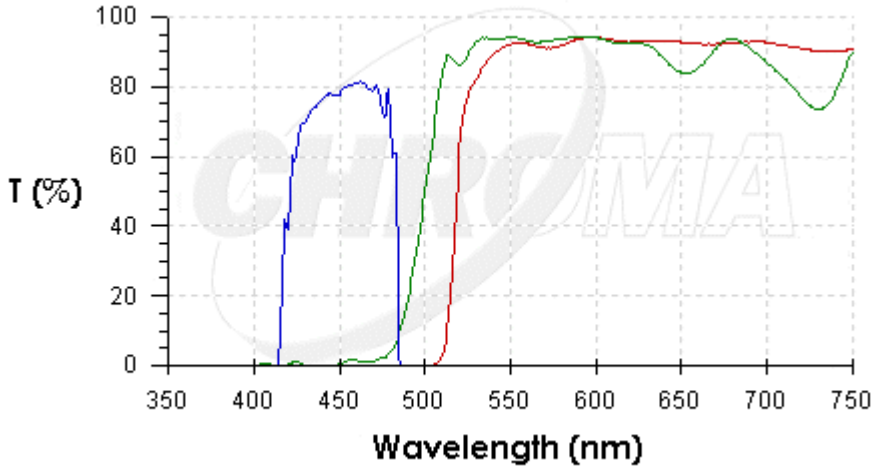

Fig. A12 Characteristics of the filter cube used in the fluorescence microscope.

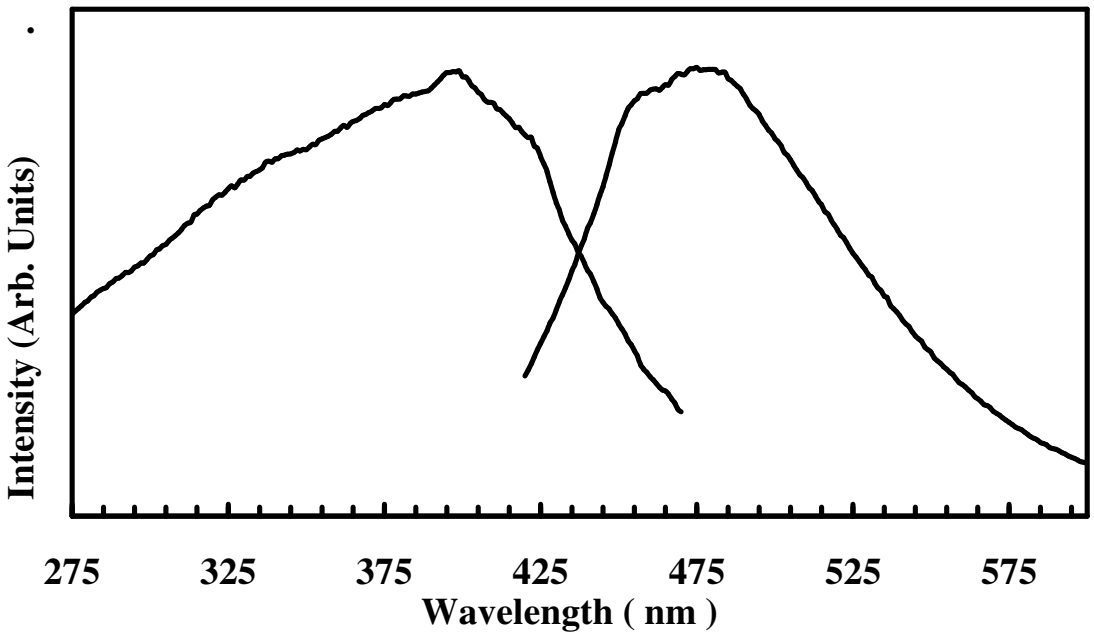

Fig. A13 Photoluminescence excitation and emission of THF extract of the photo-irradiated 1,4-diiodobenzene.

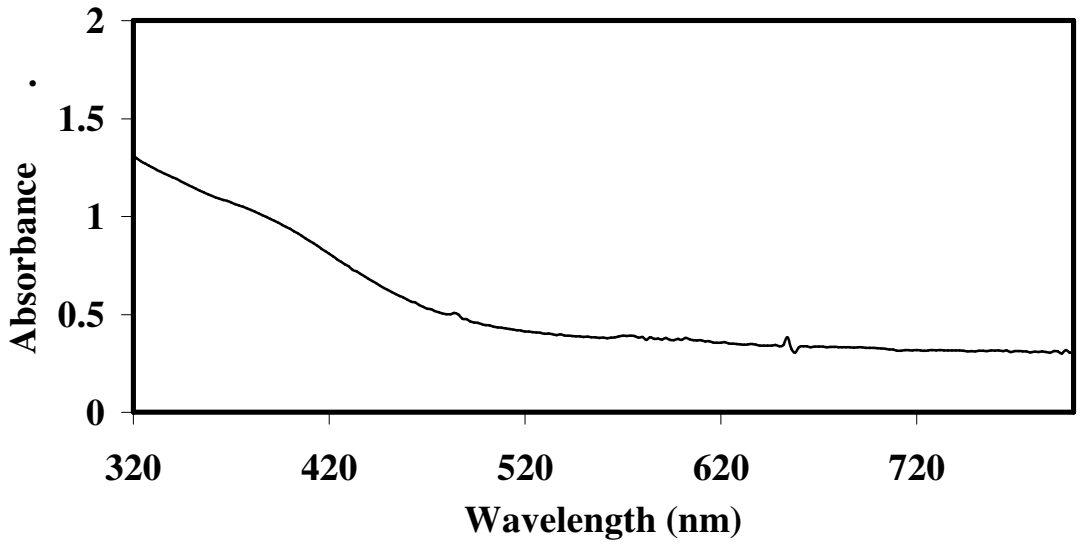

Fig. A14 UV-Vis absorption spectrum of photochemically synthesized polythiophene film on a slide glass substrate. (Note: Slide glass starts absorbing strongly below 320nm)

Appendix – B

Additional notes on chapter 3

B1. Identifying the presence of copper iodide by photoluminescence

Copper iodide is formed as a byproduct in the Ullmann coupling reaction and copper iodide has red emission (in addition to blue emission centered at 425 nm, refer JACS 1997, 119, 1439) on photoexcitation with photons of wavelength lesser than 430nm. The thin polythiophene films prepared by photo-activated Ullmann coupling reaction have copper iodide by-product mixed in it. In order to make sure that we are analyzing the polythiophene in the photoluminescence experiments, the following experiment is performed. Thin film of copper iodide is made by exposing copper metal foil to iodine vapors for 6 hours. This thin film of copper iodide is rough and white in color (as it scatter light of wavelength greater that 430nm). This film is analyzed by photoluminescence using various excitation wavelengths (404nm, 435nm, 455nm) and the results are shown in Fig. B1. As shown in the figure, on photoexciting the copper iodide film with light of wavelength lesser than 430nm (i.e. 404nm excitation) there is a red emission with the maximum at around 680nm. But excitation of the same copper iodide film with photons of longer wavelength (435 or 455nm) resulted in no emission. The corresponding set of analysis is done on polythiophene film synthesized by photo activated Ulmann coupling reaction and the results are shown in Fig B2. As shown in the figure, irrespective of the excitation wavelength we see an orange red emission centered at around 610nm. As mentioned above, in these experiments we are using copper iodide thin films, but even if the copper iodide present inside the polythiophene is in the form of

very small particulates (~diameter of 10nm or lesser) because of confinement effect the band gap of the particle will increase and the minimum wavelength with which these particulates can be photo-excited will be lesser than 430nm (refer JACS 1997, 119, 1439). Thus orange red emission observed from the thin film sample synthesized on copper is exclusively from polythiophene. Above-mentioned photoluminescence experiments are carried out using a suitable excitation filter to remove the scattered light intensity.

One of the interesting observations made during these experiments is that when a copper iodide film (prepared in the lab by exposing clean copper to iodine) is used, a distinct 425nm emission is not observed. But when copper iodide powder (purchased from Aldrich) is used, a strong 425nm emission (along with the 680nm emission) is observed as shown in Fig. B3 and this 425nm emission is in agreement with the literature (JACS 1997, 119, 1439). Also, it is noted that the red emission from the copper iodide film is stronger than that from the copper iodide powder. The reason behind these observations is not known.

B2. SERS experiments

Gold substrate for SERS experiments is prepared by electrochemical deposition using silicon with thin film of evaporated gold as cathode, stainless steel as anode and silver/silver chloride reference electrode. Electrodeposition is carried out at constant current of 20mA for 30 minutes using “Orotemp” electrolyte (purchased from Technic Inc. http:// www.technic.com/chm/goldcon.htm). Gold substrate prepared this way didn’t give significant enhancement compared to the evaporated gold film.

SERS experiments on polythiophene synthesized on copper substrate don't require any surface treatment of copper.

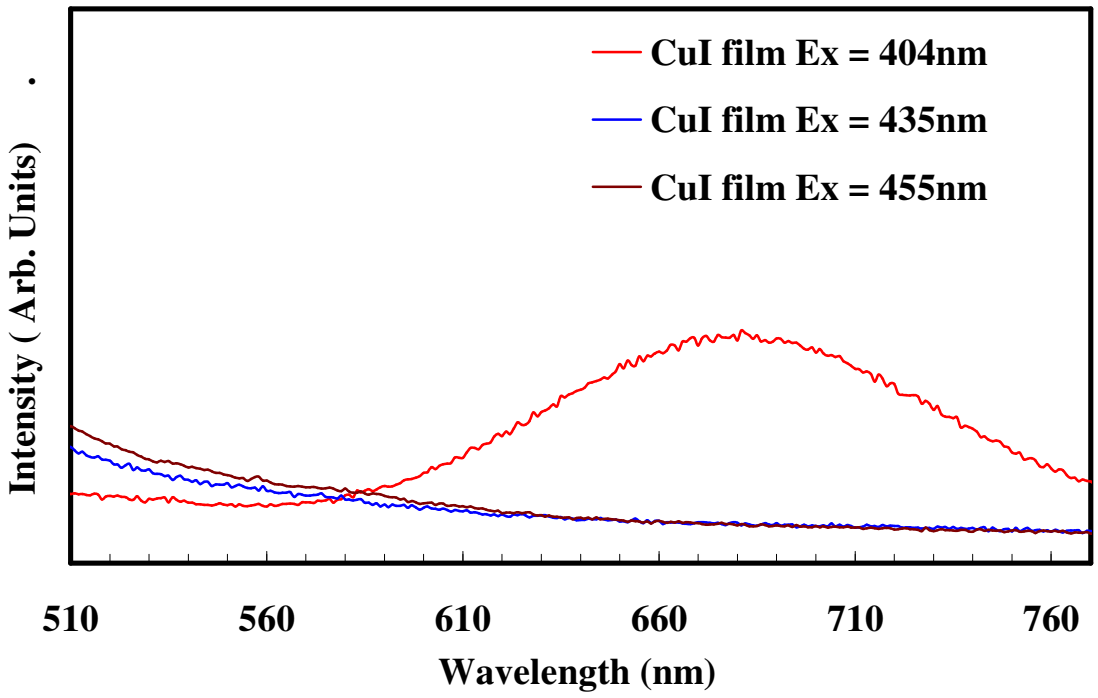

Fig. B1 Photoluminescence emission from a thin film of copper iodide synthesized in the lab.

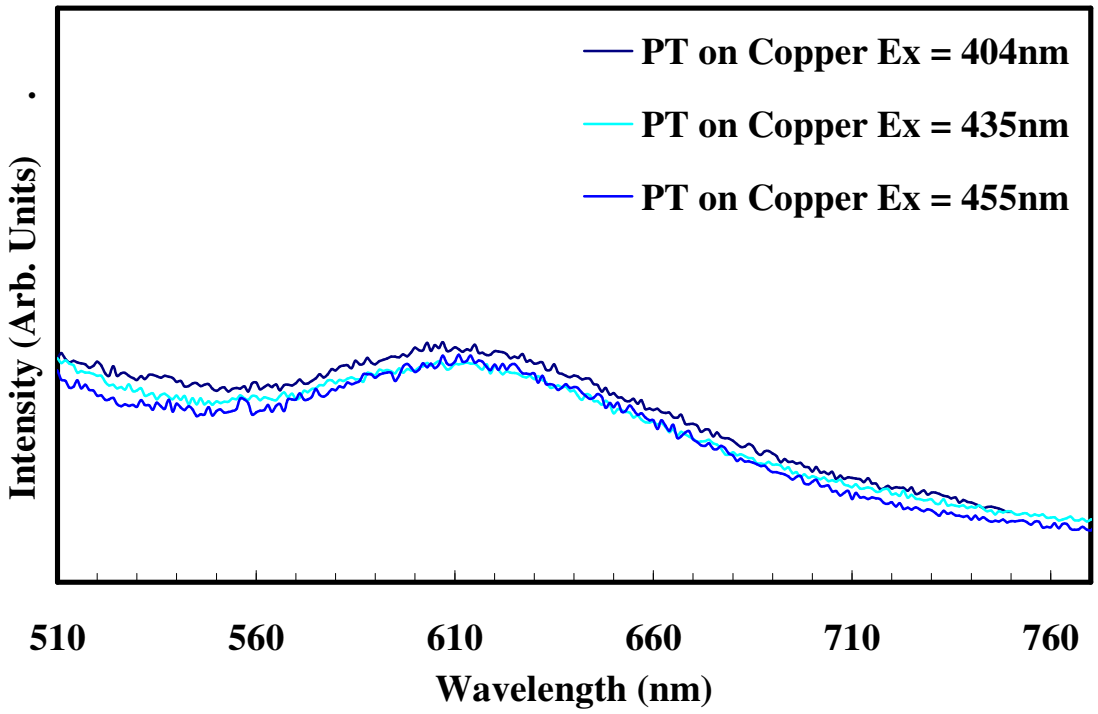

Fig. B2 Photoluminescence emission from the polythiophene film synthesized by photo-activated Ullmann coupling.

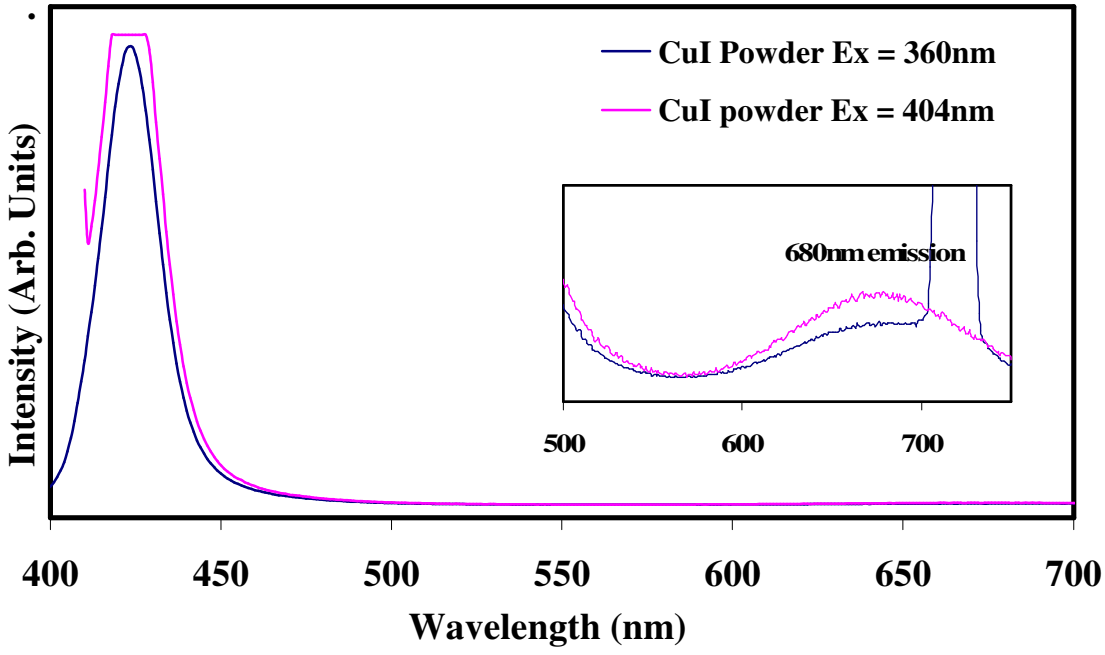

Fig. B3 Photoluminescence emission from the copper iodide powder purchased from Aldrich.

Appendix – C

Additional notes on chapter 4

C1.MALDI-MS analysis

Polymer samples are prepared on slide glass using initial monomer deposition of 20secs at the condition described in appendix A. Irradiation time for the results shown in chapter four is 3 mins. The results of the 5 and 10 mins irradiation are shown in the Fig. C1 and Fig. C2. They are essentially the same as 3 mins sample except for a few peak intensity differences in the lower molecular mass region. At this point it is difficult to conclude that these differences are real or just noise. If they are real it confirms that lower molecular mass species are mobile even after 3 mins and the polymerization is still in progress. For MALDI-MS analysis, the film on glass is scratched with a sharp blade and the fine scratched particulates are transferred to MALDI plate using acetone solvent. CHCA is used as the matrix for MALDI analysis.

C2. UV-irradiation of 2,5-diiodothiophene in thiophene

Long UV irradiation (24hr) of concentrated solution of 2,5-diiodothiophene in thiophene (~ 0.5 gm of 2,5-diiodothiophene / 1cc of thiophene) produces oligomers as shown by the MALDI-MS data in Fig. C3. Analysis of the MALDI-MS data using the spreadsheet shown in chapter 4 indicates the presence of various oligothiophene series (particularly one without any iodine or with two iodines) and that the oligomers are as long as 7 mer. D'Auria et al (Gazzetta Chimica Italiana, 119, 1989) have shown that irradiation of 2,5-diiodothiophene in the presence of thiophene produces terthiophene.

Oligomers longer than 3-mers (i.e. terthiophene) are formed in our case probably due to further reaction between terthiophene and the photo-generated thienyl radical. Thienyl radical generated by photo-dissociation of C-I bond of 2,5-diiodothiophene may substitute α or β hydrogen of terthiophene forming 4-mer and so on.

C2. UV-Vis data

The UV-Vis data is collected using a 2,5-diiodothiophene solution in hexane is as shown in the Fig. C4. The concentration of the solution is 12.86 * 10^{-8} moles/cc and the absorption at 248 nm ~ 1.01, so the extinction coefficient is 7.85 * 10^{6} cm^2/mole.

C3 Numerical Solution of PDEs

The notations used here are exactly same as Prof. Duda's ChE 546 notes. In the numerical formulation concentration C is represented by T. The subscript k represents time and i represent space.

$$\frac{\partial^2 C}{\partial x^2} = \frac{\partial C}{\partial t} + K'C$$

$$\frac{T_{k+1,i+1} - 2T_{k+1,i} + T_{k+1,i-1}}{\Delta x^2} = \frac{T_{k+1,i} - T_{k,i}}{\Delta t} + K'T_{k+1,i}$$

$$\Rightarrow \Delta t * \frac{T_{k+1,i+1} - 2T_{k+1,i} + T_{k+1,i-1}}{\Delta x^2} = T_{k+1,i} - T_{k,i} + \Delta t * K'T_{k+1,i}$$

$$\lambda = \frac{\Delta t}{\Delta x^2}$$

$$\Rightarrow \lambda T_{k+1,i+1} - 2\lambda T_{k+1,i} + \lambda T_{k+1,i-1} = T_{k+1,i} - T_{k,i} + \Delta t * K'T_{k+1,i}$$

$$\Rightarrow \lambda T_{k+1,i+1} - (2\lambda + 1 + \Delta t * K')T_{k+1,i} + \lambda T_{k+1,i-1} = -T_{k,i}$$

For every time step the following set of implicit equations is solved using tridiagonal linear equation solver (STGSL)

$$i = 1: \lambda T_{k+1,2} - (2\lambda + 1 + \Delta t * K')T_{k+1,1} = -T_{k,i} - \lambda T_{k+1,0}$$

$$2 \le i \le M - 2: \lambda T_{k+1,i+1} - (2\lambda + 1 + \Delta t * K')T_{k+1,i} + \lambda T_{k+1,i-1} = -T_{k,i}$$

$$i = M - 1: -(2\lambda + 1 + \Delta t * K')T_{k+1,M-1} + \lambda T_{k+1,M-2} = -T_{k,i} - \lambda T_{k+1,M}$$

Start with k=0

I.C: $T_{0,i}$ is known, in the specific case $T_{0,i} = 0$

B.C 1: $T_{k+1,0}$ is known, in the specific case $T_{k+1,0} = T*$

B.C 2: $T_{k+1,M}$ is known, in the specific case $T_{k+1,M} = T_{k+1,M-1}$

Then go to next time k=1, …..

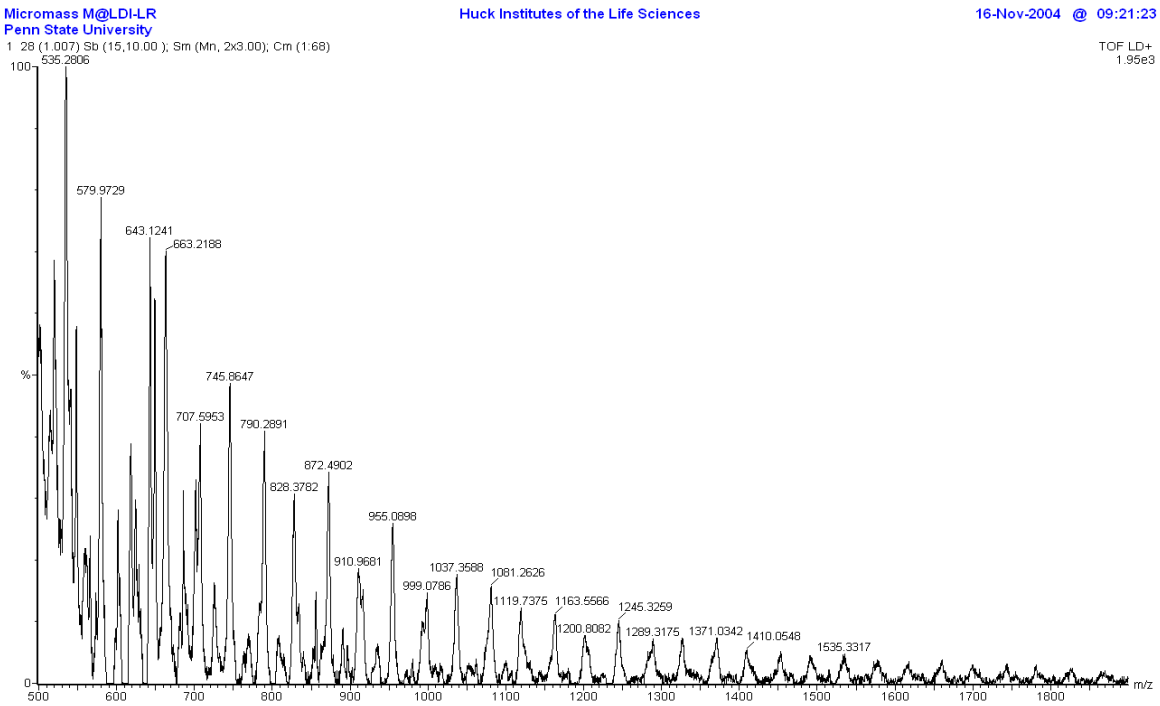

Fig. C1. MALDI data from the sample prepared by 20secs monomer deposition and 5 mins UV irradiation

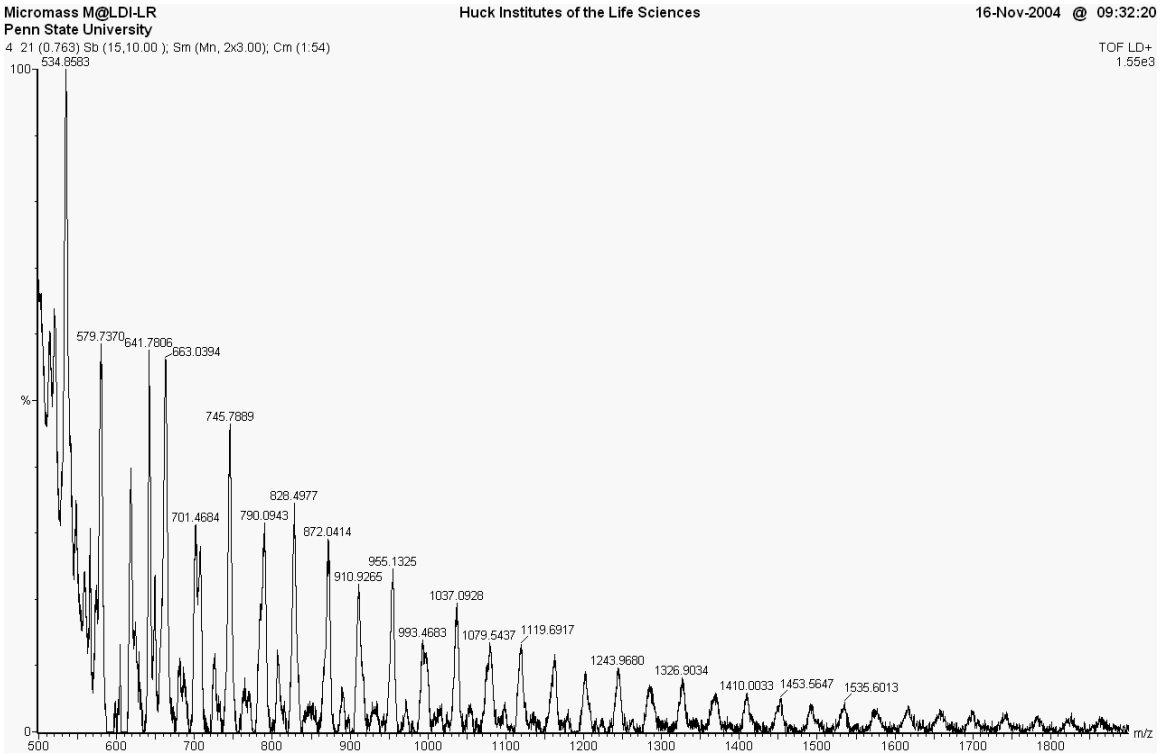

Fig. C2. MALDI data from the sample prepared by 20secs monomer deposition and 10 mins UV irradiation.

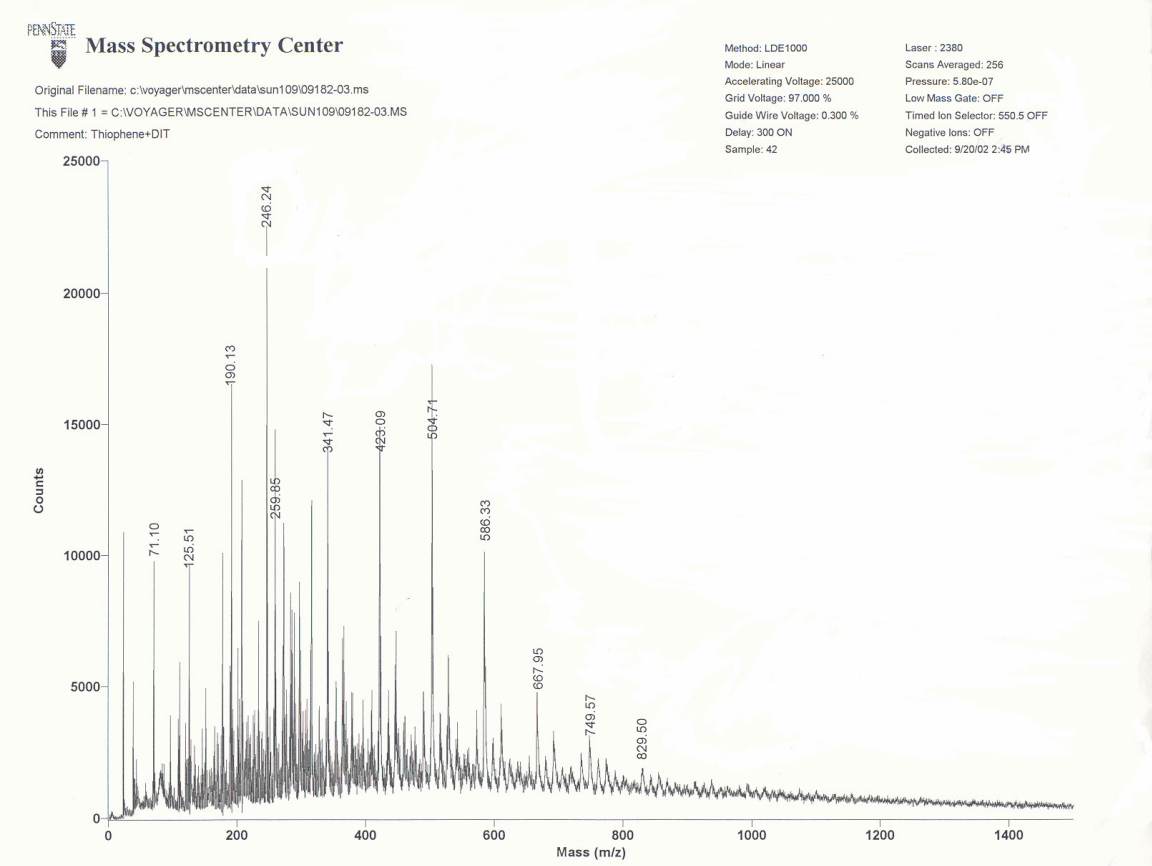

Fig. C3. MALDI data confirming oligomer formation on UV irradiation of concentrated solution of 2,5-diiodothiohene in thiophene.

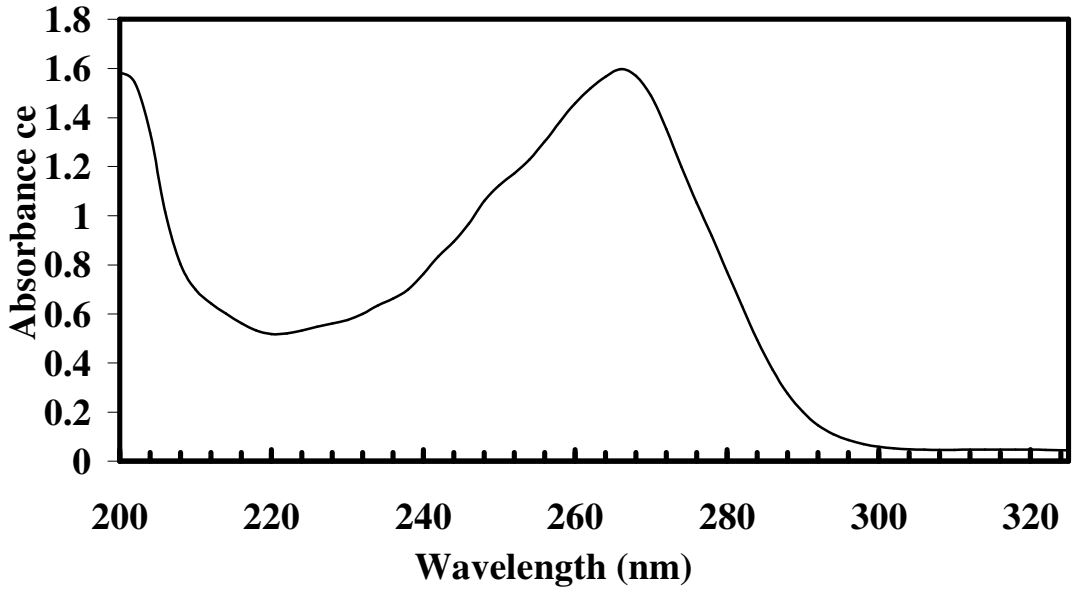

Fig. C4 UV-Vis data from 2,5-diiodothiophene solution in hexane.

Appendix – D

Additional notes on chapter 5

D1. Procedure for making PDMS stamp

Sylgard -184 elastomer kit (ordered thro a distributor, not directly from Dow Corning) is used to make the PDMS step.

1) Read the directions & safety precaution that comes with the kit.
2) Take 10:1 (by weight) mixture of the base and the curing agent and mix it thoroughly. While mixing, try your best not to make lot of trapped air bubbles.
3) Keep the master stamp on polystyrene cup (don't use glass container as PDMS bonds to glass/SiOx surface) with features on the master facing the top as shown Fig D1. For the experiments described in the fifth chapter, an optical grating is used the master. Although the master is made of glass it has some sort of surface treatment that prevents the bonding with PDMS during curing.
4) Pour the elastomer mixture up to the point the master is completely immersed. Add more elastomer mixture depending on how thick you want the final stamp to be.
5) Now place the cup with the elastomer and the master inside desiccator and pull vacuum. By pulling the vacuum air bubbles trapped in the elastomer will come to the surface.
6) Now release the vacuum quickly. Releasing the vacuum quickly bursts the air bubbles held at the surface.
7) Repeat steps 5 and 6 for few more times to remove all the trapped air bubbles.

8) Heat the setup at ~ 65C oven for a day. This procedure will harden the elastomer. Then peal the PDMS stamp off the master.

D2. Procedure for stamping

1) Clean the gold using the RCA (Radio Corporation of America) -1 etch procedure. The procedure is as follows. Heat a mixture of 5 parts of Millipore water with 1 part of 25% NH_4OH to 80 ^oC. Add 1 part of H_2O_2 gradually and maintain the mixture temperature at 70 ^oC. The solution will start bubbling vigorously. Then place the gold evaporated wafer ~ 10 mins. Take necessary safety precautions during etching and remember to keep away all the organics as this mixture is a strong oxidizing agent.
2) Prepare 3 millimolar solution of the thiol to be stamped. Use cotton swab to apply thin film of solution on the PDMS stamp.
3) Place the stamp in close contact with the cleaned gold for 30 secs and remove it.
4) Transfer the stamped sample immediately into a 5 millimolar solution of the second thiol solution. Remove the gold substrate out of the second thiol solution within 5 mins or lesser.

D3. Procedure for making gold patches on a silicon wafer

Square gold patches on a silicon wafer are made using 2000 mesh SPI (Structure Probe Inc.) TEM grid as the photomask. The procedure for photolithography is exactly as same as that described in section A7 (with the title "Conductivity measurement") of the Appendix A. The TEM grid is pressed against the photoresist film using a glass cover slip (UV transparent for wavelengths greater than 300nm).

D4. Contact angle

2,5-diiodothiophene is a solid at room temperature. So, the contact angle of 2,5-diiodothiophene is measured by melting the 2,5-diiodothiophene on the substrate. Melting is accomplished by maintaining the substrate temperature ~ 50°C. Actual photographs from which contact angles were measured are shown in Fig.D2.

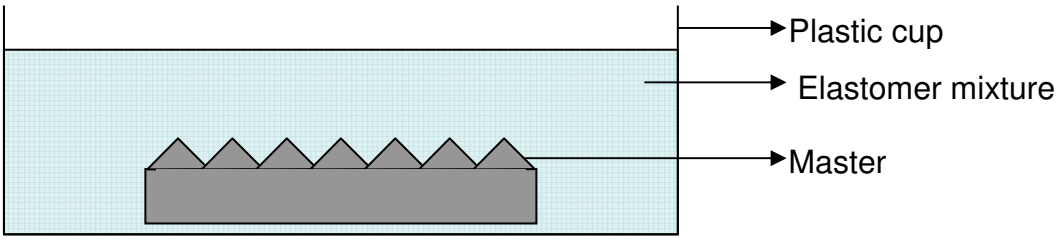

Fig. D1 Procedure for making PDMS stamp.

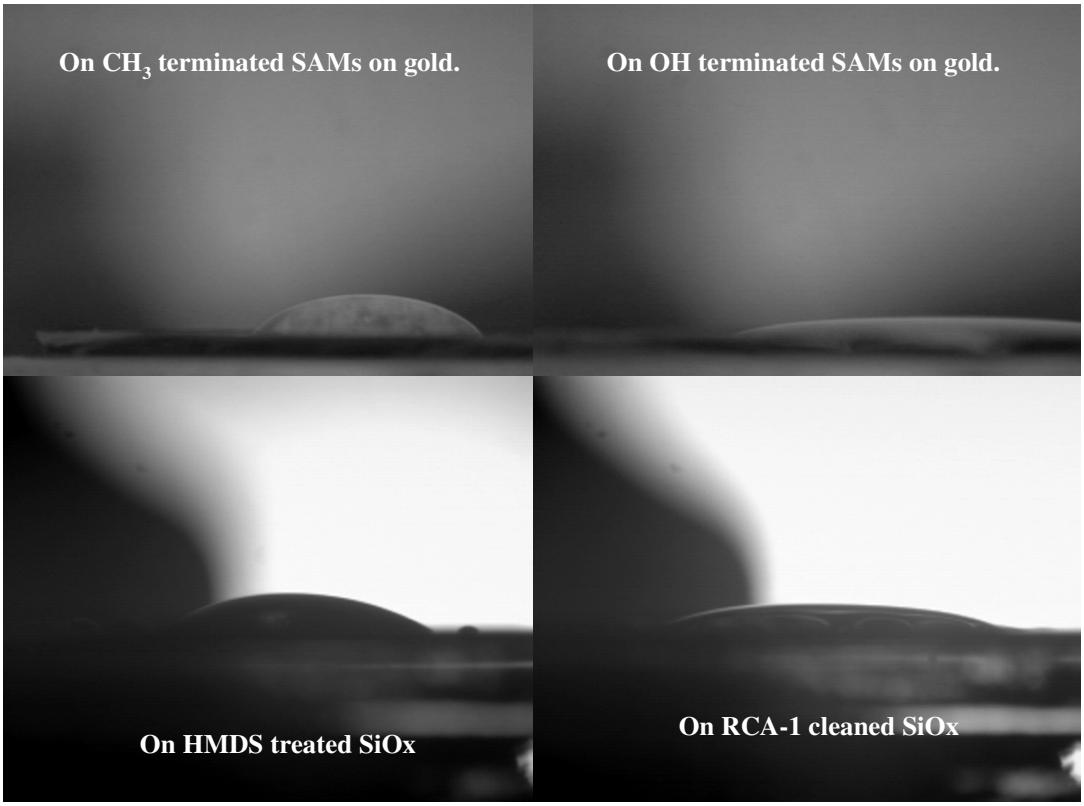

Fig. D2 Photographs from which contact angles of 2,5-diiodthiophene were measured.

Vita

Sudarshan Natarajan was born in India. He received his bachelor's degree in Chemical Engineering from Annamalai University, India in 2000. Sudarshan came to USA in 2000 for pursuing higher studies in Chemical Engineering at Texas A&M University, College Station and later transferred to Pennsylvania State University in 2001. After working on molecular simulations for a year, he joined Prof. Seong Kim's group in 2002 to pursue a Ph.D. in the area of photochemical processing of polythiophene.